CHARACTERIZATION OF A CRYOGENICALLY COOLED GLOW DISCHARGE ION SOURCE

By

SUSAN KAY OHORODNIK

A DISSERTATION PRESENTED TO THE GRADUATE SCHOOL
OF THE UNIVERSITY OF FLORIDA IN PARTIAL FULFILLMENT
OF THE REQUIREMENTS FOR THE DEGREE OF
DOCTOR OF PHILOSOPHY

UNIVERSITY OF FLORIDA

1994

To my parents

ACKNOWLEDGMENTS

I would like to express my sincere thanks to my advisor, Dr. Willard W. Harrison, for his guidance and support. My gratitude also goes out to former group members, Jeff Klingler, Yuan Mei, Philip Rafliff, and Klaus Hoppstock, for their assistance, friendship and encouragement, as well as current group members, Stefan DeGendt and Bill Walden, for their patience while I wrote this dissertation. In addition, special thanks go to Shayla Enram who assisted me while working in the lab on her undergraduate research project.

I would also like to thank Dr. J. D. Winefordner and his group for welcoming the Harrison group into their research space during the renovations to Leigh Hall. The collaborations and cooperation between the groups has worked out so well that it has become a permanent arrangement. I am deeply indebted to Monica Escobar, Ben Smith, Andi Pless, Paul Hart, Denise Imbroisi, Stephanie Pagano, Mary Ann Gunshefski, Donna Robbe, Dennis Hueber, and Sean Madden whose friendship have made this a truly enjoyable and remarkable experience. I will always cherish my status as an "official unofficial JDW group member".

Finally, I am grateful for the research support provided by the United States Department of Energy, Division of Chemical Sciences.

TABLE OF CONTENTS

Page

ACKNOWLEDGMENTS iii

LIST OF TABLES vi

LIST OF FIGURES vii

ABSTRACT xi

CHAPTERS

1 GLOW DISCHARGE MASS SPECTROMETRY 1
Historical Background 2
Recent Developments 3
Glow Discharge Fundamental Processes 8
Statement of Problem 31

2 CRYOGENIC COOLING 33
Production of Cryogenic Temperatures 33
Cryogenic Chemistry 41

3 INSTRUMENTATION 47
Mass Spectrometers 47
Glow Discharge Ion Source 51
Cryogenic Cooling Coil 57

4 CHARACTERIZATION OF THE CRYOGENICALLY COOLED GLOW DISCHARGE 64
Experimental 64
Removal of GDMS Mass Spectral Interferences 65
Glow Discharge Operating Parameters 80
Glow Discharge Characteristic Features 88
Conclusions 96

5 ANALYTICAL PERFORMANCE OF THE CRYOGENICALLY COOLED GLOW DISCHARGE 97
Experimental 97
DC Glow Discharge Analyses 98
RF Glow Discharge Analyses 110
Conclusions 126

6 DIAGNOSTICS OF THE CRYOGENICALLY COOLED GLOW DISCHARGE 127
Temperature Measurements 129
Experimental 132
Excitation Temperature Measurements 135
Rotational Temperature Measurements 151
Thermocouple Temperature Measurements 163
Conclusions 166

7 CONCLUSIONS 167
Future Studies 169

REFERENCES 173

BIOGRAPHICAL SKETCH 183

LIST OF TABLES

Table		Page
I	Ionization and excitation processes in the negative glow region of a glow discharge	25
II	Metastable energy levels of rare gas atoms.	28
III	Temperature properties of cryogens	35
IV	Comparison of Ion Signal Ratios for Aluminum Alloy NIST SRM# 1241b with and without Cryogenic Cooling	71
V	Typical spectral interferences present in a GDMS mass spectrum	77
VI	Sputter yields with and without cryogenic cooling	93
VII	Relative sensitivity factor values calculated from NIST SRM #1264 low-alloy steel standard	102
VIII	GDMS limits of detection with and without cooling	105
IX	Composition of the machinable glass ceramic (macor)	117
X	Composition of USGS geological rock standard SCo-1	120
XI	Assignment of wavelengths, excitation energies, and transition probabilities for the iron spectral lines	136
XII	Assignment of wavelengths, excitation energies, and transition probabilities for the titanium ion spectral lines	147
XIII	Assignment of the wavelengths and rotational quantum numbers for the R branch of the N_2^+ emission band	154

LIST OF FIGURES

Figure		Page
1	GDMS literature citations from Chemical Abstracts between 1980 and 1992.	4
2	Voltage-current characteristics of a low-pressure dc gas discharge	10
3	Schematic of glow discharge zones.	12
4	The effect of pressure on glow discharge sputter yields	17
5	Sputtering yields for Helium, Neon, Argon, Krypton, and Xenon ion bombardment at 400 eV	20
6	Collisional processes in gas discharges	24
7	A) Single-cylinder Stirling cooler. B) Single-stage Gifford-McMahon cooler.	39
8	Schematic diagram of cryogenic cold finger ion source	45
9	Glow discharge source with cryocooling system for the VG9000.	46
10	Schematic of the laboratory-built mass spectrometer system.	48
11	Schematic of commercial prototype mass spectrometer system.	49
12	A) Schematic of dc glow discharge instrumentation. B) Schematic of rf glow discharge instrumentation.	54
13	A) Direct insertion probe for a dc glow discharge. B) Direct insertion probe for an rf glow discharge.	55
14	A) Applied square wave voltage. B) Resultant cathode potential	56

15 Schematic diagram of the cryogenic coil coupled to the glow discharge ion source on the laboratory-built mass spectrometer. . . . 60

16 Schematic diagram of the coil flange for the laboratory-built mass spectrometer. 61

17 Schematic diagram of the cryogenic coil for the glow discharge ion source on the Finnigan mass spectrometer. 62

18 Schematic diagram of the coil flange for the Finnigan mass spectrometer 63

19 Glow discharge mass spectrum of NIST SRM 1241b aluminum alloy without cryogenic cooling 69

20 Glow discharge mass spectrum of NIST SRM 1241b aluminum alloy with cryogenic cooling 70

21 Glow discharge mass spectrum of NIST SRM 627 zinc alloy without cryogenic cooling 72

22 Glow discharge mass spectrum of NIST SRM 627 zinc alloy with cryogenic cooling 73

23 Comparison of with and without cryogenic cooling for the removal $^{12}C^+$ due to the introduction of oil vapor into the glow discharge source 76

24 The effect of cryogenic cooling versus time on the gaseous impurity and analyte ion signals 78

25 The effect of liquid nitrogen flow rate on the removal of gaseous impurity species from the glow discharge plasma 81

26 The effect of liquid nitrogen flow rate on the analyte ion signal intensities 82

27 The effect of varying the glow discharge current on the $^{56}Fe^+$ ion signal intensity 85

28 The effect of varying discharge pressure on the $^{56}Fe^+$ ion signal intensity 86

29 The effect of sample cathode to ion exit orifice distance of the GD ion signal intensity 87

30 A typical glow discharge current-voltage plot 92

31 The effect of varying the Bessel Box voltage on the $^{54}Fe^{+}$ signal intensity for the Finnigan GDMS system 94

32 The effect of varying the Bessel Box voltages on $^{56}Fe^{+}$ ion signal intensity using the laboratory-built GDMS system 95

33 Schematic diagram of the sample disk die. 99

34 The conversion of LaO^{+} to La^{+} with and without cryogenic cooling 108

35 Conversion of LaO^{+} to La^{+} using cooling for varying La_2O_3 concentrations 109

36 Mass spectra for compacted sample disks composed of 10, 20, and 50% rock standard (SCo-1) in Ag matrix 111

37 Rf-GDMS mass spectrum of an iron cathode without cooling 113

38 Rf-GDMS of an iron cathode with cooling 114

39 Rf-GDMS mass spectrum of a ceramic disk without cooling after 20 min of sputtering 118

40 Rf-GDMS of a ceramic disk after 40 min of cooling 119

41 Rf-GDMS mass spectrum of a SCo-1 rock standard disk without cooling after 30 min of sputtering 121

42 Rf-GDMS mass spectrum of SCo-1 rock standard after 37 min of cooling 122

43 The effect of argon pressure on the rf-GDMS mass spectrum of a ceramic disk 123

44 The effect of pressure on the mass spectrum of a SCo-1 sample disk 124

45 Schematic diagram of the GD optical emission system 133

46 Glow discharge Fe emission spectrum 137

47 Representative Boltzmann plot for the determination of the Fe(I) excitation temperature 138

48 Stability of the Fe(I) excitation temperature measurements 139

49 Fe(I) excitation temperature profile of the glow discharge plasma 141

50 The effect of discharge current of Fe(I) excitation temperatures 144

51 The effect of discharge voltage on Fe(I) excitation temperatures ... 145

52 Glow discharge Ti(II) emission spectrum 146

53 Representative Boltzmann plot for the determination of Ti(II) excitation temperatures 148

54 The effect of gettering versus cryogenic cooling on the Ti(II) excitation temperature 149

55 Glow discharge N_2^+ emission spectrum 153

56 Representative Boltzmann plot for the determination of the N_2^+ rotational temperature 155

57 The effect of nitrogen concentration on the glow discharge N_2^+ rotational temperature 156

58 Stability of N_2^+rotational temperature measurements 159

59 A plot of N_2^+ rotational temperature versus the distance between the sample cathode and the cryogenic cooling coil 160

60 The effect of gettering versus cryogenic cooling on the N_2^+ rotational temperature 161

61 N_2^+ rotational temperature profile of the glow discharge 164

62 Gas temperature profile of the glow discharge using a thermocouple probe 165

Abstract of Dissertation Presented to the Graduate School
of the University of Florida in Partial Fulfillment of the
Requirements for the Degree of Doctor of Philosophy

CHARACTERIZATION OF A CRYOGENICALLY COOLED
GLOW DISCHARGE ION SOURCE

By

SUSAN KAY OHORODNIK

AUGUST 1994

Chairman: Willard W. Harrison
Major Department: Chemistry

The glow discharge has been developed into an analytical technique for the analysis of metals as well as nonmetals, thin films, semiconductors, insulators, and organic materials. The atomic population in the glow discharge can be measured using atomic absorption, emission, and fluorescence spectroscopic analysis while the ionic population can be sampled by mass spectrometry.

A common problem encountered with a glow discharge source is the presence of gaseous impurities, (such as air, water vapor, and pump oil vapors) that can reduce the amount of sample sputtering, as well as quench excitation and ionization reactions. Elimination of these impurities from the glow discharge source is essential to obtaining reliable quantitative results. This dissertation

reports on the effect of cryogenic cooling for the removal of gaseous impurities from the glow discharge mass spectrometer ion source.

The effectiveness of cryogenic cooling has been demonstrated by essentially removing all impurities (except nitrogen) occurring in the m/z range between 10 and 40 where the greatest interferences from water and other impurities appear. This ability to remove efficiently impurities is crucial for the accurate analysis of compacted samples that trap water and air during pressing into sample disks. The analytical performance of the cryogenically cooled glow discharge is demonstrated for metal alloy, ceramic, and geological samples using both dc and rf glow discharge sources.

The glow discharge is quite small, and the addition of a cryogenic sink introduces an extremely cold, large surface in close proximity to the active negative glow. Plasma diagnostic measurements were performed in order to study the effect of cryogenic cooling on plasma processes in the glow discharge source. The fundamental plasma processes were investigated by optical temperature measurements from Fe(I) and Ti(II) excitation and N_2^+ rotational emission spectra and physical temperature measurements using a thermocouple probe. Fe (I) and Ti (II) excitation temperatures ranged between 3500 - 3900 K and 5500 - 7000 K, respectively. The N_2^+ rotational temperatures varied between 500 - 620 K, while the thermocouple temperatures varied between 380 - 430 K.

CHAPTER 1

GLOW DISCHARGE MASS SPECTROMETRY

Glow discharge mass spectrometry (GDMS) is a trace elemental technique for the direct analysis of solid samples in which the atomization, excitation, and ionization of the solid sample occur in the plasma. The glow discharge source can be operated using either a dc or rf power supply. If a dc glow discharge is employed, the sample must be electrically conducting, while nonconducting samples can be analyzed directly using a rf discharge. GDMS has been employed for the analysis of metals, nonmetals, thin films, semiconductors, insulators, organic materials, and solution residues with detection limits in the sub part-per-billion range. A common problem encountered with glow discharge sources is the presence of gaseous impurities (such as air, water vapor, and vacuum pump oil) that can reduce the amount of sample sputtered as well as quench excitation and ionization processes. The focus of this dissertation is the physical removal of these gaseous impurities using liquid nitrogen cooling of the glow discharge ion source.

Historical Background

Electrical discharges were the earliest ion sources in mass spectrometry. In 1886, Goldstein discovered that canal rays (positive ions) were produced in low pressure electrical discharges (1). It was the attempt to measure the velocity, charge, and mass of these cathode rays that brought about the development of the first parabola mass spectrograph by J. J. Thomson (1). F. W. Aston used a spherical discharge tube as the ion source for his velocity focussing mass spectrograph that successfully combined electric and magnetic field analyzers (1). Despite this early work, the gas discharge lost favor as a source of ions because of the relatively high gas pressures, electrical instability of the discharge, and wide range of ion energies produced.

During the early 1960's, Knewstubb and Tickner performed a series of experiments using a dc glow discharge coupled to a mass spectrometer in order to investigate ion-molecule reactions in the plasma. The ions produced in the positive column of a glow discharge were investigated using discharge gases of argon, krypton, and mixtures of the two, as well as the effect of hydrogen impurities on an argon discharge (2). The negative glow region of the glow discharge ion source was also examined using helium and helium-argon and argon-krypton discharge gases (3). They investigated the ion-molecule reactions in nitrogen (4), oxygen (5), and water vapor (6) glow discharges.

The first analytical use of GDMS occurred in 1970 when Coburn developed a planar diode rf glow discharge ion source for a quadrupole mass spectrometer

(7). Coburn and coworkers demonstrated that the rf glow discharge could be used for the elemental analysis of the bulk constituents of a sample, as well as profiling the surface layers of a solid target (8-11). Harrison and Magee (12) and Colby and Evans (13) reported the development of dc hollow cathode ion sources for the mass spectrometric analysis of solid samples. Harrison and coworkers measured trace elemental detection levels in the sub-ppm range for solution residues and low ppm range for bulk cathode analyses (12, 14). The geometry of the hollow cathode for the optimum ion production was investigated with respect to cathode length, bore diameter and bore depth by Wallace and coworkers (15). Donohue and Harrison reported a radiofrequency cavity ion source (16). From the same research group, Mattson et al. described a coaxial cathode ion source that allows the convenient exchange of samples for the analysis of solids and solutions (17). This basic design of the coaxial cathode source is still being used in our laboratory.

Recent Developments

The increase in GDMS popularity is evident by the increase in the number of GDMS literature citations in the chemical abstracts from 1980 to the present (Figure 1). The greatest increase in publications started about 1987. This increased interest in glow discharge ion sources probably was spurred on by the success of the complementary technique of inductively coupled plasma mass spectrometery and by the introduction and availability of the first commercial

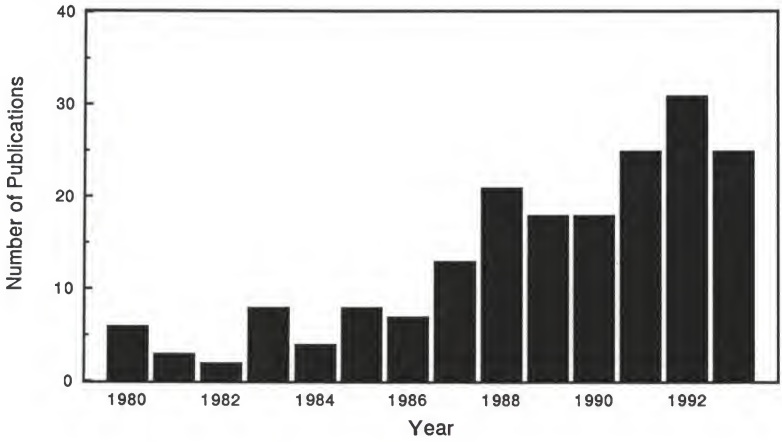

Figure 1. GDMS literature citations from Chemical Abstracts between 1980 and 1992.

GDMS instruments. A glow discharge ion source is commercially available on magnetic sector, quadrupole, and ion cyclotron resonance mass spectrometer systems. Recently, a commercial quadrupole mass spectrometer has been developed that allows the operator to switch between ICP and GD ion sources. A brief summary of GDMS research during the 1980s to the present follows.

Enhancement of the ion population in the glow discharge has been achieved by coupling the plasma with a magnetic field (18, 19), and by adding a secondary cathode to the source (20). Pulsing the dc or rf glow discharge source produced increased ion signals, and exhibited ion signal anomalies that made it possible to acquire data in different regions of the pulse period permitting discrimination against certain interfering ion signals (21-23). A dual cathode probe was developed that allowed the simultaneous analysis of two samples, usually an unknown and standard sample, under the same operating conditions (24).

A great deal of research has been expended to improve the analysis of nonconducting solid samples. Marcus and coworkers developed a direct insertion probe for an rf glow discharge ion source (25), as well as optimized the operating conditions and systems for rf glow discharges ion sources (26). Using a dc glow discharge, a secondary cathode was developed that is placed over the nonconducting sample to promote the sputtering of a glass sample (26).

The glow discharge ion source has been coupled to various kinds of mass spectrometers. Barshick and coworkers have successfully interfaced a dc glow discharge ion source to a Fourier transform ion cyclotron resonance (FTICR) mass

spectrometer (27). They have achieved mass resolutions >290,000 allowing the separation of closely spaced isobaric ions (28, 29). In addition, the rf glow discharge source has been coupled to a quadrupole ion trap mass spectrometer (30, 31). Using the ion trap, MS/MS can be performed to selectively deplete the mass spectrum of interfering species such as oxides, hydrides, argides, etc. Glow discharge sources have been interfaced to double (32) and triple (33) quadrupole mass spectrometers in order to perform collision-induced dissociation of molecular isobaric interferences (33).

The glow discharge ion source has even been used with nonsolid samples. An atmospheric sampling glow discharge ionization source was developed for direct air monitoring (34-36). Lubman and coworkers have accomplished the soft ionization of organics by injecting liquid samples into an atmospheric pressure dc glow discharge source (37). They have also coupled the atmospheric pressure glow discharge source to an ion trap storage/reflectron time-of-flight mass spectrometer (38). The glow discharge was used as the chemical ionization source for analysis of organic molecules in aqueous samples that were introduced into the ion source through microporous membranes (39) and by pneumatic nebulization (40).

Glow discharge mass spectrometry analysis has been applied to a variety of solid and solution samples. GDMS has been used for the analysis of high purity metals such as titanium (41), gallium (42-44), aluminum (45, 46), copper (47), molybdenum (48, 49), tungsten (49, 50), and steel (51, 52). The analysis of

nonconducting solid samples has also been reported for GDMS, including aluminum oxide powders (53), soils (54, 55), rare earth samples (56, 57), semiconductors (58, 59), and nuclear materials, specifically zirconium alloys and uranium oxides (60). Isotopic ratio measurements have been reported for both palladium (61) and uranium (55). The sample versatility of GDMS is demonstrated by its use for the elemental analyses of iron meteorites (62), coal fly ash (63), and coating material for a color TV Braun tube (64). GDMS continues to be used for depth profiling analysis (65, 66), including the analyses of coated wires (67) and oxide scales on metal alloys (68), as well as investigations into crater shape formations (69, 70).

Solution residue analyses have been performed using GDMS in which the solution is pipeted onto a suitable cathode, dried, and analyzed. Using this technique, the levels of lead and platinum in urine have been reported for patients receiving cancer chemotherapy (71), and the elemental composition of unrefined oils has been investigated (72). Aqueous (73) and petroleum (74) residues have also been measured by mixing an aliquot of the solution with the conducting matrix powder, following by drying and pressing the powder into a suitable GDMS sample cathode. Solution samples have also been prepared by the redox cementation of the elements (Pt and Ir) onto a copper cathode (75).

Finally, improvements in quantitative analysis using GDMS have been investigated by varying the chemical composition of the species in the plasma. Using neon as the discharge gas resulted in different spectral interferences than

an argon discharge, improving the analysis of certain elemental constituents (76). The ion signal intensities of most elements increased when an argon-hydrogen gas mixture ranging between 0.1 - 0.5 % was used (77). The use of a gettering matrix (e.g., Ta, W, Ti) for compacted powder samples was shown to "clean up" the plasma by effectively removing oxygen-containing impurity species (78).

Glow Discharge Fundamental Processes

General Characteristics

A gas discharge is a general term meaning the conduction of electricity through a gaseous medium (79). There are two classifications of gas discharges: self-sustaining and non-self-sustaining discharges. A self-sustaining discharge occurs when the electrical current is maintained without an external aid, while a non-self-sustaining discharge requires an external source to supply a sufficient amount of electrons and ions into the discharge. Removal of the external source extinguishes the discharge.

It is possible to produce gas discharges over a wide range of gas pressures and currents. At low pressures, 1-10 Torr, three general types of gas discharges can exist based on their current-voltage characteristics: the Townsend discharge, the glow discharge, and the arc discharge (Figure 2). The Townsend discharge is an invisible non-self-sustaining discharge at very low currents ($<10^{-6}$ A). The electrons are supplied by photoemission from the cathode or photoionization of the gas by external sources such as ultraviolet light, x-rays, or

cosmic rays. As the current is increased, the electrons acquire sufficient energy that upon collision with gas molecules it is possible to produce ions, excited species, and secondary electrons. The positive ions are attracted to the negative cathode, bombarding it, and releasing electrons and atomic species from the surface. This charge multiplication process or "avalanche" increases rapidly with increasing current and voltage reaching a point called the breakdown voltage (V_b); the voltage required for the gas to start behaving as a conductor instead of as an insulator, and the discharge becomes self-sustaining (79). The breakdown voltage is dependent on the discharge gas, cathode material, and cathode configuration. As the current increases further, the potential drops until reaching the normal glow discharge region. The decrease in voltage with rising current results because at larger currents the discharge potential is no longer determined solely by the applied voltage but also by the net space charge (80). It is in this region that a glow first appears at the cathode surface. As the current is increased, the glow spreads over the entire cathode surface while the voltage and current density remain relatively constant. Once the glow encompasses the whole cathode, increases in current cause an increase in the current density and voltage in the abnormal glow discharge region. Further increases in current result in the development of an arc discharge. The arc is a non-self-sustaining discharge that results from the thermal emission of electrons due to the heating of the cathode material by an external source or the discharge itself.

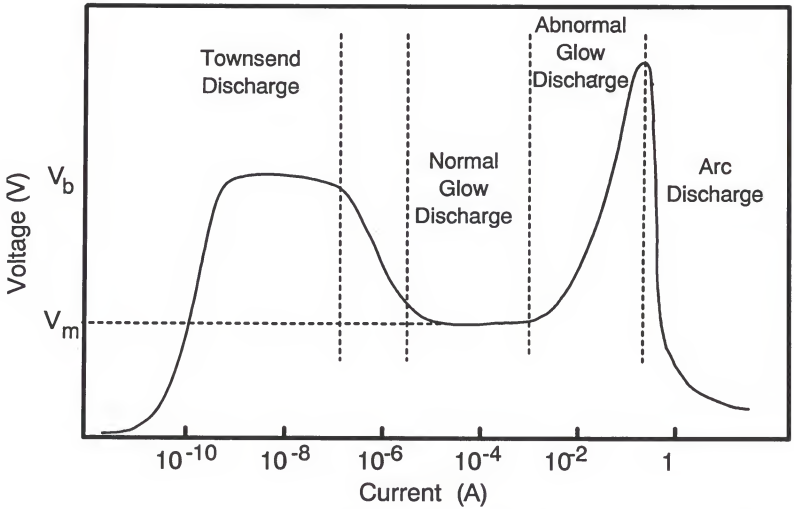

Figure 2. Voltage-current characteristics of a low-pressure dc gas discharge. Adapted from references 82 and 104.

While glow discharges can be operated within a wide range of pressures, voltages, currents, and cathode geometry conditions, all are capable of developing distinctive light and dark luminous zones. For a glow discharge developed between two parallel plates several centimeters apart, eight zones are apparent (81, 82) (Figure 3). Adjacent to the cathode surface is the Aston dark space. In this region, electrons are produced by the bombardment of the cathode surface with ions and fast atoms that have been accelerated through the cathode dark space. There is a net negative charge due to the accumulation of low energy (slow) electrons emitted from the surface. The electrons are accelerated away from the negative cathode surface into the cathode glow region. The cathode glow results from the release of photons upon the recombination of incoming positive ions and slow outgoing electrons. The electrons are next accelerated through the cathode dark space due to the potential drop in this region called the cathode fall. The electrons will accumulate sufficient energy to cause charge multiplication in the cathode dark space producing an efficient supply of electrons and ions. The positive ions move toward the cathode creating a space charge field responsible for the cathode fall, while the electrons are accelerated into the bright negative glow region. The negative glow is formed when the electrons have gained sufficient energy to excite and ionize the gas species upon collision. Two types of electrons are present in the negative glow: fast electrons produced near the cathode that are accelerated through the

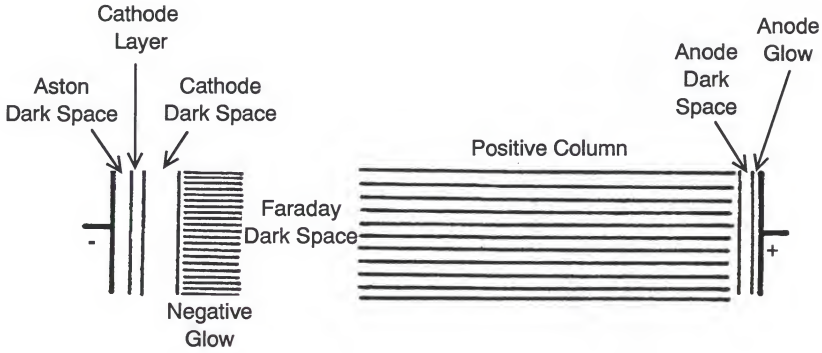

Figure 3. Schematic of glow discharge zones.

cathode dark space, and slow electrons that are produced from election impact ionization of the gas molecules. The negative glow is a relatively field-free region having no net charge, meaning the electron and ion concentrations are nearly equal. The electrons undergo many collisions in the negative glow resulting in the loss of electron energy and glow intensity with increasing distance from the cathode. The Faraday dark space results when the electrons no longer have enough energy to excite and ionize the gas atoms. In the Faraday dark space, the electrons continue to undergo inelastic collisions gaining enough energy to ionize and excite the gas molecules producing the glow of the positive column. The negative glow, Faraday dark space, and positive column are field-free regions (no net charge) and are called a plasma. The anode glow is produced when the electrons have gained excess energy from the space charge effects near the anode. The anode dark space is a region where positive ions are created due to the anode fall that results from electrons leaving the positive column toward the anode surface.

The length of the positive column will depend on the length of the discharge tube. As the tube is shortened, the length of the positive column is reduced, while the rest of the zones remain unchanged. The distance between the cathode and anode can be decreased until the positive column and anode glow completely disappear resulting in an "obstructed" discharge. Therefore, in order to maintain a glow discharge, the presence of the cathode dark space and negative glow is required. An obstructed glow discharge ion source was used in

this research because the "reactive" negative glow is the region of most importance in analytical applications.

Sputter Atomization

The usefulness of the glow discharge as an analytical source lies in its ability to produce an atomic vapor representative of the solid cathode. The following processes may occur when the solid cathode (analytical sample) is bombarded by positive ions in the glow discharge: (1) ejection of electrons from the surface (the process responsible for maintaining the discharge), (2) reflection of the ions typically resulting in their neutralization and loss of energy, (3) implantation of the ions, (4) structural rearrangement and damage of the surface, and (5) ejection of atomic species (sputtering) (83).

Sputtering occurs when the energized species impart their kinetic energy through inelastic collisions with surface atoms that dissipate their energy to their neighbors producing a "collision cascade" (83). If the energy released in the collision cascade is sufficient to overcome the binding energy of the surface atoms, an atomic species will be ejected into the gas phase. This minimum energy required to dislodge a target atom is called the sputtering threshold, and is usually approximated by the heat of sublimation of the elemental species (84). At kinetic energies greater than the binding energy of the atoms, the atoms can undergo surface rearrangement and damage. At energies greater than 4x the binding energies, dislodging of the atoms and ejection into the gas phase can occur (84). The sputtering threshold is characteristic of the sputtering gas-target

material combination. The atomic species can be sputtered from the surface as neutrals, negative and positive ions, and clusters, with neutral atoms making up the majority of the sputtered material (85).

The most important parameter for characterizing the sputtering process is the sputter yield, *S*, and is defined as the number of atoms ejected per incident ion. The experimental expression for the sputter yield is (86):

$$S = \frac{WNe}{Mi^{+}t} \qquad (1)$$

where *W* is the weight loss (g), *N* is the Avogardro number ($mole^{-1}$), *e* is the electron charge (C), *M* is the atomic mass of the sputtered atom (g), i^{+} is the ion current (A), and *t* is the sputtering time (s). The ion current is related to the discharge current, *i*, by:

$$i^{+} = \frac{i}{1 + \gamma} \qquad (2)$$

where γ is the number of electrons released by one ion, and is equal to 0.1 for argon, the gas used most often for analytical GD sources.

To obtain accurate sputter information, the mean free path of the sputtering gas must be larger than the dimensions of the source. The glow discharge operating at pressures between 0.1 -10 Torr has atomic and ionic mean free paths that are small compared to the glow discharge source dimensions. The higher

operating pressure of the glow discharge appears to have two effects on sputtering. First, due to the short mean free paths, the sputtered atoms might be unable to escape completely from the cathode due to collisions and are redeposited on the sample surface. As the pressure is increased, the sputter yield decreases due to the back diffusion of the sputtered material (87) (Figure 4). It has been commonly estimated that 90-95% of the sputtered atoms are redeposited in glow discharge sputtering (88). Second, the length of the cathode dark space is larger than the mean free paths of the ions; consequently, the ions can undergo multiple collisions as they are accelerated through the cathode fall toward the cathode surface. These multiple collisions produce bombarding ions with undetermined angles of incidence and a wide energy spread, anywhere between zero and the maximum energy of the cathode fall (84). In addition, the inherent nature of a gas discharge can affect the sputtering process. The secondary emission of electrons due to ion bombardment is responsible for maintaining the self-sustaining discharge, but these emitted electrons can also neutralize incoming ions resulting in bombardment by fast atoms instead of ions. Also, if the sputtered species is ejected as a positive ion, it will be attracted to the negative cathode surface and will redeposit.

As a result of these complications, sputter measurements made with glow discharge sources are typically inaccurate and irreproducible. Therefore, most sputtering experiments are performed with low-pressure ion beam systems that have long mean free paths and known ion bombardment energies. The

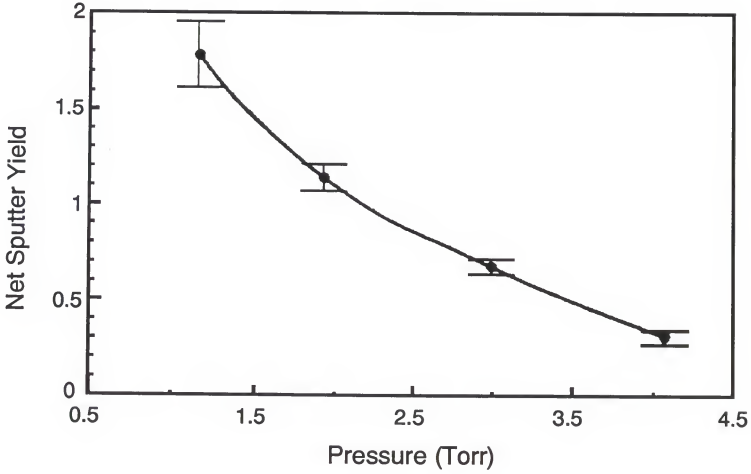

Figure 4. The effect of pressure on glow discharge sputter yields (87).

mechanisms are assumed to be similar between ion beam and glow discharge sputtering; therefore, comparisons with ion beam systems have been used to gain a better understanding of GD sputtering mechanisms.

It has been shown using ion beam bombardment that the efficiency of sputtering depends on the incident ion energy, angle of incidence, type of sputtering gas, and the nature of the cathode material. Some general observations on the effect of these parameters on sputter yields follows; references 84, 89, and 90 are suggested for a detailed discussion of sputtering and its parameters. Once the threshold energy is reached, the sputter yield rises exponentially then linearly as the energy of the incident ion increases. At high ion energies (ca. 1 keV), the sputter yield reaches a maximum or plateau and then decreases with further ion energy increase (89). This maximum ion energy corresponds to the energy required to implant the incident ion into the cathode surface, and is usually higher than what is normally available with a glow discharge source. The angle of incidence of the bombarding ion has been found experimentally to produce a maximum sputter yield for angles between 40-80° (91). The higher sputter yields result because more energy is transferred to the surface atoms at oblique angles than at larger angles where greater penetration into the cathode results (84). It is possible that the increase observed in glow discharge sputtering after an initial preconditioning is the result of the roughing of the sample that produces more oblique incident angles for bombarding ions. Noble sputtering gases have been found to produce the largest sputter yields

because of their "hardness" and chemical inertness resulting from their filled orbital shells. There is also a periodicity effect with regard to the target material. Sputter yields measured by Wehner and coworkers for He, Ne, Ar, Kr, and Xe ion bombardment were plotted versus their atomic number, and the sputter yields were found to increase in any one period of the periodic table corresponding to the increased filling of the d-shells (92, 93) (Figure 5). It is believed that as the d-shell is filled, the depth of penetration into the cathode is smaller and the transfer of energy back to the surface is larger, resulting in increased sputtering.

It is possible for sputtering to produce an atomic gas phase representative of a solid composed of elements that have differing sputter yields, and this process is called differential sputtering (94). While the sputter yields do differ, the difference is rarely larger than a factor of 10 (see Figure 5). The elements having higher sputter yields are preferentially depleted at the solid surface because they are more easily sputtered, while the elements with lower sputter yields accumulate on the surface. A steady state condition is reached on the cathode surface between the different elemental species that results in the production of a gas phase representative of the bulk sample composition.

The presence of impurities on the cathode surface or in the discharge gas can influence the sputtering rate. Sample sputtering does not begin immediately upon turning on the discharge, but only after an initial "cleaning" period of the cathode surface by bombardment. The time it takes to clean the cathode surface depends on the sample material, the purity of the discharge gas, the type of

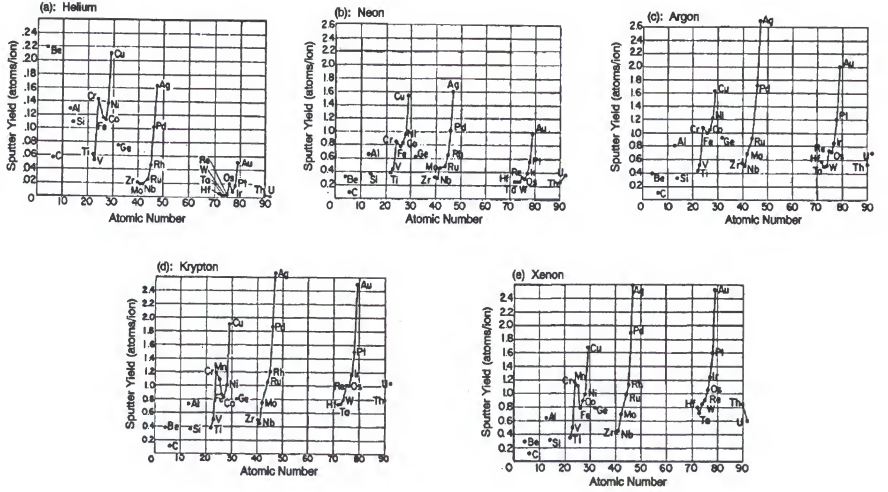

Figure 5. Sputtering yields for Helium, Neon, Argon, Krypton, and Xenon ion bombardment at 400 eV (92, 93).

impurities present, and the cleanliness of the discharge chamber. In addition, sputtering of the sample will only occur if the sputtering rate is greater than the deposition rate of the impurities onto the cathode surface. Jones et al. found that the sputtering rate of SiO_2 decreased rapidly when oxygen was added to the argon sputtering gas (95). Their results were explained by using a model where the sputter rate is lowered by the replacement of the oxygen atoms that have already been sputtered; consequently, a monolayer of oxygen is always being sputtered. If the impurity species has a lower molecular weight than the sputtering gas, a decrease in the sputter yield can result since the efficiency of energy transfer equals $\frac{4M_1M_2}{(M_1 + M_2)^2}$ where M_1 and M_2 are the molecular weights of the colliding species, and maximum energy transfer occurs when M_1 equals M_2. A common impurity in the glow discharge is water vapor that has been found to produce numerous ionic species in the plasma such as H^+, H_3^+, O^+, OH^+, H_2O^+, and H_3O^+ (96). Larkins observed that when trace quantities of water vapor were present in the glow discharge the sputtering rate decreased, and this decrease was dependent on the cathode material (97). In the case of water vapor, the decreased sputtering could be due to the lower molecular weight bombarding species or the adsorption of the water vapor ion species on the cathode surface.

Sputtering is an inefficient process with more than 95% of the bombarding energy converted to target heating (84). Sputter yields tend to vary only slightly with target temperature, but rise sharply when the temperature nears the vaporization point of the elements. At low bombarding energies, such as for glow

discharge sputtering, sputter yields tend to decrease with increasing target temperature due to the annealing of the surface species producing more strongly bound atoms (84). At higher bombarding energies, the sputter yields increase as the temperature approaches the melting point of the metal resulting in the thermal emission of the atomic species ("thermal sputtering") that is superimposed on the collisional sputtering process. Hence, to achieve higher sputter yields by increasing the bombarding energy usually requires that the cathode or target be cooled.

Ionization and Excitation

The neutral atomic population introduced into the glow discharge by sputtering has been probed using atomic absorption (98, 99) and atomic fluorescence (100). In addition, the atomic population can be excited and ionized in the plasma allowing both atomic emission (101) and mass spectrometric (102, 103) measurements to be made. Therefore, the glow discharge can be thought of as an atomic reservoir as well as an excitation and ionization source.

At the pressures typically required to operate the glow discharge, collisional processes are responsible for the observed excited and ionized species. The discharge collisions can be classified into two broad categories: elastic and inelastic collisions. When two particles undergo an elastic collision, they retain their internal structure (potential energy) but their velocities change and, consequently, their temperatures change. If an inelastic collision occurs, the state of the atom is changed (excitation or ionization) resulting in an increase or

decrease of potential energy of the atom. An inelastic collision is the conversion of kinetic energy to potential energy or vice versa. For example, ionization of an atom can take place upon collision if an electron has a kinetic energy greater than the ionization potential of the atom.

The glow discharge plasma contains electrons, ground state and excited atoms, ground state and excited ions, and photons resulting in the possibility of collisions between any two species. All the collisional permutations that can result in a gas discharge were summarized over fifty years ago by Penning (104) as illustrated in Figure 6. Fortunately, only some of the processes are important in glow discharge ionization and excitation. The two primary processes responsible for ionization and excitation in the glow discharge are collisions with electrons and excited discharge species (Table I).

Collisions with electrons. The electrons present in the negative glow region can be classified into three groups based on their energies and where they are formed in the discharge (83). First, the *primary electrons* are high energy electrons (20 - 25 eV) that are emitted from the cathode surface during ion bombardment and gain energy as they are accelerated through the cathode dark space toward the negative glow. Second, the *secondary electrons* (2 - 10 eV) are produced from ionizing collisions or from primary electrons that have lost energy through collisions. Third, the *ultimate electrons* are low energy electrons (0.05 - 0.6 eV) that result from primary and secondary electrons being thermalized to the plasma temperature through numerous inelastic and elastic collisions with plasma

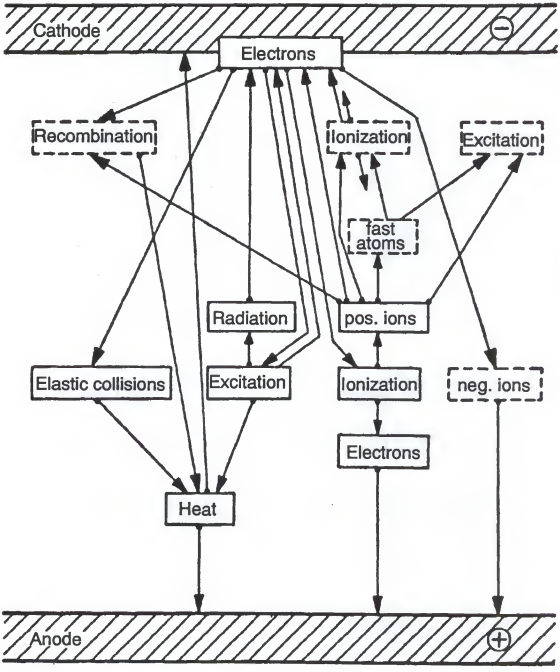

Figure 6. Collisional processes in gas discharges (104).

Table I. Ionization and excitation processes in the negative glow region of a glow discharge.

I. Primary Ionization and Excitation Processes

A. Electron Impact

$$M^\circ + e^- \rightarrow M^+ + 2\,e^-$$
$$M^\circ + e^- \rightarrow M^* + e^-$$

B. Penning Collisions

$$M^\circ + A_m^* \rightarrow M^+ + A^\circ + e^-$$
$$M^\circ + A_m^* \rightarrow M^* + A^\circ$$

II. Secondary Processes

A.1. Nonsymmetric Charge Transfer

$$M^\circ + A^+ \rightarrow M^+ + A^\circ$$
$$M^\circ + A^+ \rightarrow M^{+*} + A^\circ$$

2. Symmetric (Resonance) Charge Transfer

$$X^+_{(fast)} + X^\circ_{(slow)} \rightarrow X^\circ_{(fast)} + X^+_{(slow)}$$

3. Dissociative Charge Transfer

$$MX + A^+ \rightarrow M^+ + X + A^\circ$$

B. Associative Ionization

$$M + A_m^* \rightarrow MA^+ + e^-$$

C. Photoionization and excitation

$$M^\circ + h\nu \rightarrow M^+ + e^-$$
$$M^\circ + h\nu \rightarrow M^*$$

D. Cumulative Ionization

$$M^\circ + e^- \rightarrow M^* + e^- \rightarrow M^+ + 2e^-$$

M° - sputtered neutral; A_m^* - metastable atom of discharge gas; X - any gas atom

species (83, 105). Electron densities on the order of 10^6, 10^7 - 10^8, and 10^9 - 10^{11} cm^{-3} have been reported for the primary, secondary, and ultimate electrons respectively (105).

The ability of an electron to ionize or excite an atom upon collision depends on its energy. Very slow ultimate electrons will produce no ionization or excitation upon collision with ground state atomic species, while secondary electrons, having a moderate speed and less energy than required for ionization, are capable of exciting atoms upon collision. The excited atoms can undergo further collisions with electrons and be ionized (cumulative ionization) (81). Ionization of neutral atoms is accomplished by collisions with primary electrons or secondary electrons that have energies larger than the ionization potential of the atomic species. It would seem logical that the higher the electron velocity, the more collisions, and therefore the more excited and ionized atoms produced. This assumption is false; most gases exhibit a maximum in their ionization and excitation cross sections between 0.1 - 200 eV (106). A maximum is produced because the period of interaction between a very fast electron and an atom becomes very short resulting in a decrease in the amount of kinetic energy transfer that can occur (106). While it might be possible for some high energy primary electrons to pass through the glow and collide with the anode, collisions between ground state atoms and primary electrons appear to be the main source of total ionization in the negative glow (83).

Collisions with excited species. Ionization and excitation of the plasma species can also occur due to collisions with long-lived excited atoms in a process called Penning ionization/excitation (Table I). The metastable atom is created when it has been excited to a "forbidden" transition level and cannot lose its energy by emitting radiation. Therefore, the metastable atoms are deexcited by collisional relaxation processes, resulting in metastable lifetimes on the order of several milliseconds (107). The metastable atom is capable of ionizing a ground state atom if its excitation energy is greater than the ionization potential of the atom. The metastable energies for the rare gases used in GDMS are higher than most elemental first ionization potentials (Table II). The metastable atoms are produced with high efficiency in the glow discharge by electron collisions and are considered to play a principal role in the ionization mechanism for sputtered species in the negative glow (8).

A second and less important ionization process involving metastable atoms is associative ionization, in which a polyatomic ion is formed between the metastable and its collision partner (Table I, II-B). The products formed by associative ionization are often found in GDMS, often causing spectral interferences. Typical interferences include dimers that result from the combination of the discharge gas with the sputtered matrix species (ArM^+), impurity species (ArO^+, ArN^+) and other gas discharge species (Ar_2^+).

Table II. Metastable energy levels of rare gas atoms.

Element	Energy (eV)	Species Not Ionizable
He	20.61 19.82	He, Ne
Ne	16.72 16.62	He, F, Ne
Ar	11.72 11.55	H, He, N, O, F, Ne, Cl, Ar
Xe	9.45 8.32	H, He, C, N, O, F, Ne, P, S, Cl, Ar, As, Se, Br, I, Xe, Kr, Hg, Rn

Additional Collisional Processes

While collisions with electrons and metastable atoms appear to be the dominant ionization and excitation mechanisms in the negative glow region of the discharge, other secondary processes are present and should be considered. The presence of charge exchange reactions as a source of excitation and ionization has been observed, but is highly dependent of the identity of the gas, the sputtered species, and discharge conditions. Using GDMS, Hecq determined that charge exchange was the dominant ionization mechanism for oxygen in an argon-oxygen discharge and for sputtered metal species in an oxygen discharge (108, 109). Hess et al. reported that for a coaxial cathode geometry GD operated at typical GDMS operating conditions of low currents (1 - 10 mA) and pressures (0.3 - 1.5 Torr Argon), charge exchange reactions did not contribute to ionization in the negative glow (110). Photoionization of the plasma species can occur if the energy of the photons, released during the radiative relaxation of the excited discharge species, corresponds closely to the ionization potential of the element. Photoionization was found to play a minor role in ionization of copper and carbon in a neon glow discharge (111).

The effect of impurity species. The presence of impurity species, such as water vapor, nitrogen, carbon dioxide, and hydrocarbons, can reduce the intensity of the ion signals of the sputtered species. This reduction in sputtered species ion signal as monitored by mass spectrometry appears to be caused by several methods including: (1) quenching of the metastable discharge atoms that are

responsible for ionization, (2) gas phase reactions between the sputtered and impurity species, and (3) reduced sputter rate due to the adsorption of the impurity species on the surface and lower molecular weight bombarding species, such as H^+, O^+, and H_2O^+ (97, 110, 112).

As it was previously mentioned, the primary ionization mechanism for the sputtered species is Penning ionization, the collision between metastable discharge gas atoms and the sputtered atoms. It has been observed that the presence of water vapor and organic molecules can quench the metastable atom population by an energy transfer from the metastable atom to the impurity species; thereby, reducing the analyte ion signal (110, 113). Typically, the impurities are molecular species which can be dissociated in the plasma producing byproducts such as H, O, C, and N. These byproducts are very reactive and produce dimers with the discharge gas and sputtered species. When water vapor is present in the discharge the following species can be found in the mass spectrum: ArH^+, ArO^+, ArN^+, MO^+, and MH^+. Whether the sputtered species, M, reacts with a reactive atom depends on its affinity for that species. For example, it was found that the reactivity of several elements (Ti > Fe > Cu) toward oxygen corresponded to their M-O bond strength (159.3, 97.7, and 65.2 kcal/mol respectively) (112, 114). Therefore, the ion signals of different elements are affected to varying degrees when impurities are present in the discharge.

Statement of Problem

A common problem encountered with glow discharge sources, particularly for mass spectrometry, is the presence of gaseous impurities (such as water vapor, carbon dioxide, nitrogen, and hydrocarbons) in the plasma even after proper outgassing and presputter cleaning of the GD source. The primary contaminant in the glow discharge is water vapor that can be introduced by the discharge gas, vacuum leaks, chamber surface desorption, and sample outgassing. Other contaminants include N_2, O_2 , and CO_2, which are introduced mainly from vacuum leaks, and hydrocarbons that result from backstreaming of the vacuum pump oil.

The gaseous impurities can influence the sputtering, atomization, and ionization processes in the glow discharge. Larkins (97) observed a reduction in atomic absorption for various elements upon addition of water vapor, with the amount of reduction dependent on the type of sample. Ratliff and Harrison (112) have shown that the ion signals of different elements are affected by varying degrees in the presence of water. The reduction in analyte signal due to the presence of water can be attributed to a combination of effects, including inefficient sample sputtering, oxidation of the sample surface, loss of analyte atoms through gas-phase reactions, and quenching of argon metastable atoms that are responsible for ionization (97, 112). Eliminating these impurities from the GD source is essential for obtaining reliable quantitative results, especially in mass spectrometry, where the impurities may obscure analyte ion signals.

Efforts to reduce or eliminate water vapor and other gaseous impurities have included: (1) use of ultra-high purity gases to reduce impurity introduction, (2) application of gettering agents to purify further the discharge gases, (3) frequent baking of the source chamber to eliminate absorbed species, and (4) general maintenance of high-vacuum conditions in the system. Cryogenic cooling in the source chamber is also a method for removing the impurities from the glow discharge by physically freezing out the impurities, particularly water vapor, from the gas onto the source chamber walls.

The purpose of this research was to study the effect of cryogenic cooling on the glow discharge's analytical performance and fundamental discharge processes using mass spectrometry and optical spectroscopy. In order to perform these studies a simple, effective design for cryogenic cooling was developed that could be adapted to many different types of GD source configurations.

CHAPTER 2
CRYOGENIC COOLING

In 1877, Pictet working in Geneva and Cailletet in Paris separately liquefied oxygen marking the start of cryogenics (115), which is defined as the science that deals with the production of very low temperatures and their effect on matter. Cryogenics literally means relating to cold (116). Cryogenic temperatures range from -100°C to absolute zero, -273° C, and can be obtained by using liquid cryogens, such as liquid nitrogen and liquid hydrogen, or cryogenic refrigerators.

Production of Cryogenic Temperatures

Liquid Cryogens

Determining what equipment to use for the production of low temperatures depends on the desired temperature range, precision of temperature control, and the length of cooling time. The simplest type of cryostat, an apparatus for maintaining low temperatures, is a dewar filled with a liquid cryogen. A variety of cryostats are commercially available, and include options such as automatic level and feed controls for the liquid cryogen and temperature probes for measuring the sample temperature. One disadvantage of commercial cryostats is that they

are not easily modified. Hence, depending on the need, a laboratory built cryostat might be more appropriate.

Cryostats can be built out of glass, metal or a combination of the two. Glass dewars are inexpensive, light, and can be made into complicated shapes, but they are susceptible to thermal stress and failure. Glass is also an excellent insulator; therefore, good thermal contact with the cryostat must be attained to achieve the desired low temperature (117). Metal cryostats are easily machined and are very sturdy. Copper alloys, aluminum alloys, and stainless steels are the most commonly used metals for the construction of cryostats due to their strength at low temperatures (116). The thermal conductivity of the material is also an important consideration. In the temperature range between 20 - 50 K, pure metals have conductivities 100 times larger than their alloys, while the alloys differ from one another by a factor of ten (116). Copper is considered an excellent material for heat exchangers because of its large thermal conductivity, which increases with lowering temperature. Copper alloys also can easily adsorb gaseous species and might not be suitable for experimental systems requiring high vacuum integrity over a large temperature range (i.e., 0 - 300 K). Consequently, stainless steel is the recommended material for vacuum cryostats.

The properties of the liquid cryogen determine the temperature operating range of the cryostat (Table III). The four most common liquid cryogens are oxygen, nitrogen, helium, and hydrogen. They are produced in the greatest quantities, and account for most of the cryogenic research and applications (116).

Table III. Temperature properties of cryogens (118).

	Boiling Point °C (K)	Freezing Point °C (K)
He	-269 (4.2)	---
H_2	-253 (20.3)	-259 (14.1)
Ne	-246 (27.1)	-249 (24.5)
N_2	-196 (77.4)	-210 (63.3)
Ar	-186 (87.3)	-189 (84.0)
O_2	-183 (87.3)	-219 (54.8)
CH_4	-161 (111.7)	-183 (90.6)
Kr	-152 (121.4)	-169 (104.2)
Xe	-109 (164.1)	-140 (133.2)
C_2H_4	-104 (169.3)	-169 (104.2)
C_2H_6	- 89 (184.6)	-183 (89.9)

The use of liquid helium is necessary to obtain the lowest possible temperature, while liquid nitrogen provides the cheapest and safest refrigerant. In choosing the optimum liquid cryogen for the glow discharge source, it is desired that the cryogen will condense all the gaseous impurities but not the discharge gas. From matrix isolation experiments, it has been found that isolation requires temperatures approximately 1/2 of the melting (freezing) point of the matrix (119). Therefore, to freeze out and isolate the argon discharge gas in a glow discharge source would require temperatures near 30 K, meaning liquid hydrogen or helium must be used for cooling. For the glow discharge source, liquid nitrogen and higher boiling point cryogens would be appropriate for cooling.

Cryogenic Refrigerators

While liquid cryogens are the most common method for producing cryogenic temperatures, the use of cryogenic refrigerators is finding wider application in chemical instrumentation due to improvements and miniaturization prompted by the electronics, military, and space industries. Several common types of small cryogenic refrigerators that might be found in an analytical research laboratory include the Joule-Thomson, Stirling, Gifford-McMahon, and thermoelectric coolers.

Joule-Thomson coolers. The Joule-Thomson cooling effect occurs when a high-pressure gas is passed through a small orifice into a low pressure region. Gas molecules separate as they expand into the low pressure region, moving against the Van der Waals force of attraction between them. The energy required

for this motion comes from the gas molecules' kinetic energy. The lowering of the kinetic energy results in a decrease in internal energy and a drop in gas temperature (116). In the Joule-Thomson cooler, the high pressure gas passes down a heat exchanger and is cooled as it expands into a low pressure. The cooled gas is passed back up through the heat exchanger to precool the next quantity of incoming high pressure gas. With each successive pass, the gas gets cooler and cooler until liquefaction of the gas occurs and a minimum temperature is reached (120). Performance of the Joule-Thomson cooler depends on the gas used and its operating pressure and flow rate.

Stirling coolers. In the Stirling cooler, cold is produced by the reversible expansion of a gas. The gas, usually helium, is compressed at ambient temperature in a compression space with the heat produced extracted by a heat exchanger (Figure 7A). The gas is then transferred through a regenerator, a porous connector having a high heat capacity, to the expansion space. The gas is cooled down in the regenerator with the heat being stored within the regenerator's mass. In the expansion space, the gas is expanded producing the cold that is available for use. To complete the cycle, the gas is transferred back to the compression space, regaining the heat stored in the regenerator (121, 122). There are two common types of Stirling coolers: the single-type where the compressor and expander are housed within the same cylinder, or the split-type where the compressor and expander are located in separate cylinders joined by

the appropriate piping (122). The miniature Stirling coolers can typically cool a few watts at 80 K and fractions of a watt at 10 K (122).

Gifford-McMahon coolers. The Gifford-McMahon cooler also uses gas compression and expansion to produce refrigeration. This method extracts heat from the gas at a low temperature and then adds the heat to the gas at a higher temperature (123). The cooler consists of a cylinder closed at both ends containing a piston that fills approximately 5/6 th of its volume (Figure 7B). The ends of the cylinder are connected in parallel with a regenerator; therefore, any gas in the system flows into both the cylinder and regenerator. Gas intake and outlet valves are located at the top of the regenerator. Compressed gas at room temperature is introduced into the cylinder and regenerator; the piston is moved upwards transferring the warm gas in the top volume through the regenerator and into the cold bottom volume. During this transfer, the intake valve allows some gas into the system to compensate for the pressure loss due to the cooling of the gas through the regenerator. The intake valve is closed and the outlet valve is opened, allowing the gas in the bottom of the cylinder and the regenerator to undergo expansion. The cold produced during the expansion is now available for cooling applications. To complete the cycle, the piston is moved downward transferring the cold gas into the regenerator and the warm top volume (122, 123). The Gifford-McMahon coolers are capable of producing refrigeration temperatures as low as 6.5 K (122).

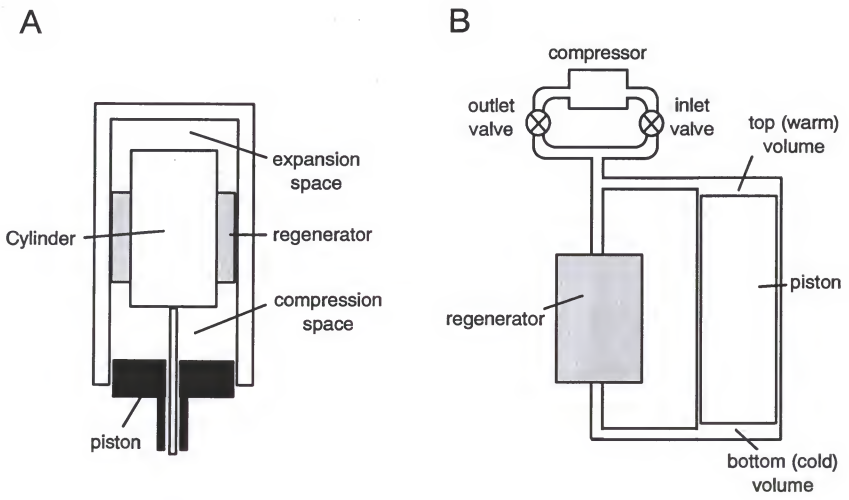

Figure 7. A) Single-cylinder Stirling cooler. B) Single-stage Gifford-McMahon cooler.

Thermoelectric coolers. When electrical current is passed through a junction between two dissimilar metals, a change in heat occurs that is proportional to the quantity of the electrical charge transferred between the two metals (124). If heat is liberated for current flow from metal A to metal B, then heat is absorbed for current flow from metal B to metal A (124). The heat absorbed by electrons at the cold junction is pumped to the hot junction, at a rate proportional to the electrical current, where the energy is expelled to a heat sink as the electrons move from a high energy level to a lower energy level (125). Thermoelectric cooling devices can be coupled electrically in series and thermally in parallel. The devices are available in a great variety of sizes, shapes, and heat pumping capacities.

To remove the gaseous impurities from the glow discharge plasma, the cryogenic cooling method must compensate for the heat given off by the glow discharge. Hence, the minimum amount of cooling required can be estimated by the amount of heat given off by the glow discharge to its surroundings. A glow discharge ion source, operating at 4.0 mA and 1000 V, assuming most of the power goes into heating the cathode, produces a maximum heat load of 4 watts. Therefore, any cryogenic cooling method must have at least a cooling capacity of 4 watts.

There are several types of commercial miniature Joule-Thomson cryorefrigerators currently available, such as coolers manufactured by R. G. Hansen & Associates [Model RDG P/N 5002, Santa Barbara, CA] and NMR

Technologies Inc. [Model S-10, Mountain View, CA] that can handle heat loads of 2 and 0.25 watts respectively. These miniature Joule-Thomson coolers should not cool the plasma, and the NMR cooler proved unable to due so when it was tested. The Stirling coolers can produce several watts (0.25 - 4 watts) of cooling capacity at 80 K (122). Whether the Stirling cooler can be used will depend on the individual model. Coolers based on the Gifford-McMahon cycle can produce temperatures as low as 7.5 K with cooling capacities between 1 - 20 watts. They can also produce 20 - 120 watts of cooling at 80 K. Gifford-McMahon cryorefrigerators are capable of producing more cooling than necessary, which increases the risk of freezing out the argon discharge gas if not controlled carefully. The thermoelectric cooling device can also produce temperatures cold enough for use in the glow discharge source, but the device would have to be mounted outside the ion source in order to maintain the glow discharge vacuum integrity. As a result, numerous coolers would be required to obtain the desired amount of impurity removal from the plasma, making thermoelectric coolers impractical. Due to the availability and ease of use, the research reported here was carried out at temperatures obtained by using liquid cryogens.

Cryogenic Chemistry

In its broadest definition cryogenic chemistry is the combination of low temperatures and chemistry. For the analytical chemist, cryogenic chemistry might mean the use of cryogenic methods to cool samples for the purposes of

sharpening spectral lines, improving resolution, slowing exchange processes and investigating phase changes (119). Cryogenic chemistry might also be defined as the investigation of chemical species, reactions, or processes that would not occur or could not be studied except at low temperatures (119). For example, matrix isolation is used to trap reactive species in a solid noble gas matrix to study the unstable intermediates in chemical reactions.

The coupling of cryochemistry and mass spectrometry has been accomplished in many manners depending on the need of the analyst. For example, cryogenic trapping has been carried out to preconcentrate gaseous species on adsorbents or cold surfaces before analysis by MS or GC/MS (126, 127). Cryogenic desolvation has been used to reduce the water load nebulized from the aqueous sample solution into an inductively-coupled plasma mass spectrometer, reducing polyatomic interferences such as MO^+ and ArO^+ (128). Removal of water vapor by cryogenic cooling has also been employed on an ion trap mass spectrometer interfaced with an inductively coupled plasma to reduce the production of metal-polyoxide, -hydroxide, and -H_2O ions in the trap (129). In secondary ion mass spectrometry, cryogenic cooling of the sample has allowed the analysis of solid water (130), nitrogen (131), carbon monoxide (131), rare gases (132), and small hydrocarbons (133). Frozen aqueous solutions have also been analyzed using ion induced desorption and multiphoton resonance ionization coupled with time-of-flight mass spectrometry detection (134).

Some of the first low temperature mass spectrometric studies were performed to isolate and investigate reactive unstable species, typically reaction intermediates. The cryogenic experiments were carried out using two methods: (1) cooling the entire ionization chamber, or (2) cooling the sample external to the ionization chamber then introducing the products through a cooled inlet tube and into the ionizing beam (135). Blanchard and LeGoff studied the condensation and recombination of free radicals at low temperatures by cooling the walls of the ionization chamber with liquid nitrogen (136). McGee et al. constructed a separate cryogenic facility with a refrigerated delivery system that injects the cooled sample directly into the ionizing beam (135). The cryogenic facility consisted of a reactor chamber, temperature control system, and the mass spectrometer injection system, where the reactor chamber is completely immersed in the refrigerant. Several different reactor designs were used to create the reactive species including glow discharges, spark and electric arcs, exploding wires, and furnace pyrolyses (135).

Daughtrey and Harrison (137) introduced a liquid nitrogen cold finger into a glow discharge ion source in 1975, but cooling was inefficient due to unsatisfactory contact between the glass cold finger and the metal conductor (Figure 8). In 1983, Foss et al. reported using a cryogenic hollow-cathode ion source for the elemental analysis of 20 - 50 μL aliquots of aqueous solution samples (138). The sample was deposited onto the cathode, inserted into the source, and quickly cooled by the liquid nitrogen temperatures, freezing the

aqueous sample. The discharge was thn turned on and the ice was sputtered. While many elements were present as singly charged ions, the presence of water in the discharge also contributed to the formation of oxides, hydroxides, and water clusters. Commercial GDMS instruments also have provisions for cryogenic cooling of the source, utilizing a flow of liquid nitrogen through a cryocell block in contact with the source (Figure 9), resulting in the entire GD source being cooled (139). Using this cryocell GD source, Donohue and Petek (20) have shown that interfering gas-phase reactions can be eliminated. They demonstrated that the formation of palladium hydride was eliminated when the source was cooled. Cryogenic cooling also allows the glow discharge to be used for analyzing difficult elements that would otherwise melt under normal GD conditions (42).

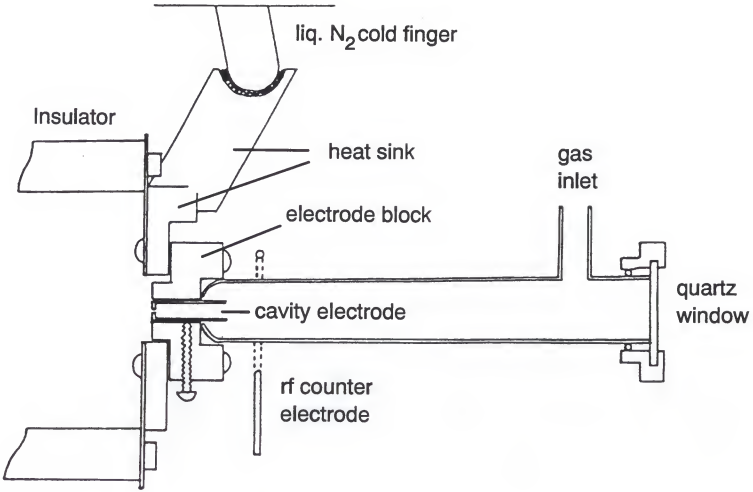

Figure 8. Schematic diagram of cryogenic cold finger ion source (137).

CHAPTER 3
INSTRUMENTATION

Mass Spectrometers

The research in this dissertation was performed on two separate quadrupole mass spectrometer systems. The first mass spectrometer is a laboratory-built quadrupole system, while the second is a commercial prototype built by the Finnigan MAT corporation (Figures 10 & 11). The mass spectrometers have been described in detail elsewhere (140-142); therefore, only a brief overview of the instruments will be given here.

The laboratory-built instrument was designed so that the ion source is external to the mass spectrometer and can be isolated from it by a gate valve. This system allows both optical and mass spectrometric measurements to be made simultaneously from the same glow discharge source, making it very useful for diagnostic investigations of the glow discharge. The mass spectrometer consists of four components: the Einzel lenses, Bessel box, quadrupole mass analyzer, and detector. The first component is the electrostatic lenses (Einzel lenses), which are used to transport the ions formed in the external source to the second component, the Bessel box. An exact description of the Einzel lenses can be found in reference 142. Only the ions near the exit orifice

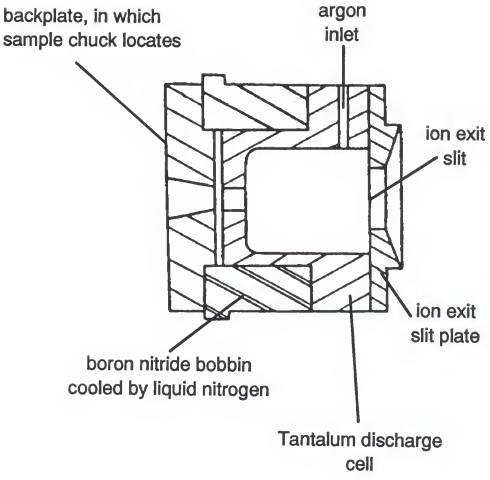

Figure 9. Glow discharge source with cryocooling system for the VG9000.

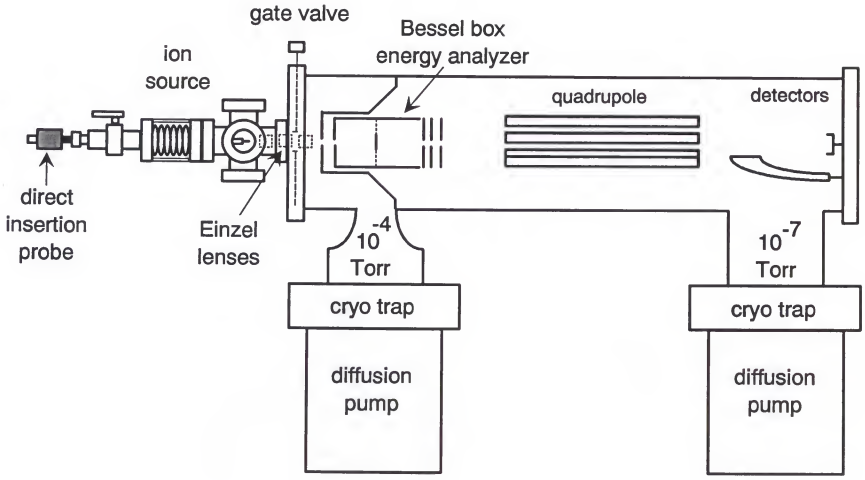

Figure 10. Schematic of the laboratory-built mass spectrometer system. Adapted from reference 140.

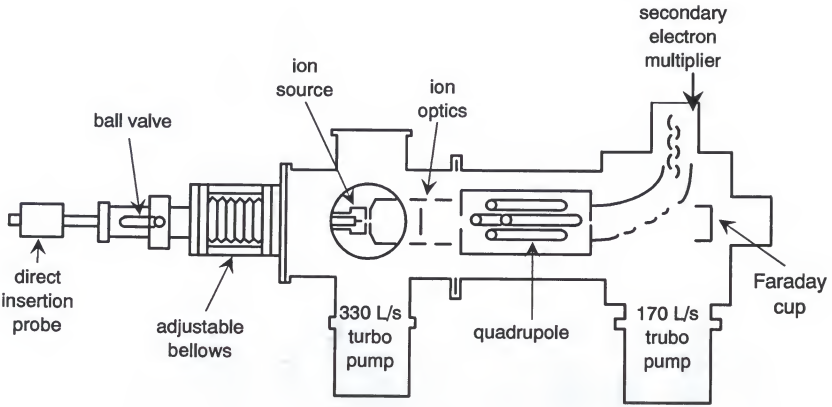

Figure 11. Schematic of commercial prototype mass spectrometer system (140).

opening are extracted by the Einzel lenses and transported to the Bessel box, which passes ions of a selected kinetic energy, without mass discrimination, to the quadrupole mass filter. The Bessel box consists of several lenses, one of which has a center beam stop that prevents photons, neutrals, and very high energy ions from entering the quadrupole. Only the ions of the correct energy bandpass will symmetrically traverse around the beam stop, then out of the box and to the mass analyzer. If the ion's energy is too low, the ion is reflected inside the box. If the ion's energy is too high, the ion has an unsymmetrical trajectory and does not pass out of the box. Once in the quadrupole mass analyzer, the ions are resolved based on their mass-to-charge ratio resulting in typical mass resolutions of $\leq$ 1 amu. The mass resolving ability of the quadrupole results from an ion's stability or instability within the electric field produced from the rf and dc potentials applied to the four parallel rods symmetrically arranged. For a detailed explanation of quadrupole mass analyzer theory see references 143, 144. The mass resolved ions are then detected by either a Faraday plate or an electron multiplier.

The major difference between the Finnigan mass spectrometer and the laboratory-built model is that the glow discharge ion source is located within the high vacuum chamber of the Finnigan mass spectrometer system. As a result, the ion source cannot be isolated from the mass spectrometer and optical measurements are not feasible. One advantage of this system is that the ions formed in the source are transported directly to the Bessel box, resulting in less

ion loss due to transport and therefore to lower detection limits. The Finnigan mass spectrometer has detection limits in the low ppb range while the laboratory-built mass spectrometer has detection limits in the sub ppm range. Deciding which mass spectrometer to use for an experiment will depend upon the capabilities of the system one wishes to exploit. If simultaneous optical measurements are desired, the laboratory-built system is used. In addition, the laboratory-built mass spectrometer is used to test any new instrumental designs or sources being investigated. Investigations into fundamental ion plasma processes or studies requiring quantitative results are usually done on the Finnigan instrument.

Glow Discharge Ion Source

There are many glow discharge source configurations including the co-axial cathode, planar diode, Grimm-type, hollow cathode plume, and hollow cathode glow discharges. Both mass spectrometer systems employ co-axial type glow discharge ion sources, thus allowing the use of direct insertion probes that result in faster and easier sample exchange. In this configuration, the cathode is the sample, which is affixed on the end of the direct insertion probe, and the anode is the source chamber walls.

The glow discharge can be operated using either dc or rf power supplies. When a dc power supply is used, the sample must be electrically conducting such as a metal alloy. If the sample is a nonconducting powder, it can be mixed with

a conducting powder and pressed into a suitable cathode shape. The instrumental setup for a dc glow discharge is simple, and includes a high voltage power supply [Kepco, Flushing, NY, Model OPS 3500] (capable of producing up to 3000V and 10mA), direct insertion probe, and glow discharge chamber (Figure 12A). The dc direct insertion probe consists of an electrical feedthrough welded to 1/2 in. stainless steel tubing (Figure 13A). A copper sample holder that fits on the end of the feedthrough is used to hold the cathode sample in place. A nonconducting machineable ceramic [Macor, Corning Glass Works, Corning, NY] shield is placed over the copper holder to isolate the glow discharge plasma to the sample surface. The gap between the shield and the sample cathode must be no larger than the dark space length or a discharge will form behind the shield.

The use of rf power is more complicated and difficult than dc, but allows both conducting and nonconducting samples to be sputtered directly in the glow discharge. The major difference between a rf and a dc discharge is that the rf discharge is oscillating between a positive and negative voltage while the dc has a steady negative voltage. A nonconducting sample in a rf discharge behaves like a capacitor as the sample surface alternates between negative and positive potentials. When a high negative voltage is applied to the nonconducting sample, the cathode potential drops to a negative value and decays with time to a more positive potential as the bombarding ions neutralize the cathode surface (145). When the oscillating voltage goes positive, the cathode surface develops a positive charge, and electrons are attracted to the surface neutralizing it. As the

frequency of the ac is increased, the cathode surface develops a negative charge called the dc bias. This bias results because of the differences in mobilities between the ions and electrons. The faster electrons can neutralize the surface before the potential polarity is switched again while the positive ions cannot. After several cycles, the negative charge build-up reaches a constant negative dc offset (Figure 14). While the cathode is bombarded by both ions and electrons, a continuous dc discharge is formed with an ac potential superimposed on it.

The rf glow discharge system consists of a rf power supply, matching network, direct insertion probe, and the glow discharge chamber (Figure 12B). The power supply [RF Power Products, Marlton, NJ, Model RF5] can produce up to 500 watts of rf power at a frequency of 13.56 MHz. (The Federal Communications Commission has set aside 13.56 MHz as the operating frequency for sputtering systems.) The rf generator is designed to terminate into a 50 ohm impedance; therefore, a matching network [RF Power Products, Marlton, NJ, Model AM-5] simulating a 50 ohm impedance is placed between the rf power supply and the glow discharge. By adjusting the capacitance of the matching network, it is possible to maximize the forward power while minimizing the reflected power. The direct insertion probe is then connected to the matching network by a coaxially shielded cable. The distance between the matching network and the discharge is kept to a minimum ($\langle$1 m) to reduce any power losses. Due to the heat produced by the rf circuit, the direct insertion probe also had to be modified (Figure 13B). The most common type of probe failure results

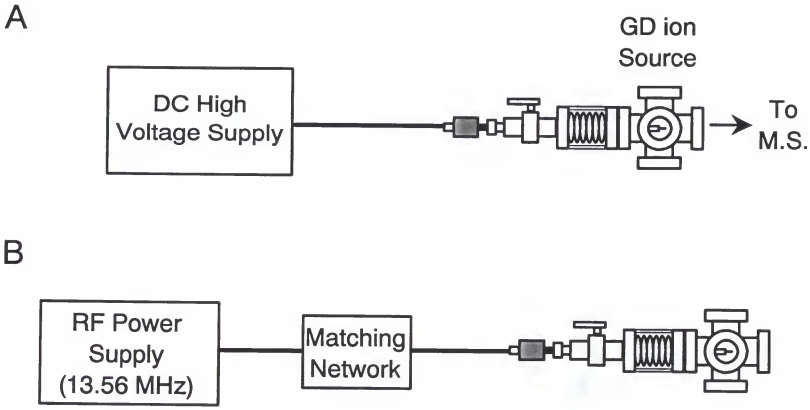

Figure 12. A) Schematic of dc glow discharge instrumentation. B) Schematic of rf glow discharge instrumentation.

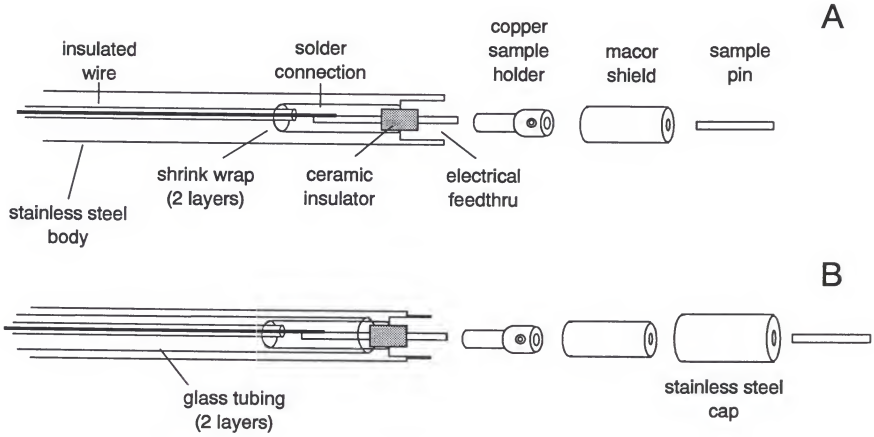

Figure 13. A) Direct insertion probe for a dc glow discharge. B) Direct insertion probe for an rf glow discharge.

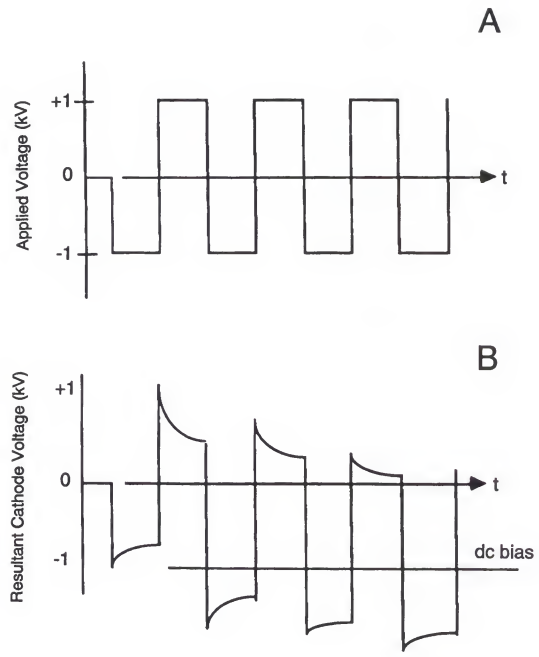

Figure 14. A) Applied square wave voltage. B) Resultant cathode potential (83).

from the heat burning away the insulation surrounding the electrical wire and contacts which then short to the grounded probe body. The first modification involved improving the electrical insulation of the probe's electrical contacts. This was accomplished by insulating the wire and solder connection inside the probe with two layers of glass tubing. The second modification was the addition of a grounded metal cap to cover the ceramic shield. Since the rf can travel through both conducting and nonconducting materials, it will attempt to follow the path of least resistance, which is not necessarily the sample. As a result, sputtering of the ceramic shield and sample holder can occur, making it imperative that all surfaces surrounding (but not touching) the sample be at ground potential in order to force the rf power through the sample. One of the major difficulties with the rf system is the development of a discharge on the conducting sample holder when analyzing a nonconducting sample. The slightest gap between the sample and grounded metal shield will result in the sputtering of the sample holder (path of least resistance); therefore, the gap must be smaller than the cathode dark space or else a discharge will develop behind the shield.

Cryogenic Cooling Coil

A cryogenic cooling coil has been developed whose cold surface acts as a cryopump for all the condensible vapors (gaseous impurities) in the glow discharge chamber. The glow discharge ion source for the laboratory-built mass spectrometer, constructed from a six-way cross with 2.75 in. flanges, was modified

by the insertion of a cryogenic cooling coil as illustrated in Figure 15. The coil is made of 1/8 in. stainless steel tubing welded to a double-sided 2.75 in. flange allowing the coil to be on axis with the direct insertion probe (Figure 16). The bellows assembly allows the distance between the coil and the exit orifice of the mass spectrometer to be adjusted from 0 to 2 cm. For the Finnigan mass spectrometer, the coil is introduced through a side port into the glow discharge source such that the coil is at right angles to the direct insertion probe (Figures 17 & 18). Due to the smaller size of the glow discharge ion source, the coil is in a fixed position and cannot be moved.

Liquid nitrogen is introduced into the top of the flange from an 80 L self-pressuring dewar [Cryofab Inc., Kenilworth, NJ] with the flow controlled by a stainless steel bellows regulating valve [Nupro, Willoughby, OH]. To minimize losses in cooling capacity, the liquid N_2 transfer line, cryogenic coil flange, and surrounding flanges are insulated with CMHC No. 10892 pipe insulation [Industrial Thermo Polymers Ltd., Mississauga, ON, Canada]. The flow of gaseous N_2 is monitored downstream from the cryogenic coil using a rotameter [Dwyer Instruments, Michigan City, IN]. Pressure relief valves [Whitey, Highland Hts., OH] are also installed between the dewar and regulating valve and between the coil and flowmeter. For the laboratory-built mass spectrometer, heating tape is wrapped around the bellows assembly and gently warmed during cryogenic operations, otherwise after several hours of cooling a leak develops in the bellows assembly. For simpler operation, the pressurized dewar can be replaced by a

small insulated reservoir mounted on top of the flange, allowing the liquid N_2 to flow unregulated through the coil by gravity. The efficiency of cooling with this gravity delivery system depends on keeping the reservoir full of liquid N_2. When the liquid N_2 level drops too low, the cooling ability of the coil drops and the gaseous impurities are desorbed from the coil surface.

Cryogenic fluids are usually at or near their boiling point. Heat is always being absorbed from the surroundings to the colder coil, resulting in the additional boiling of the liquid N_2 in the coil and piping. This produces a two-phase mixture of vapor and liquid. This mixture has poor flow properties and severe pressure oscillations which may result in the cessation of flow (115). One way to prevent the development of a two-phase mixture in the pipes, is to use a pressurized flow of the liquid cryogen (115). For consistent, long-term use, the self-pressurized dewar is the recommended liquid N_2 introduction method, and is the method used throughout this research.

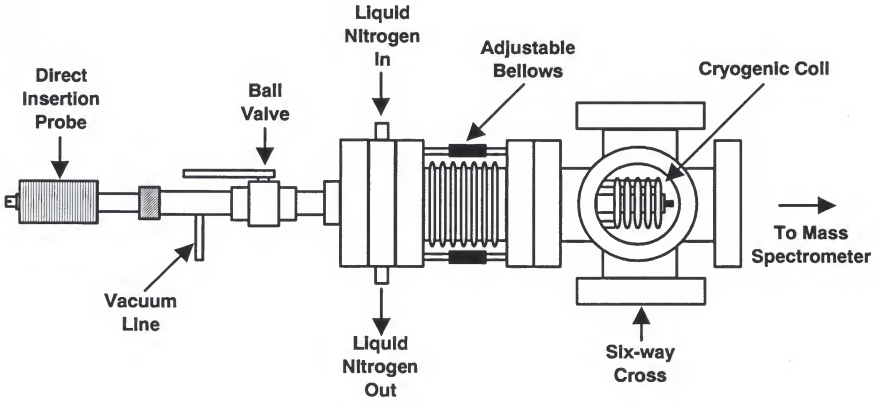

Figure 15. Schematic diagram of the cryogenic coil coupled to the glow discharge ion source on the laboratory-built mass spectrometer.

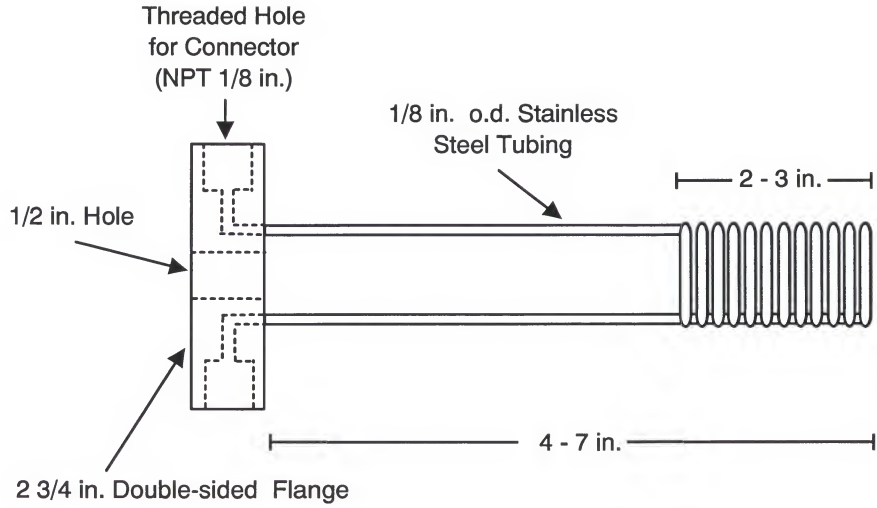

Figure 16. Schematic diagram of the coil flange for the laboratory-built mass spectrometer.

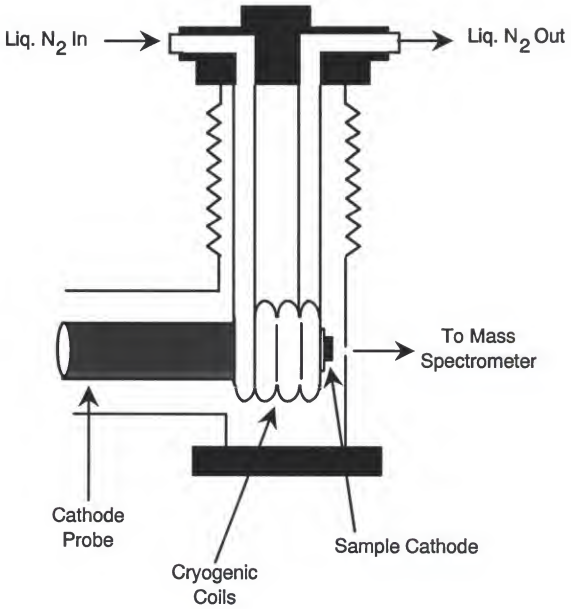

Figure 17. Schematic diagram of the cryogenic coil for the glow discharge ion source on the Finnigan mass spectrometer.

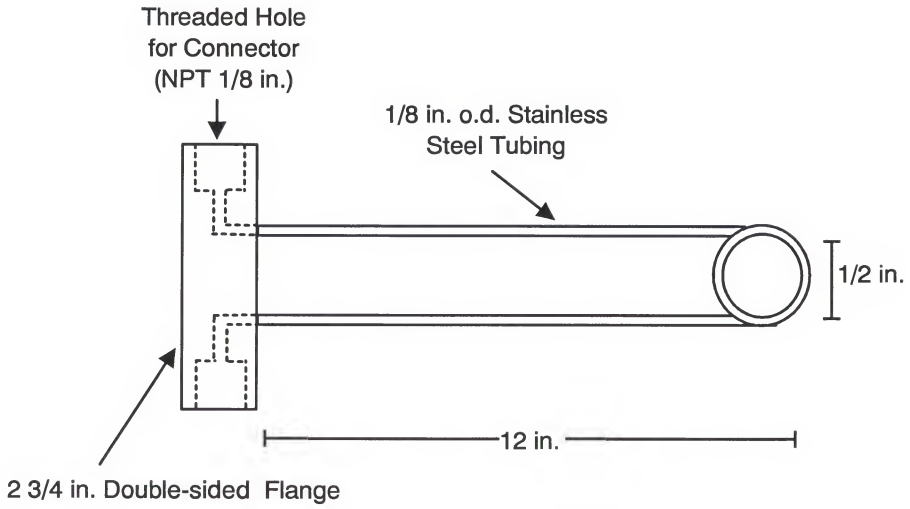

Figure 18. Schematic diagram of the coil flange for the Finnigan mass spectrometer.

CHAPTER 4
CHARACTERIZATION OF THE CRYOGENICALLY COOLED GLOW DISCHARGE

Even under the best experimental precautions, gaseous impurities are still commonly present in the GD chamber. The cryogenic coil was designed to reduce further certain gaseous impurities such as water vapor, carbon dioxide, and hydrocarbons. This chapter will demonstrate qualitatively the effectiveness of the cryogenic cooling for GDMS analyses and to characterize glow discharge operating trends with and without cooling.

Experimental

Both mass spectrometer systems, as described in chapter 3, were used to characterize the effect of cryogenic cooling on the gaseous impurity and analyte ion signals. Ultra-high-purity grade argon (Liquid Air Corp., San Francisco, CA) was used in all experiments with an operating pressure of approximately 1 Torr. Analytical samples were prepared from aluminum alloy (National Institute of Standards and Technology, standard reference material #1241b), low alloy steel (NIST SRM #1265), zinc alloy (NIST SRM #627), copper wire (Johnson Matthey Chem. Ltd., Royston, England, 99.999% pure (metals basis)), and iron wire (Johnson Matthey Chem. Ltd., Ward Hill, MA, 99.9985% pure (metals basis)). The NIST samples were machined into 2 mm pins from a bulk disk, while the copper

was purchased as a 2 mm diameter wire. Approximately 5 mm of the sample pins were exposed to the discharge for sputtering. The sample pin was approximately 9 mm from the ion exit orifice of the mass spectrometer. For the laboratory-built system, the cryogenic coil was positioned 5-7 mm from the ion exit orifice so that the coil surrounded the sample pin without touching it or the probe. The cryogenic coil in the Finnigan GDMS system is in a fixed position approximately 1 cm from the ion exit orifice. All experiments were performed using a dc glow discharge, either in the constant voltage or constant current mode.

Removal of GDMS Mass Spectral Interferences

Water Vapor Impurities

To demonstrate the effectiveness of cryogenic cooling, an aluminum alloy was chosen as the sample cathode, since the greatest interferences from water and other impurities occur in the m/z range between 10 - 40, potentially obscuring analyte ion signals. Figure 19 is the mass spectrum of the aluminum alloy after sputter cleaning the cathode for 30 minutes at a discharge current of 3.6 mA. The major species in the spectrum are H_3^+ and ArH^+; both are a result of residual water vapor. H_3^+ can arise from the dissociation products of water within the plasma (96) or adsorbed on the source walls (146). ArH^+ can be produced from the argon ion reacting with water or hydrogen molecules (3, 147). The peaks at m/z of 14, 28, 29 are a result of air contamination in the GD source, while the

peak at 12 is probably due to contamination from backstreaming of the GD source roughing pump.

Upon turning on the liquid nitrogen flow through the coil, reduction in gaseous impurities begins almost immediately. After approximately five minutes of liquid nitrogen flow, the water species are no longer detected. After 15 minutes the H_3^+ and the ArH^+had been essentially removed. Typically it requires about 20 minutes of cryogenic cooling to "clean up" the glow discharge to a level satisfactory for trace analysis. The glow discharge, operated at constant voltage, showed an increase in discharge current upon elimination of the gaseous impurities, indicating a drop in plasma resistance. This could be explained by removal of quenching agents in the discharge and by changes in surface oxidation of the cathode.

A mass spectrum of the aluminum sample taken after 30 minutes of cooling with liquid nitrogen is shown in Figure 20. The cryogenic cooling removes or reduces many of the gaseous impurities. A comparison of the ion signal ratios with and without cooling is listed in Table IV. Nitrogen impurities are not removed, of course, but these can be reduced by careful attention to the vacuum integrity. H_3^+, N_2H^+, and ArH^+ signals drop sharply as the source of their protonation reactions (H_2O) is removed. Other argon containing species such as metal-Ar^+, Ar^{2+}, and Ar_2^+ were not greatly affected by the cryogenic cooling. There is also an increase in the analyte ion signals (Mg, Al) upon cooling. The behavior of the analyte ion signals upon the removal of water vapor depends partly on their

reactivity toward atomic oxygen (a by-product of water dissociation in the glow discharge). Tantalum, which forms a strong metal-oxide bond, has a higher reactivity toward oxygen than does iron and copper, which exhibit lower bond strengths. The magnitude of increase in the analyte ion signal depends upon the reactivity of that element with residual water vapor (148).

When the liquid nitrogen flow is turned off, the gaseous impurities desorb quite rapidly (approx. 3 min.) from the coil, producing once again a mass spectrum resembling Figure 19. Therefore, to maintain the suppression of the impurity ion signals, a constant flow of liquid nitrogen is required. By controlling the flow rate of the liquid, an optimum degree of cooling can be reached. In our GD source we have incorporated a ball valve to allow for easy sample exchange when the cryogenic cooling is in use. Because the direct insertion probe becomes very cold upon cryo-cooling, when the probe is removed for sample exchange, water from the atmosphere immediately condenses on the sample and probe assembly. It is convenient to have available a second direct insertion probe to reduce additional introduction of water and to allow quick sample turnover. This alternate clean, dry probe is inserted into the GD source with the new sample, while the first probe is dried and prepared for the next analysis.

Next, the cryogenic coil was evaluated for its ability to eliminate unwanted gas-phase reactions. Zinc is a difficult sample to analyze by GDMS. The discharge currents required to obtain useful analyte ion intensities usually result in the melting of the zinc pin. Therefore, the sample must be operated at low

currents and voltages where the gaseous impurities dominate. In other words, the operating current and voltage are too low for sputter cleaning of the GD source. Shown in Figure 21 is a mass spectrum of a zinc pin without cooling after 30 min of presputtering. The zinc isotope fingerprint is not correct due to the formation of zinc hydride dimers appearing at m/z 65, 67, 68, and 69. The zinc readily reacts with the hydrogen present in the plasma due to the dissociation of the water vapor. The argon hydride is the predominant argon species while spectral interferences due to the formation of CO_2^+, CO_2H^+, and ArN^+ are also present. After cooling for only 20 min, the zinc hydrides are eliminated (Figure 22). Therefore, as expected, the cryogenic cooling eliminates gas-phase reactions involving condensible gaseous impurities. The ion signals due to CO_2^+ and CO_2H^+ are also eliminated while the ArH^+ is dramatically reduced. The ArN^+ dimer appears not to be affected by cryogenic cooling.

Using a double focusing sector GDMS instrument, Donohue and Peteck measured the isotopic abundances of palladium with and without liquid nitrogen cooling (61). Without cooling, PdH^+ was detected at m/z 107, 109, and 111. Using the cooled glow discharge source, the hydride interferences were eliminated and the isotope ratios were measured with precisions better than 0.1% RSD. Therefore, cryogenic cooling is essential for quantitative analysis of elements that will readily react with the by-products of water dissociation.

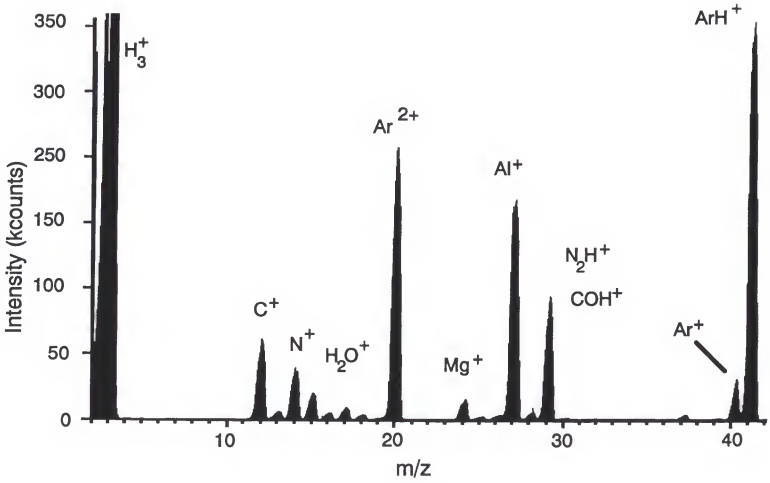

Figure 19. Glow discharge mass spectrum of NIST SRM 1241b aluminum alloy without cryogenic cooling. Spectrum taken after a presputter time of 30 min. Discharge voltage: 1000 V, discharge current: 3.6 mA.

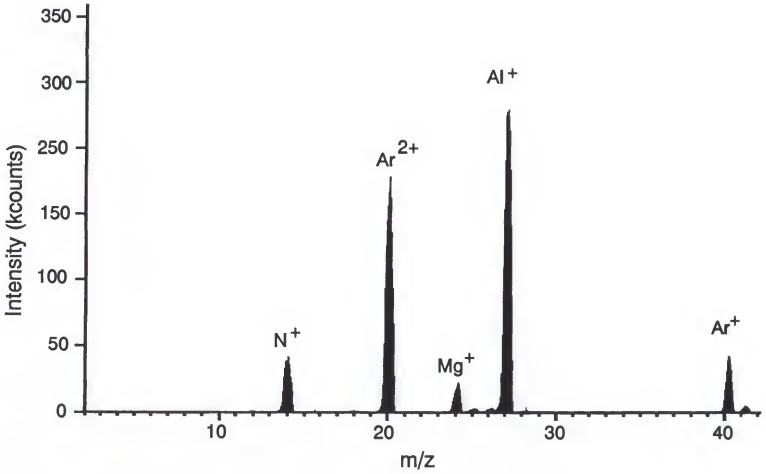

Figure 20. Glow discharge mass spectrum of NIST SRM 1241b aluminum alloy with cryogenic cooling. Spectrum taken 30 min after turning on liquid nitrogen flow through the coil. Discharge voltage: 1000 V, discharge current of 6.2 mA.

Table IV. Comparison of Ion Signal Ratios for Aluminum Alloy NIST SRM# 1241b with and without Cryogenic Cooling.

		(ion peak area)/($^{27}Al^+$ peak area)*		
m/z	ion	without cooling	with cooling	difference (%)
3	H_3^+	4.06×10^{0}	1.99×10^{-4}	-99.995
12	C^+	3.30×10^{-1}	2.21×10^{-3}	-99.3
14	N^+	2.14×10^{-1}	1.79×10^{-1}	-16.4
18	H_2O^+	2.02×10^{-2}	3.46×10^{-3}	-82.9
24	Mg^+	7.96×10^{-2}	8.45×10^{-2}	6.2
29	COH^+, N_2H^+	4.86×10^{-1}	8.65×10^{-4}	-99.8
40	Ar^+	1.35×10^{-1}	1.57×10^{-1}	16.3
41	ArH^+	1.70×10^{0}	1.69×10^{-2}	-99.0

* $^{27}Al^+$ peak area without cooling = 1,180,627 counts, with cooling = 1,365,212 counts

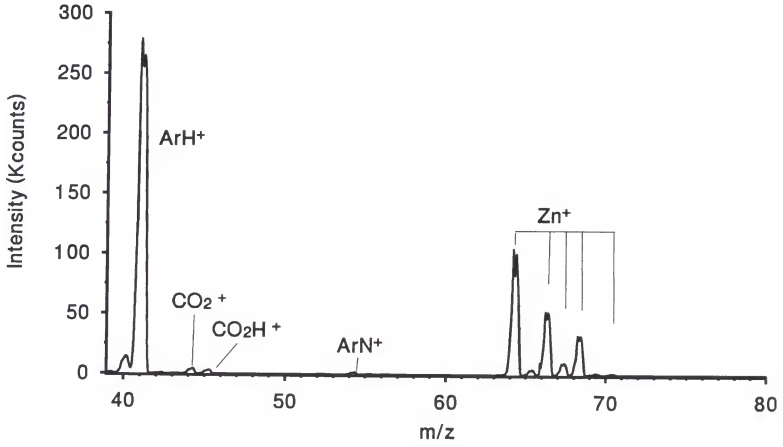

Figure 21. Glow discharge mass spectrum of NIST SRM 627 zinc alloy without cryogenic cooling. Spectrum was taken after a presputter time of 30 min. Discharge voltage: 800 V, discharge current: 2.7 mA.

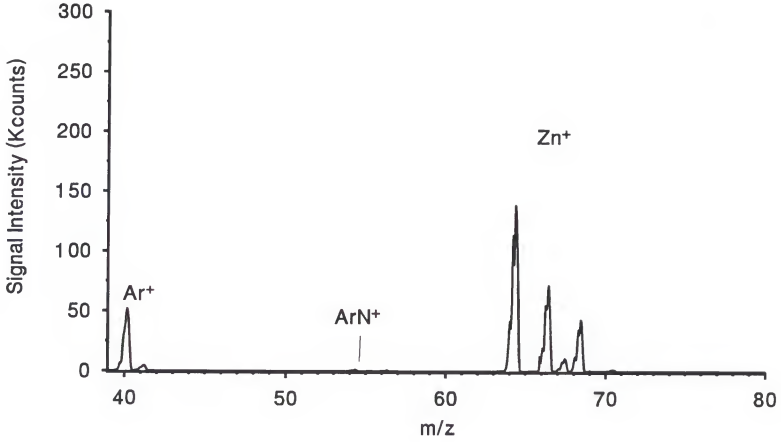

Figure 22. Glow discharge mass spectrum of NIST SRM 627 zinc alloy with cryogenic cooling. Spectrum was taken after 20 min after turning on the liquid nitrogen flow through the coil. Discharge voltage: 800 V, discharge current: 3.6 mA.

Hydrocarbon Impurities

Another prominent gaseous impurity in the GD is oil vapor, which is introduced by the backstreaming of the rotary pumps required for differential pumping of the MS system. The oil vapors present in a vacuum vessel can be cracked when bombarded by the electrons, atoms and ions in the glow discharge, causing carbon to deposit on the cathode and ion source surface (149). This deposition can inhibit the sputtering rate of the cathode since carbon is sputtered at a lower rate (150). Therefore, the ability of cryogenic cooling to remove oil vapors was investigated.

A standard oil sample (Constan Base Oil 75, Conoco, Inc., Ponca City, OK) was introduced into the glow discharge chamber through a needle valve. While the discharge was off, the oil was gently warmed contaminating the GD chamber. The oil introduction was stopped, and the removal of the oil vapor impurities with and without cooling was monitored. Once the oil introduction was stopped, the glow discharge was turned on. In the case of cryogenic cooling, the liquid nitrogen flow was started simultaneously with the discharge. The C^+ ion signal intensities were plotted as a function of sputtering time with and without cooling (Figure 23). The glow discharge is very efficient at cracking the hydrocarbon compounds, resulting in C^+ and H_3^+ as the major impurity ion species. For the noncooled plasma, the C^+ signal actually increases for the first 20 min., probably due to the dissociation of the hydrocarbons in the plasma, then starts to decrease. After an hour of sputtering, the C^+ signal is decreased by 50%. For the H_3^+ ion

intensity, an initial increase was also observed before the signal decreased about 25%. With cryogenic cooling, both impurities are removed approximately 30 min after turning on the liquid nitrogen flow. Even under the extreme conditions of oil vapor introduction, the cryogenic cooling coil can effectively clean the plasma of the hydrocarbon impurities.

The typical spectral interferences present in a GDMS mass spectrum and the ability of cryogenic cooling to remove them are summarized in Table V. Interferences that result from the by-products of water and hydrocarbon dissociation can be removed by cooling at liquid nitrogen temperatures. In general, any interferences composed from impurities that are condensible at liquid nitrogen temperature should be removed upon cooling. Polyatomic species containing any combination of the discharge gas (Ar), nitrogen, and sputtered species will not be eliminated or reduced by cooling. The nitrogen impurities can be eliminated by maintaining high vacuum conditions since the nitrogen is usually introduced by atmospheric leaks in the system.

Cryogenic Cooling Time Profile

As previously mentioned, cryogenic cooling is capable of removing the gaseous impurities rapidly (20 - 30 min). A typical time profile for the removal of impurities from the plasma is illustrated in Figure 24. Under normal operating conditions without cooling, the plasma is allowed to sputter for 10-15 min before starting any mass spectral analyses to sputter clean and stabilize the glow discharge. In this plot, the glow discharge is allowed to stabilize without cooling

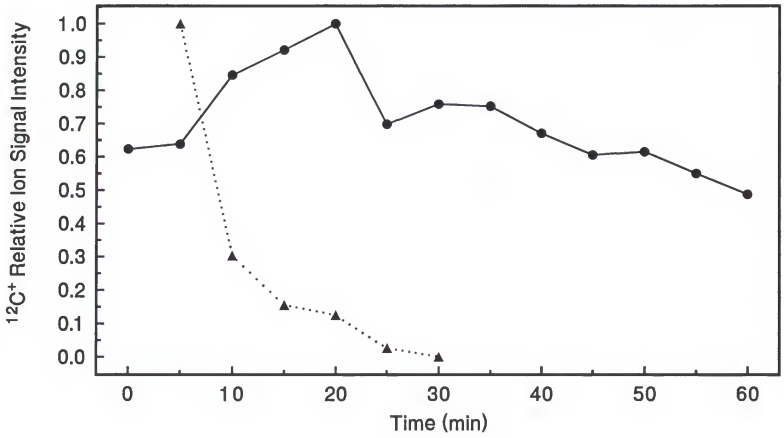

Figure 23. Comparison of with and without cryogenic cooling for the removal $^{12}C^+$ due to the introduction of oil vapor into the glow discharge source. Sample cathode: NIST SRM #1265, discharge current: 5.0 mA. ● - without cooling, ▲ - with cooling.

Table V. Typical spectral interferences present in a GDMS mass spectrum.

m/z	Possible Contributing Ion(s)	Removal by cryogenic cooling
1	H	yes
2	H_2	yes
3	H_3	yes
12	C	yes
13	C	yes
14	N	no
16	O, NH_2	yes
17	OH, NH_3	yes
18	H_2O, NH_4	yes
19	H_2O	yes
20	Ar^{+2}	no
27	CNH	yes
28	CO	yes
28	N_2^+	no
29	COH, N_2H	yes
30	NO	yes
37, 39, 41	ArH	yes
42	CNO	yes
43	CNOH	yes
44	CO_2	yes
45	CO_2H	yes
	MH	yes
	MO	yes
	MN	no
	MAr	no

M = sputtered analyte species

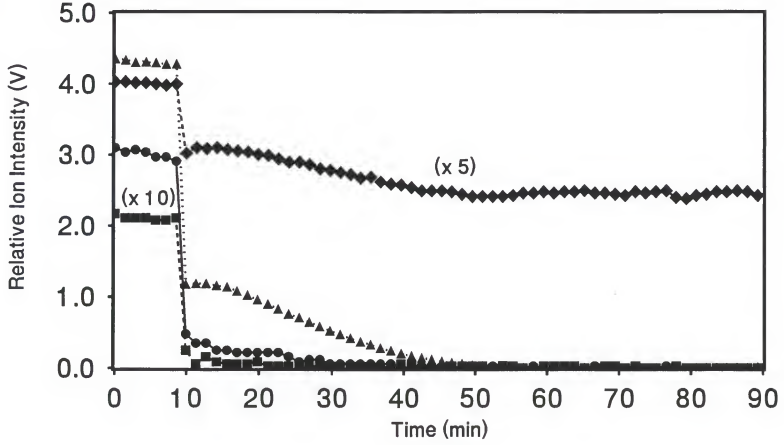

Figure 24. The effect of cryogenic cooling versus time on the gaseous impurity and analyte ion signals. Cathode material: NIST SRM #1265, constant discharge voltage: 1100 V. ◆ - $^{54}Fe^+$, ■ - H_2O^+, ● - H_3^+, ▲ - m/z = 29 (COH^+, N_2H^+).

for the first 10 minutes. At 10 min, the liquid nitrogen flow is turned on. An immediate drop in the impurity ion signals, as illustrated by m/z 3, 18, and 29, is observed. After approximately 30 minutes, the impurity signals are undetectable. The effect of cooling on the analyte ion signal, $^{54}Fe^{+}$, is also shown. In this case, the analyte ion signal decreases with cooling. The noncooled glow discharge plasma is irreproducible, and depending upon the magnitude of the gaseous impurities in the GD source the analyte ion signal will either increase or decrease upon cooling. In general, it has been observed that if a large amount of water vapor is present, the analyte ion signals increase upon cooling. If the gaseous impurities are present in trace amounts, the analyte ion signals will decrease upon cooling. After the gaseous impurities were eliminated or reduced (ca. 40 min), the analyte ion signal was very stable having a RSD of 2% over approximately 50 min. Hutton and Raith found, using a precooled glow discharge cell, that the gaseous contaminants were removed or reduced and the ion signals stabilized within 5 - 10 min of presputtering (47).

Effect of Liquid Nitrogen Flow Rate

One way of controlling the temperature of the cryogenic coil is by the flow rate of the liquid nitrogen through the coil. Hence, the effect of the flow rate of liquid nitrogen through the coil on the analyte and gaseous impurity ion intensities was investigated. The flow rate of the liquid nitrogen was not measured, but was monitored by measuring the nitrogen gas exhaust from the cooling system.

The effect of $N_2(l)$ flow rate on the gaseous impurities is shown in Figure 25. At low flow rates (2 lpm), H_3^+ and H_2O^+ were efficiently removed. Higher flow rates were required to remove completely the impurities at m/z 17 and 29 (6 and 13 lpm respectively). By controlling the $N_2(l)$ flow rate, it is possible to selectively eliminate impurities, and investigate the effect of the different impurities on plasma chemistry. The effect of $N_2(l)$ flow rate on the analyte ion intensity was also examined. At low flow rates (2-6 lpm), the $^{54}Fe^+$ ion signal drop slightly (Figure 26). As the flow rate continued to increase (>6 lpm), a larger decrease in ion signal was observed. Similar behavior was observed for the $^{40}Ar^+$ ion signal. At low flow rates, the signal intensity increased, but started to decrease at even higher flow rates. If the decrease in analyte ion signal is a crucial concern, a compromise in $N_2(l)$ flow rate can be achieved that removes most gaseous impurities without detrimentally affecting the analyte signal.

Glow Discharge Operating Parameters

The intensity of the analyte ion signals depends on the operating parameters of the glow discharge plasma. The most important parameters include the discharge operating current, voltage, and pressure and the distance between the sample cathode and the mass spectrometer exit orifice. These parameters are usually optimized to give the largest analyte ion signal. Therefore, the effect of cryogenic cooling on these operating conditions was investigated.

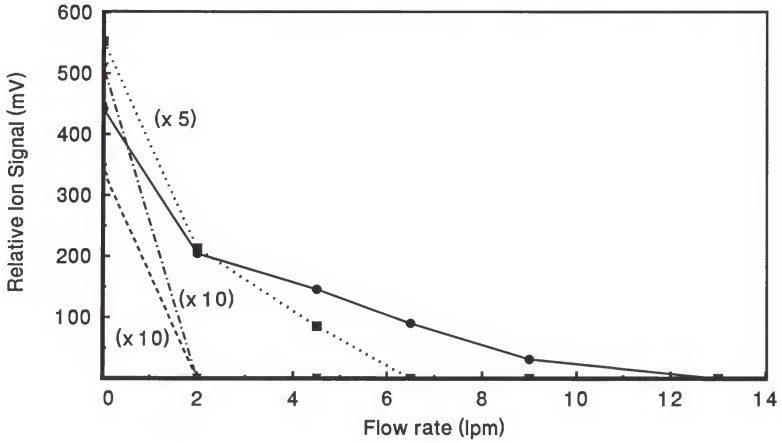

Figure 25. The effect of liquid nitrogen flow rate on the removal of gaseous impurity species from the glow discharge plasma. Cathode material: NIST SRM #1265, constant voltage: 1100 V. ● - m/z = 29 (N_2H^+, COH^+), ■ - m/z = 17 (OH^+, NH_3^+), ▲ - H_2O^+, ▼ - H_3^+.

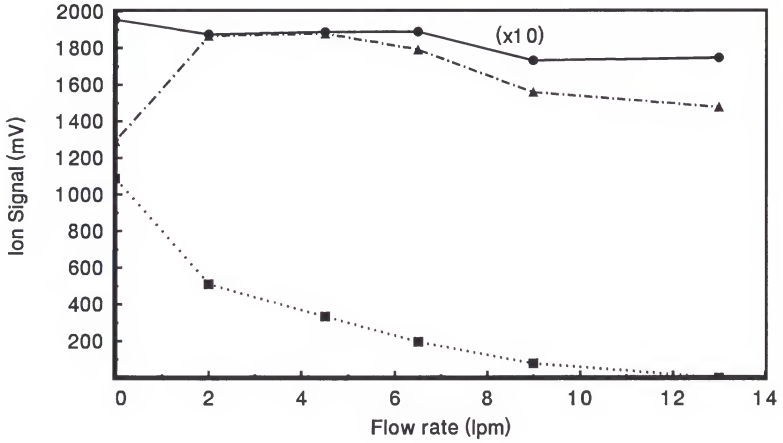

Figure 26. The effect of liquid nitrogen flow rate on the analyte ion signal intensities. Cathode material: NIST SRM #1265, constant voltage: 1100V. ● - $^{54}Fe^{+}$, ▲ - Ar^{+}, ■ - ArH^{+}.

Effect of Discharge Operating Parameters

The formation of ions or atoms can be favored in the glow discharge plasma by varying the discharge operating current, voltage, and pressure. Typically, the optimum operating conditions for the formation of atomic neutral species are at high pressures (2-10 Torr) and currents (20-50 mA) and low voltages (100-500 V). The formation of ionic species is favored at low pressures (0.1- 2 Torr) and currents (2-10 mA) and high voltages (1000-2000 V).

First, the effect of varying the discharge current, with and without cooling, on the ion signal intensities was investigated. The $^{56}Fe^{+}$ ion signal was plotted versus increasing discharge current (Figure 27). The maximum analyte ion signal at each individual operating condition was obtained by optimizing the ion lenses on the mass spectrometer. For both the cooled and noncooled glow discharge plasmas, the ion signal increased with increasing current. The noncooled plasma had larger ion intensities than the cooled except at low currents. A similar effect was observed when the discharge voltage was varied. The ion intensity increased with increasing voltage, and the cooled plasma had lower intensities than the noncooled. It is possible to operate at higher currents or voltages to compensate for the lower ion signals that can result from cooling.

The discharge current and voltage can be increased to a point where the sample starts to overheat, becoming red hot and melting. Therefore, the current and voltage are kept at a value low enough to avoid overheating of the sample. The operating conditions that cause overheating of an iron cathode sample were

investigated with and without cooling. The discharge voltage was continually increased until the cathode either melted or became red hot. For the iron cathode, there was no significant difference in the voltage required to overheat the cathodes (ca. 1750V and 10 mA). The cryogenic coil is not in direct contact with the sample cathode, and the sample does not appear to be cooled although the direct insertion probe does become very cold.

The effect of varying the discharge pressure at constant voltage with and without cooling is shown in Figure 28. In both cases, the optimum discharge pressure is approximately 0.8 Torr argon, and the ion intensities from the cooled plasma are larger than the noncooled plasma. An increase in ion intensities was observed upon cooling during this study because the noncooled glow discharge source was "wet" (i.e., the rigorous procedures for removing all gaseous impurities were not undertaken). In summary, the operating parameters of the glow discharge (current, voltage, and pressure) appear to behave similarly for both the cooled and noncooled plasmas.

Effect of Sampling Distance

Since only the ions directly in front of the exit orifice are extracted into the mass spectrometer, the cathode position is optimized to give the largest ion signal. As shown in Chapter 1, Figure 3, the glow discharge consists of several different luminous zones of varying energy content. The optimum sampling position usually corresponds to the interface region of the negative glow and Faraday dark space. The optimum distance will change with pressure since

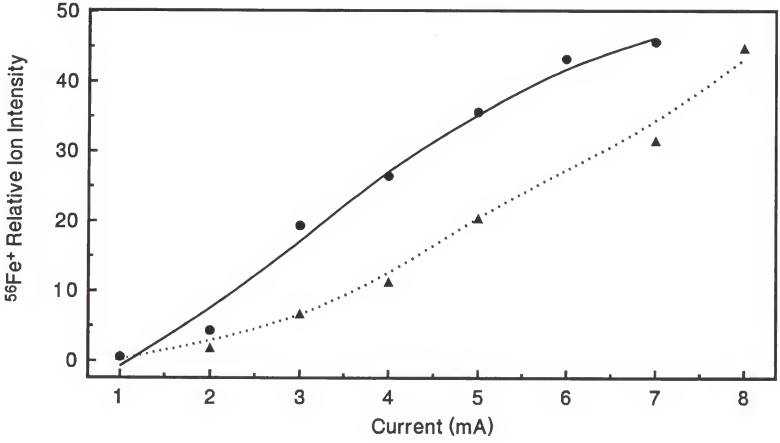

Figure 27. The effect of varying the glow discharge current on the $^{56}Fe^{+}$ ion signal intensity. Cathode material: iron wire. ● - without cooling, ▲ - with cooling.

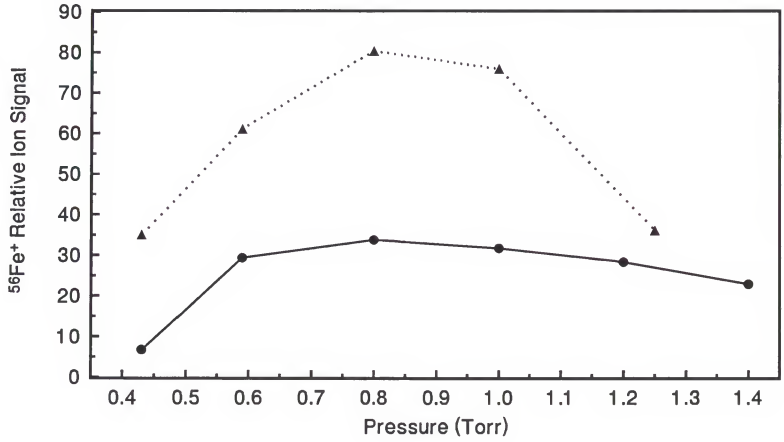

Figure 28. The effect of varying discharge pressure on the $^{56}Fe^{+}$ ion signal intensity. Cathode material: iron wire, constant voltage: 1000 V. ● - without cooling, ▲ - with cooling.

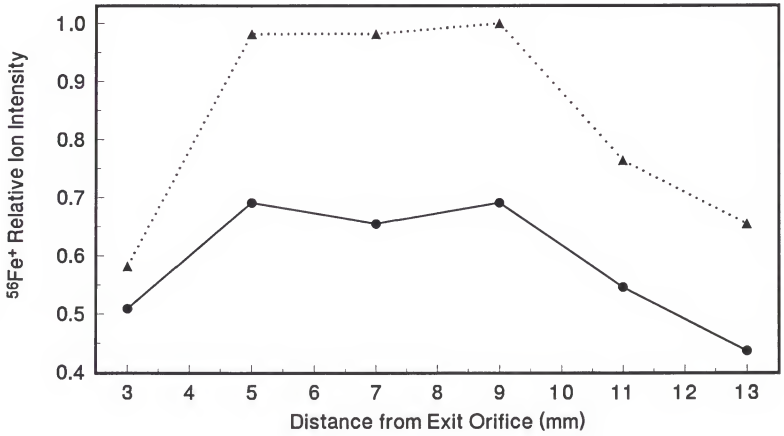

Figure 29. The effect of sample cathode to ion exit orifice distance of the GD ion signal intensity. ● - without cooling, ▲ - with cooling.

the length of some GD zones change with pressure. No difference was found for the optimum sampling distance for the plasma with and without cooling (Figure 29). This is a good indication that cooling is not changing the pressure in the glow discharge source. No pressure changes are observed in GD source pressure upon cooling as monitored by the pressure gauge (Teledyne Hastings-Raydist, Hasting, VA, Thermocouple gauge DV-4D, 0 - 20 mm Hg). If the amount of gaseous impurities was very large or if the argon discharge gas was being condensed, a change in GD pressure would result and the optimum sampling position would change.

Glow Discharge Characteristic Features

It is easy to understand the reason for the increase in ion signal intensity upon cooling. Upon the removal of the gaseous impurities, there could be more efficient sputtering of the sample as well as increased excitation and ionization of the sputtered analyte as discussed in chapter 1. The reason for the analyte ion intensity decrease is not so apparent. Therefore, the effect of cryogenic cooling on the general characteristics of the glow discharge was examined in order to understand the mechanisms responsible for the changing ion signal intensities.

Current-Voltage Characteristics

Each operating regime of the glow discharge has a characteristic current-voltage plot. For an applied voltage (or current), a resultant current (or voltage) is developed that depends on the discharge pressure, cathode material, and GD

source configuration. The I-V plot for the GD source made from the six-way cross is shown in Figure 30 with and without cooling. In this plot, a constant voltage is applied and the resultant current is measured. At a constant voltage, the resultant current increases when cooling is applied. For example, at 1000 V, the resultant current is 1.5 mA without cooling and 3.4 mA with cooling. Assuming that Ohm's law applies to the glow discharge plasma, upon cooling the impedance of the plasma is reduced. Therefore, less voltage is required to produce the same amount of current.

There are at least two possible explanations for the decrease in plasma resistance. The discharge current is composed of an ionic and electronic fraction with the ion fraction (ca. 90%) related to the number of ions generated per unit time. In the presence of impurities, the total ionization rate can be reduced due to energy consumption by the excitation of molecules vibrations, by dissociation of the molecular impurities, and their easier atomic excitation (151). Since the plasma has less resistance, there is more efficient movement of the charged species to their respective electrodes and fewer collisions with interfering gaseous species. A second mechanism involves the formation of negative ions by the impurities through electron attachment. As the electron population is depleted, larger discharge voltages are required to maintain the desired current. To determine whether the elimination of negative ions is responsible for the lower plasma impedance upon cooling, the mass spectrometer can be modified to measure the negative ion population with and without cooling.

Attempts were made to measure the effect of cryogenic cooling on the electron number density using Stark broadening of the H_δ 486.1 nm line, but the electron densities in the glow discharge are too low (10^9 - 10^{11} cm^{-3}) to obtain accurate optical measurements with the medium resolution monochromators that were available for this research. Langmuir probe measurements could also have been used to measure the electron densities with and without cooling, but it would not have been possible to distinguish between the electrons and the negative ions since both are measured by the probe.

Sputter Yields

It was observed with cooling that less voltage is required to maintain the plasma at a given current. If the discharge voltage is an indication of the energy of the plasma, the sample sputtering should be affected by this lower energy bombardment. The sputter rates for copper, iron, and tantalum with and without cooling are given in Table VI. Although the discharge voltage is lowered with cooling, iron and tantalum show no significant difference in their sputter yields while copper's sputter yield increases with cooling. The drop in the discharge voltages for these experiments was typically about 30%, which may not be large enough to affect the sputter yields. But larger voltage drops (> 50%) have also been observed with cooling, and it cannot be assumed that such large drops in GD voltage would not cause a decrease in sputtering. Fischer et. al reported that the GD sputtering rates were not significantly altered when less than 0.1 mass % of N_2 or O_2 was added to Ar discharge gas, but at higher concentrations the

sputtering rate decreased with increasing impurity addition (151). Larkins observed that the addition of 140 ppm water vapor produced a reduction in sputter weight loss varying from 3% for steel to 71% for aluminum (97). In general, the sputter yields measured with and without cooling behave similarly, increasing or changing little with the removal of the gaseous impurities.

Relative Ion Energies

A second effect that might arise from a lower discharge voltage is a reduction in ion energy. Both mass spectrometer systems have energy discriminating Bessel box lenses. If the ion energies are changing, the lower analyte ion signal intensities could be due to their discrimination by the Bessel box lenses. The Fe^+ ion intensity was monitored as the Bessel box lens voltages were varying for both mass spectrometers (Figures 31 & 32). For the Finnigan system, there is little difference between the optimum lens voltage for the cooled and noncooled discharge. For the laboratory-built system, the cooled plasma exhibited a slightly higher range of relative ion energies than the noncooled plasma. A slight difference in relative ion energies is observed for both the constant current and constant voltage operating mode. Whether this difference is large enough to explain the decrease in analyte ion signal is questionable. The decreased analyte ion signal is observed on both mass spectrometer systems, and attempts to regain the original signal intensity by retuning the ion lenses were unsuccessful. Therefore, it is inconclusive whether the decreased ion signal with cooling is due to lower ion energies.

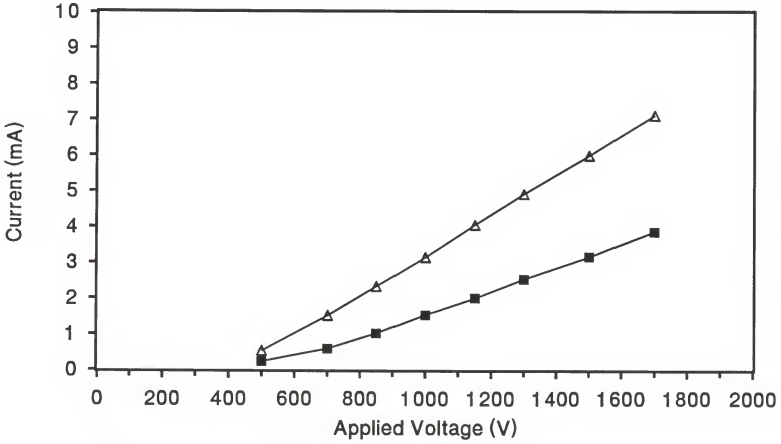

Figure 30. A typical glow discharge current-voltage plot. Cathode material: copper wire. ■ - without cooling, △ - with cooling.

Table VI. Sputter yields with and without cryogenic cooling.

Cathode	Sputter Yields Without Cooling	With Cooling
Fe	0.79 (±0.03)	0.91 (±0.09)
Cu	2.6 (±0.4)	3.4 (±0.4)
Ta	0.81 (±0.1)	0.71 (±0.06)

Mean and standard deviation were determined with n=3.

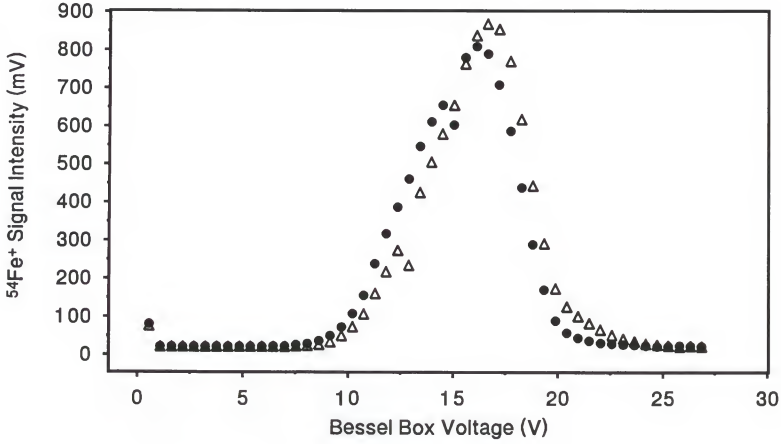

Figure 31. The effect of varying the Bessel Box voltage on the $^{54}Fe^{+}$ signal intensity for the Finnigan GDMS system. Cathode material: NIST SRM #1265, constant voltage: 1100 V. ● - without cooling, Δ - with cooling

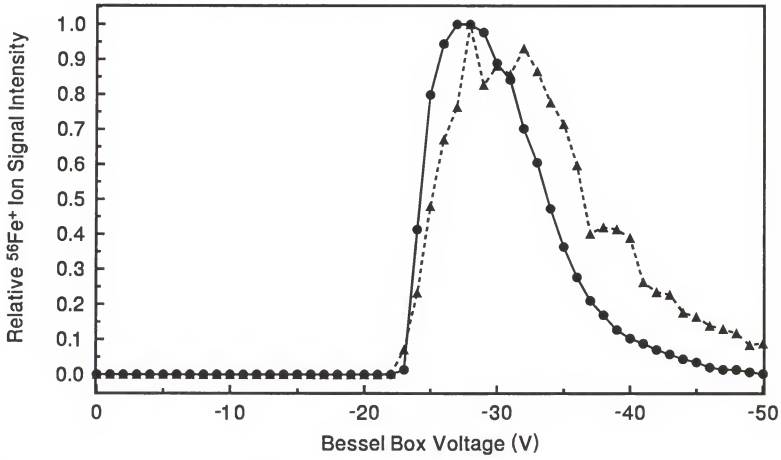

Figure 32. The effect of varying the Bessel Box voltages on $^{56}Fe^{+}$ ion signal intensity using the laboratory-built GDMS system. Cathode material: iron wire, constant : 1100 V. ● - without cooling, ▲ - with cooling.

Conclusions

Cryogenic cooling has been shown to be effective in the removal of gaseous impurities from the glow discharge plasma. The removal of these impurities results in the elimination of many mass spectral interferences due to the impurities, their dissociation products, and their gas-phase reaction products. One difficulty in describing the results of coupling cryogenic cooling with the glow discharge source, is comparing the noncooled and cooled glow discharge plasmas. For the noncooled case, the condition of the glow discharge source is typically unpredictable and irreproducible, depending on the amount of impurities present. The condition of the glow discharge will depend on the operating history of the source chamber and mass spectrometer, including the type of samples analyzed, operating parameters, purity of discharge gas, and frequency of venting the GD chamber and mass spectrometer to atmospheric pressure. As a result, it is difficult to reproduce accurately the noncooled glow discharge for both the long- and short-term. This accounts for the relatively high errors (5-30% RSD) that are sometimes associated with GDMS analyses. With cryogenic cooling, it should be possible obtain clean, reproducible plasma conditions, thereby, improving the precision and accuracy of GDMS elemental analyses. The optimum operating parameters for the dc glow discharge appear to be similar for both the noncooled and cooled plasmas. The lower analyte ion signal intensities usually observed upon cooling do not appear to be a result of lower sputter yields and relative ion energies, but could possibly be a combination of these effects.

CHAPTER 5
ANALYTICAL PERFORMANCE OF THE CRYOGENICALLY COOLED GLOW DISCHARGE

In the previous chapter, it was shown that cooling with liquid nitrogen effectively removed many gaseous impurities from the glow discharge plasma. This chapter will demonstrate the analytical performance of cryogenic cooling for the elemental analysis of conducting and nonconducting samples. The effect of cryogenic cooling on the analysis of metal alloys, compacted powders and ceramics was investigated using both dc- and rf-powered glow discharges.

Experimental

Both mass spectrometer systems were used in these studies. The Finnigan MS system was used for the determination of the relative sensitivity factors, while all other studies were performed on the laboratory-built MS system. The 2 mm diameter sample cathodes were prepared from the NIST low alloy steel series SRM #1261, 1262, 1263, 1264, 1265. Conducting compacted powder disk samples were prepared by mixing 10 - 50%, by weight, of the nonconducting analyte with a conducting matrix. The analyte samples included La_2O_3 (RG, Fisher Scientific Co.) and a sedimentary rock standard (United States Geological Survey,

SCo-1), and the matrix powders included silver (Gallard-Schlesinger Chemical Mfg. Corp., City, 99.9% pure (metals basis)) and iron (AESAR, Johnson Matthey Inc., Seabrook, NH, 99.9% pure (metals basis)). The analyte and matrix were mixed together using a WIG-L-BUG mixer for 2 min. The mixtures were pressed into 4.3 mm diameter sample disks using a stainless steel die (Figure 33). The nonconducting samples were prepared from a machinable ceramic (Corning Glass Works, Corning, NY, Macor) and the SCo-1 USGS rock standard. The ceramic sample was machined into a 5 mm diameter disk having a 1.5 mm thickness. The rock standard was prepared by pressing 100% SCo-1 powder in the stainless steel die. The rock disk was then sliced into approx. 2 mm thick sample cathodes. The sample disks were affixed onto a flat sample holder with silver paint adhesive (Ernest F. Fullam, Latham, NY, #14810). The conducting samples were analyzed using the dc glow discharge, while the rf glow discharge was used for the nonconducting samples. The operating pressure was maintained at approximately 1 Torr of argon (Liquid Air Corp., San Francisco, CA, 99.999% pure) for all experiments.

DC Glow Discharge Analyses

Relative Sensitivity Factors

One difficulty in performing any type of elemental solids analysis is the limited supply of solid standards. Typically it is impossible to find a set of solid standards containing the desired elements at varying concentrations in the matrix

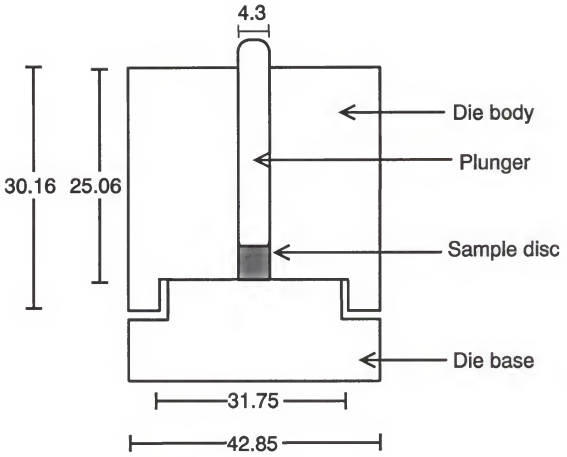

Figure 33. Schematic diagram of the sample disk die. Units are in mm.

of interest. As a result, the use of calibration curves for quantitative analysis is not possible. One technique employed in GDMS is the use of an internal standard. The internal standard is the matrix element, and is assumed to be known or is determined by another procedure. In this method, the sensitivity (signal intensity/concentration) of the matrix element is used to determine analyte concentration:

$$Conc_{anal} = Signal\ Intensity_{anal} \times \frac{Conc_{ref}}{Signal\ Intensity_{ref}} \qquad (3)$$

Using equation 3, semi-quantitative analyses are possible in GDMS because the variation in elemental sensitivities is within a factor of three and is relatively matrix independent (103).

In order to obtain precise quantitative analysis, the external standard technique of using relative sensitivity factor (RSF) values was developed. RSF values were originally employed in spark source mass spectrometry to correct for the variations observed in the elemental sensitivities due to physical, chemical, and instrumental effects. The RSF is the ratio of the sensitivity of an analyte element to the sensitivity of the reference (matrix) element. For this method, only one standard material of similar composition to the unknown sample is required. For a standard of known concentration, the RSF value of the desired element can be calculated from the following equation:

$$RSF = \frac{Signal\ Intensity_{anal}}{Conc_{anal}} \times \frac{Conc_{ref}}{Signal\ Intensity_{ref}} \quad (4)$$

The RSF value is then used as a correction factor for the quantitative analysis of the analyte element in the sample using:

$$Conc_{anal} = \frac{1}{RSF} \times \frac{Signal\ Intensity_{anal} \times Conc_{ref}}{Signal\ Intensity_{ref}} \quad (5)$$

where the concentration of the reference element is known or assumed known in the sample. RSF values in GDMS have been reported for a variety of elements in varying matrices (152). Attempts are being made to develop a theoretical expression for determining RSF values to eliminate the need for standard materials altogether (152, 153).

The use of RSF values has become the accepted method for quantitative analysis in GDMS. Therefore, the effect of cryogenic cooling on RSF values was examined. Using a low-alloy steel standard (NIST SRM #1264), the RSF values were determined for selected elements over the typical elemental m/z range of 0 - 200 (Table VII). The RSF value for $^{27}Al^+$ decreases when cryogenic cooling is applied. This can be explained by the reduction or removal of impurity species that occur at m/z 27, such as CNH^+. For $^{48}Ti^+$, $^{181}Ta^+$, and $^{186}W^+$, the RSF values increase upon cooling. This increase could be due to the elimination of their

Table VII. Relative sensitivity factor values calculated from NIST SRM #1264 low-alloy steel standard.

	Without Cooling		With Cooling	
	Mean	%RSD*	Mean	%RSD*
$^{27}Al^+$	4.21	18.6	1.44	8.2
$^{48}Ti^+$	2.10	4.5	4.26	0.41
$^{51}V^+$	1.69	3.2	3.78	0.61
$^{57}Fe^+$	1.00		1.00	
$^{59}Co^+$	0.77	1.6	1.60	0.62
$^{63}Cu^+$	0.38	5.5	0.26	0.94
$^{93}Nb^+$	0.84	4.9	2.32	0.40
$^{98}Mo^+$	0.68	2.9	1.54	1.1
$^{181}Ta^+$	0.11	7.4	0.38	1.7
$^{186}W^+$	0.081	5.2	0.23	1.4

reference analyte = $^{57}Fe^+$
*n=3

oxide formation. Titanium, tantalum, and tungsten are all gettering agents, oxygen scavengers, and will readily form oxides when oxygen is present in the plasma. All the other RSF values increased except $^{63}Cu^+$. The increased RSF values could be due to a relative decrease in the reference element ($^{57}Fe^+$) signal intensity, which could happen if an impurity species was present at m/z 57. Possible impurities include $ArOH^+$ or $^{56}FeH^+$. It should be noted that all the analyte and reference ion signals decreased with cooling.

A difference in %RSD for the RSF calculations was also observed between the noncooled and cooled glow discharge analyses. Lower %RSD were reported for the cryogenically cooled plasma. Therefore, better precision for the RSF values and, consequently, quantitative analyses result with cooling. It is rather apparent that the plasma chemistry changes upon cooling, and as a result, the RSF values change. Therefore, RSF values developed for noncooled glow discharge sources should not be used for cooled sources. In addition, any attempted to use theoretical expressions for determining RSF values must include the effect cooling has on the plasma chemistry.

Limits of Detection

The effect of cooling on the GDMS detection limits was determined using two methods. The first method determined the limit of detection from the calibration curve, and is defined as $LOD = \frac{k\, s_{bk}}{m}$ where k=3, s_{bk} is the standard deviation of the blank, and m is the slope. A calibration curve was obtained for several elements using the NIST low alloy steel series. A suitable blank sample

was not available; therefore, the s_{bk} was estimated by the standard deviation of the background. The second method calculates the limit of detection from a single point, and is commonly used in elemental mass spectrometry.

$$LOD = \frac{3 \; x \; \sqrt{background}}{signal \; / \; conc} \qquad (6)$$

The background is typically the count rate at 1/2 amu above or below the most abundant isotope being used. For both LOD calculations, the background was taken at m/z = 67. It was the closest m/z to the matrix signal (Fe) that did not have an elemental ion signal. The limits of detection obtained by both methods are reported in Table VIII, and are similar for both calculation techniques. In addition, there was no significant difference between the detection limits determined with and without cooling. While an overall decrease in the analyte ion signals was observed with cooling, it did not appear to affect the detection limits. The detection limits measurements were performed on the laboratory-built mass spectrometer system, which inherently has higher detection limits due to the inefficient ion transport lenses.

Nonconducting Samples

The number one advantage of GDMS is its ability to analyze solids directly. This is of great importance with respect to geological materials that can be very difficult to put into solution, often requiring complex dissolution and digestion steps. However, geological materials are difficult to analyze by GDMS due to the

Table VIII. GDMS limits of detection with and without cooling*.

	Slope Method (ppm)		Single Point** (ppm)	
	Without	With	Without	With
Cu	9.6	9.9	9.8 ± 6.1	7.8 ± 3.5
Ni	6.3	2.7	8.2 ± 3.5	3.2 ± 1.3
Cr	4.0	2.6	5.1 ± 2.4	2.9 ± 1.0
Co	5.5	1.5	6.7 ± 2.8	1.9 ± 7.8

* Fe was used as an internal standard, k=3

** Mean and standard deviation were determined with n = 15. Three analyses of each: NIST SRM# 1261, 1262, 1263, 1264, and 1265.

presence of molecular interferences, in particular monoxides. The molecular interferences can arise from the sputtering of the monoxide species into the plasma along with the elemental atoms. The monoxides can also form in the gas phase as a result of combination reactions of the atomic species and the gaseous impurities. In addition, when compacted samples are used, gaseous impurities can be pressed within the cathode during the sample preparation and then released into the plasma by sputtering. For strongly bound oxide samples, the effect of gaseous impurities on the analyte atoms can be generalized by:

$$MO \rightleftharpoons M + O \qquad (7)$$

where *M* and *MO* are the atomic and monoxide species. For precise elemental analyses, a high atomic population is desired, requiring the elimination or reduction of the monoxide formation. Using lanthanum oxide (La_2O_3) as the sample, it has been shown that the LaO can be converted to La when getter reagents are used as the sample matrix (78). The getter reagent reacts with the oxygen depleting it from the plasma with the $\frac{La^+}{La^+ + LaO^+}$ ratio reaching 98% (78).

The ability of cryogenic cooling to promote the formation of the atomic species by physical removal of the gaseous impurities was investigated. Lanthanum oxide was used as the sample because of its strong oxide bonds (La-O 8.3 eV). The ratio of $\frac{La^+}{La^+ + LaO^+}$ was plotted versus time with and without cryogenic cooling for a 10% La_2O_3 in iron matrix sample disk (Figure 34). For the

sample without cooling, no La^+ signal is observed for the first 15 min probably corresponding to the time required to sputter away the oxides formed on the cathode surface. The La^+ concentration steadily increased until after 90 min of sputtering, the $\frac{La^+}{La^+ + LaO^+}$ ratio neared 0.99. With cooling, the $\frac{La^+}{La^+ + LaO^+}$ ratio approached 0.99 after only 10 min of sputtering. In these studies, the liquid nitrogen flow was turned on 30 min before inserting the sample and turning on the discharge.

The greater the concentration of nonconducting samples in the cathode disk, the less dilution of the sample and the greater the analytical sensitivity for GDMS analysis. Therefore, the ideal sample would contain only enough conducting material to support the glow discharge plasma. It is possible to have 90% nonconducting sample to 10% conducting material. However, for large concentrations of geological samples, the mass spectra consist mainly of the gaseous impurities sputtered from the sample. The ability of cryogenic cooling to influence the $\frac{La^+}{La^+ + LaO^+}$ was examined using sample cathodes composed of 10, 20, and 50% La_2O_3 (Figure 35). Regardless of the percentage of the nonconducting material in the sample cathode, the cryogenic cooling eliminated the LaO formation within 20 - 30 min. When getter reagents were used to reduce oxide formation, an increased time to remove all the LaO from the plasma was observed for increased La_2O_3 concentrations (78). Therefore, the effect of cooling is relatively independent of the cathode composition, and is less time-consuming than using getters to clean the GD plasma.

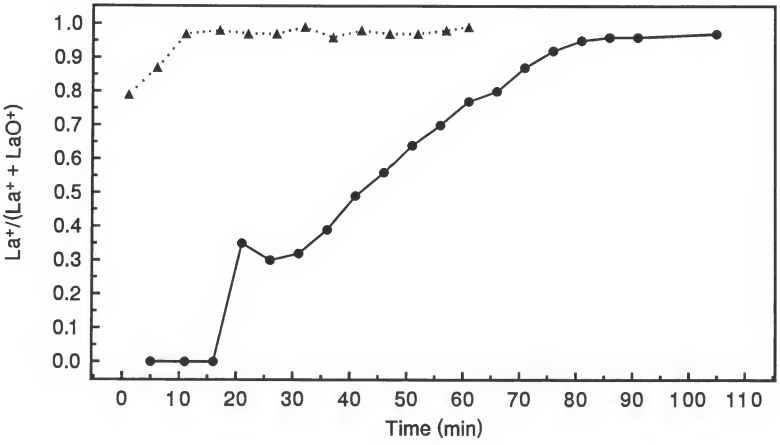

Figure 34. The conversion of LaO^+ to La^+ with and without cryogenic cooling. Sample cathode: 10% La_2O_3 in Ag matrix, argon pressure: 1 Torr, and constant current: 5.0 mA. ● - without cooling, ▲ - with cooling.

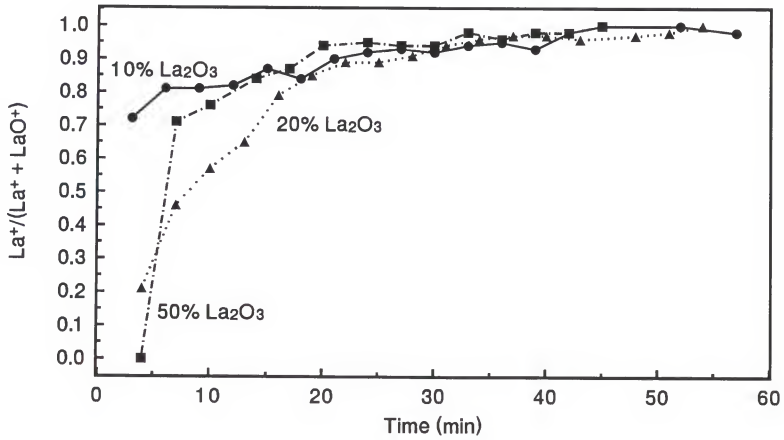

Figure 35. Conversion of LaO^+ to La^+ using cooling for varying La_2O_3 concentrations. Argon pressure: 1 Torr, constant current: 5.0 mA. ● - 10% La_2O_3, ▲ - 20% La_2O_3, ■ - 50% La_2O_3 in Ag matrix.

It was shown, using an ideal nonconducting sample, that cryogenic cooling could effectively remove the gaseous impurities and monoxide formation. Sample cathode disks were also prepared from geological samples containing 10, 20, and50% of the USGS rock standard SCo-1 in a silver matrix. For the 10 and 20% SCo-1 samples, the gaseous impurities were removed or significantly reduced within 30 min (Figure 36). The 50% SCo-1 in Ag matrix required 60 min of cooling to clean up the plasma (Figure 36). For all the SCo-1 samples, the largest ion signals are C^+, N^+, and O^+, and are probably due to gaseous impurities, oxides and carbonates sputtered from the sample. While the cryogenic cooling does effectively remove or reduce the gaseous impurities, the analyte ion signals (Al^+ and Si^+) are weak due to the dilution of the sample in a nonconducting matrix. To increase analyte ion signal sensitivity and reduce contaminants introduced from the matrix material, the pure nonconducting sample should be analyzed directly.

RF Glow Discharge Analyses

In 1971, the first glow discharge ion source used for elemental analysis was rf-powered (8, 9). The rf glow discharge never really gained in use because of the difficulties associated with using rf power. Due to the success of the dc-powered glow discharge ion sources, the rf glow discharge sources have been rediscovered, and are gaining in popularity because of their ability to sputter nonconducting materials. Ionization in the rf glow discharge is quite efficient, due

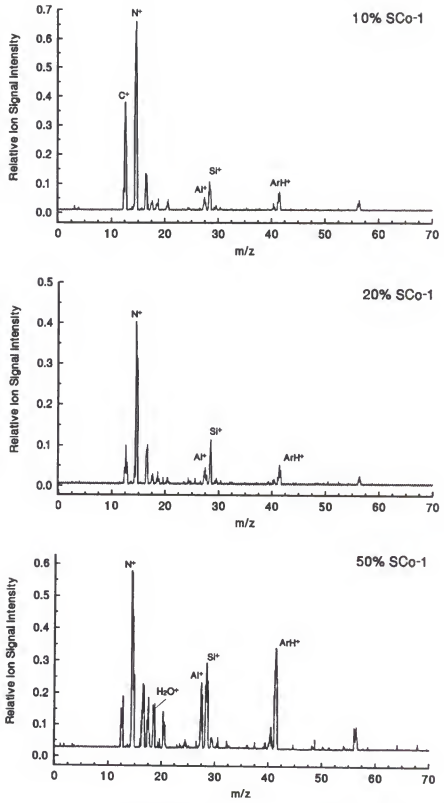

Figure 36. Mass spectra for compacted sample disks composed of 10, 20, and 50% rock standard (SCo-1) in Ag matrix. Argon pressure: 1 Torr, constant current: 5.0 mA.

partially to the oscillating nature of the rf discharge typically producing ion energies between 20 - 30 eV (145). While Penning ionization is believed to be the dominate ionization mechanism in a dc glow discharge, it is believed that electron impact may predominate in the rf glow discharge.

The mass spectrum of a conducting sample obtained using a rf glow discharge is very similar to its dc counterpart except that the molecular interferences due to gaseous impurities are usually larger in rf glow discharges than dc. This is probably a direct result of the higher electron energies associated with the rf discharge. The mass spectra of an iron cathode obtained with and without cryogenic cooling are shown in Figures 37 & 38. Without cooling, the same spectral interferences between m/z 0 and 30, as observed in the dc plasma, are present. Similar to the dc discharge, the cryogenically cooled glow discharge plasma produced a relatively impurity free mass spectrum except for the N^+ ion peak. One difference from the dc discharge is that it was possible to regain any lost analyte ion intensity by retuning the ion lenses. Using rf GDMS, Duckworth and Marcus have reported that the optimum sampling distance differed for the sputtered species (ca. 5 mm) and the gaseous species (ca. 9 mm) (25). This was also found true with our discharge, allowing further discrimination of the sputtered species from the gaseous impurities interferences and the discharge gas species. Using the iron cathode, optimum operating conditions were found to be a 5 - 6 mm sampling distance, 25 watts, and 0.7 Torr argon (operating conditions similar to that reported by Marcus (25)).

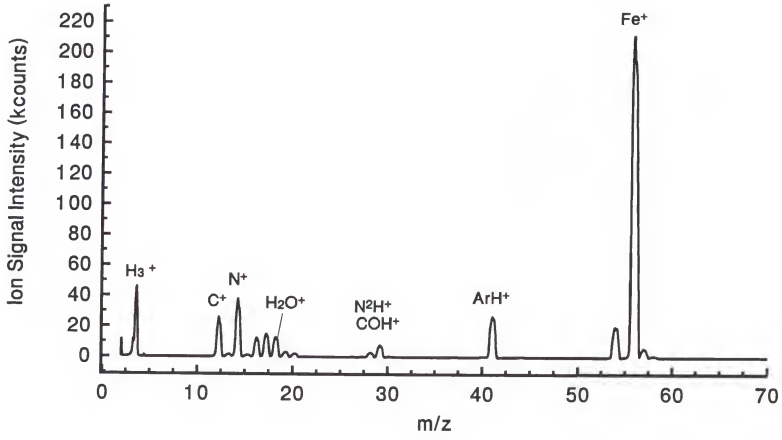

Figure 37. Rf-GDMS mass spectrum of an iron cathode without cooling. Argon pressure: 0.7 Torr, Power: 40 watts.

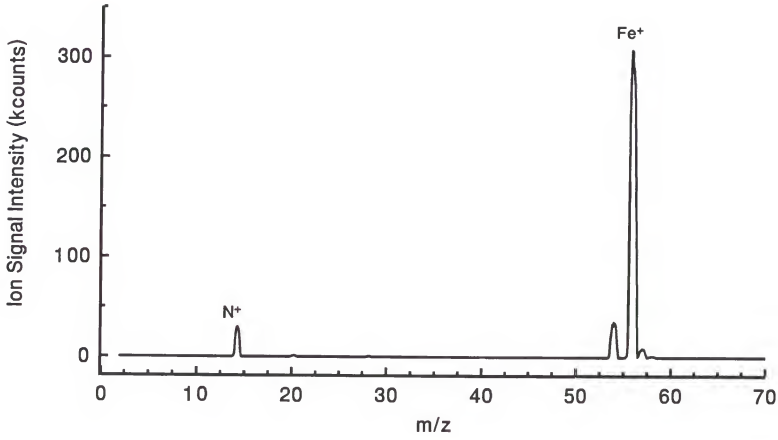

Figure 38. Rf-GDMS of an iron cathode with cooling. Argon pressure: 0.7 Torr, power: 40 watts.

In order to develop a rf glow discharge plasma using a nonconducting cathode, the thickness of the cathode was critical. In this research, glow discharge plasmas would develop upon cathodes of 2 mm or less thickness. Using thicker disks, it was not possible to initiate a plasma. The placement of the sample cathode in relation to the grounded shield was also critical. If a gap larger than the dark space existed between the cathode and shield, a discharge would develop behind the shield on the sample holder.

The first nonconducting sample analyzed by the rf glow discharge was a solid ceramic (Table IX). A ceramic material is an ideal rf sample material since outgassing of gaseous impurities should not be large, but as shown in Figure 39 the gaseous impurity species again dominate the mass spectrum with the ArH^+ gas discharge species producing the largest ion signal. However, with cryogenic cooling, the gaseous impurities are removed and the analyte species dominate (Figure 40). Analyte ion signals due to Al^+, Si^+, Mg^+, K^+ and B^+ are easily detected. Considering the large quantity of oxygen in the ceramic (Table IX), there is very little atomic oxygen or oxide formation present in the mass spectrum. The weak ion signal at m/z 44 is believed to be SiO^+, and not CO_2. The liquid nitrogen cooling will freeze out any CO_2 in the glow discharge source. The ion signals due to copper and zinc are introduced from the sputtering of the brass holder. The large ion signal at m/z 14 is probably due to nitrogen impurities. Careful positioning of the cathode relative to the ion exit orifice could probably result in the elimination or reduction of the nitrogen peak.

The more difficult test of cryogenic cooling is the GDMS analysis of a compacted sample composed entirely of a geological material. A sample disk of 100% USGS SCo-1 rock standard was pressed into a 4.3 mm diameter disk cathode. To minimize the adsorption of water by the standard, the SCo-1 sample was stored in a vacuum oven before and after pressing the disk cathode. The composition of the rock standard is listed in Table X. The mass spectrum of the rock standard after 30 min of sputtering in shown in Figure 41. In contrast to the ceramic sample, the water impurity species are the largest, even dwarfing the ArH^+ ion signal. The large impurity signals are probably due to the water adsorbed or entrapped into the cathode during exposure to the surrounding atmosphere or during pressing. The major components of the rock sample are SiO and Al_2O_3, with isotope peaks at m/z 27 and 28 corresponding to Al^+ and Si^+ respectively. The isotope ratios for Si and Mg are incorrect suggesting that gaseous impurities are primarily responsible for the peaks between m/z 24 and 30. Upon cooling, the water impurities are removed and the analyte ion signals appear (Figure 42). The isotope ratios for the Mg^+ and Si^+ are now correct. Ion signals due to minor components such as Fe^+, Na^+, K^+, and possibly Ca^+ are also present. Without cryogenic cooling, it would be very difficult and time consuming to achieve the same quality mass spectrum.

The mass spectra obtained for the ceramic and rock sample cathodes were obtained under optimum conducting discharge conditions. To improve the analyte ion signals, the effect of discharge pressure and rf power was examined.

Table IX. Composition of the machinable glass ceramic (macor).

Compound	Approximate Weight %
SiO_2	46
Al_2O_3	16
MgO	17
K_2O	10
F	4
B_2O_3	7

H_2O, CO, N_2, CO_2, HF, BF_3, and BF_3 gases will also be evolved from the ceramic as it is heated.

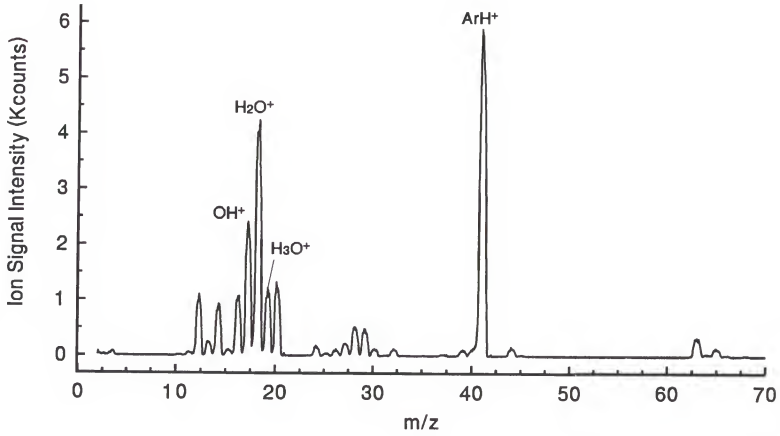

Figure 39. Rf-GDMS mass spectrum of a ceramic disk (Macor machinable ceramic) without cooling after 20 min of sputtering. Argon pressure: 0.6 Torr, power: 25 watts.

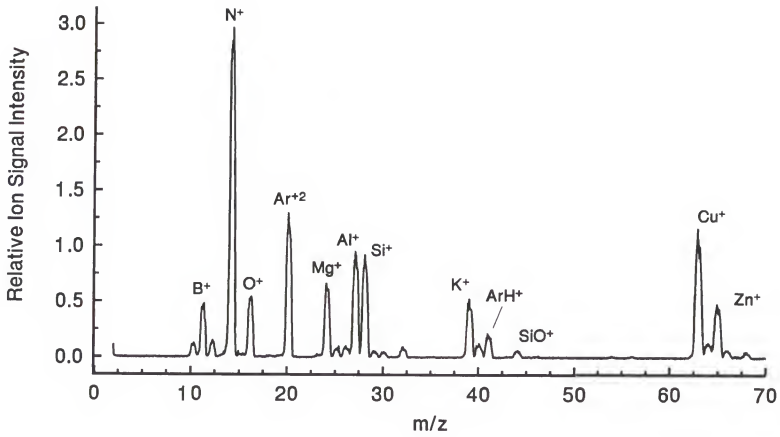

Figure 40. Rf-GDMS of a ceramic disk (Macor machinable ceramic) after 40 min of cooling. Argon pressure: 0.6 Torr, power: 25 watts.

Table X. Composition of USGS geological rock standard SCo-1.

Compound	Weight %
SiO_2	61.84
Al_2O_3	13.40
Fe_2O_3	3.83
FeO	1.15
MgO	2.69
CaO	2.68
Na_2O	0.97
K_2O	2.8
H_2O	6.3
TiO_2	0.83
P_2O_5	0.44
MnO	0.05
CO_2	2.55
SO_3	0.44
Cl	0.16
F	0.15
S	0.12
organic material	0.18

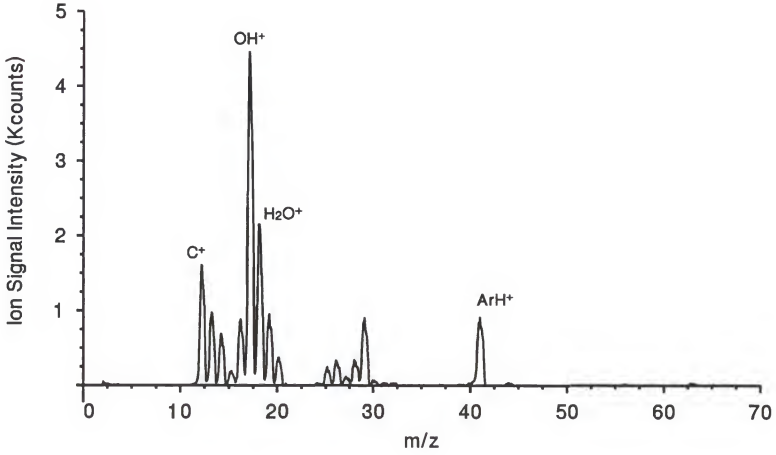

Figure 41. Rf-GDMS mass spectrum of a SCo-1 rock standard disk without cooling after 30 min of sputtering. Argon pressure: 0.7 Torr, power 30 watts.

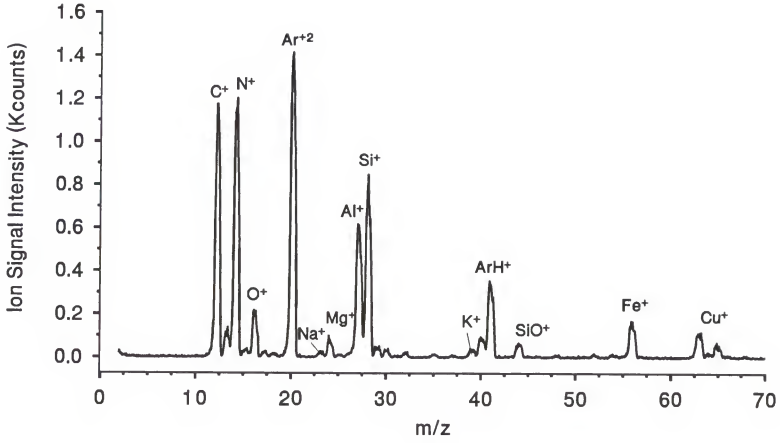

Figure 42. Rf-GDMS mass spectrum of SCo-1 rock standard after 37 min of cooling. Argon pressure: 0.7 Torr, power: 30 watts.

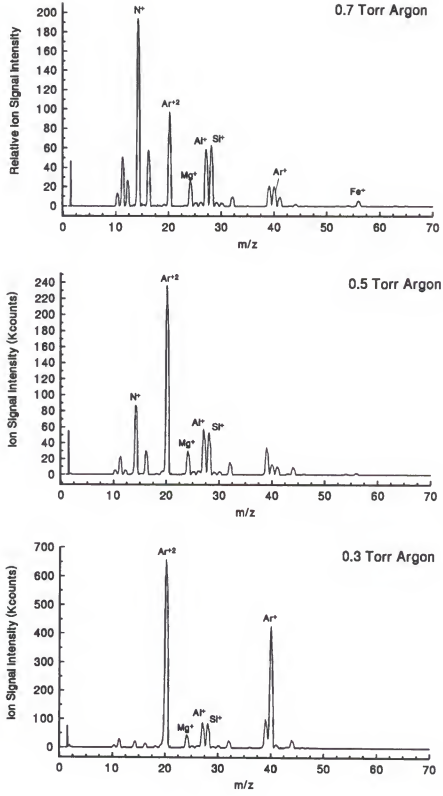

Figure 43. The effect of argon pressure on the rf-GDMS mass spectrum of a ceramic disk (Macor machinable ceramic). With cooling, power: 45 watts.

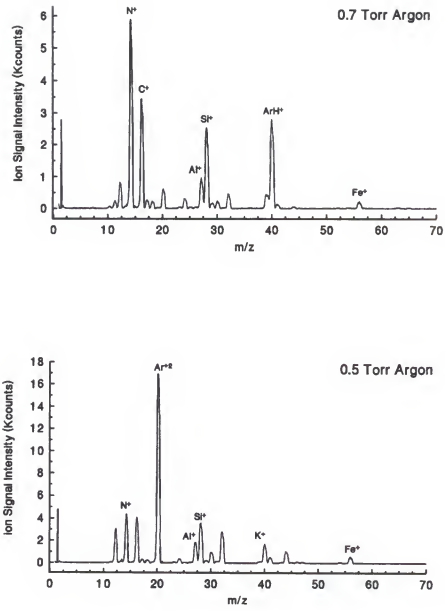

Figure 44. The effect of pressure on the mass spectrum of a SCo-1 sample disk. With cooling, power: 45 watts.

The mass spectra were obtained at varying discharge pressures for both the ceramic and rock sample. For the ceramic sample at 0.7 Torr argon pressure, the dominate ion signal was the N^+ followed by Ar^{+2} peak (Figure 43). When the argon pressure was lowered to 0.5 Torr, the major ion species became Ar^{+2}, and the gaseous impurities (N^+, C^+) were roughly the same magnitude as the sputtered matrix material (Al^+, Si^+). At still lower pressures (0.3 Torr), the Ar^{+2} ion signal nearly tripled, and the Ar^+ (which was very low at 0.7 and 0.5 Torr) increased greatly. The gaseous impurities were now lower than the matrix ion signals. While the discharge gas and impurity ion signals changed greatly with changing pressure, the analyte ion signals appeared to only increase slightly. Using the rock sample, the same effect was observed for 0.7 and 0.5 Torr argon (Figure 44). A mass spectrum was not obtained at 0.3 Torr argon because a stable glow discharge could not be maintained. The ion signals for the gaseous species and the sputtered species in the rf glow discharge optimize at different pressures; therefore, in addition to cooling, it is possible to minimize further the gaseous impurities by the judicious choice of discharge pressure. The rf operating power was also varied between 19 - 40 watts with cooling. The analyte and gaseous ion species both increased with increasing power. Similar to dc glow discharges, the rf discharge should be operated at a power as high as possible without overheating the sample or probe assembly.

The success of rf glow discharges developed by Marcus and co-workers is probably responsible for the renewed interest in their application. Few results

for nonconducting materials have been reported. While they have reported results for glasses, ceramics, and fused geological materials, smooth, flat samples were required since a vacuum seal is being made between the sample and source chamber. A GD source for pin samples has been reported, but only conducting samples have been analyzed. Although the glass matrices were >50% oxygen, mass spectra were observed to be predominantly atomic in nature with minimal single and higher order oxide signals (154). In order to analyze geological materials, they have to be made into fused glass samples requiring the sample to be diluted with the flux material at a mixing ratio between 1:2 and 1:20. With such a requirement, there is no advantage of using rf-powered glow discharges; one might as well mix the sample with a conducting matrix and use the simpler dc-powered glow discharge. The results reported in this dissertation are the first successful analysis of 100% compacted geological material.

Conclusions

Cryogenic cooling is essential to obtain accurate and precise elemental analysis of conducting and nonconducting materials using either dc or rf glow discharge ion sources. As mentioned in chapter 4, a decrease in the analyte ion signal can occur upon cooling, but this effect does not appear to adversely affect GDMS detections limits. While nonconducting samples can be analyzed using the dc glow discharge by mixing with a conducting matrix, better results were obtained using a cryogenically cooled rf glow discharge with 100% pure sample.

CHAPTER 6
DIAGNOSTICS OF THE CRYOGENICALLY COOLED GLOW DISCHARGE

While cryogenic cooling is extremely effective at removing gaseous impurities, the glow discharge cell is usually quite small, and dropping the temperature dramatically to liquid nitrogen levels introduces an extremely cold, large surface in close proximity to the active negative glow region of the GD. In order to understand how the plasma processes in the glow discharge are affected by cryogenic cooling, diagnostic measurements in the glow discharge were performed. This chapter reports the results of investigating fundamental discharge processes, specifically through the measurement of excitation and rotational temperatures.

The number of diagnostic temperature measurements reported for glow discharges is small compared to the number of studies reported for the higher energy ICP. For a coaxial glow discharge source, Marcus and Fang measured excitation temperatures between 2000-4000 K for argon lines, finding little variation with changing sample composition (155). In addition, the same authors measured electron temperatures ranging from 2300 to 4100 K using a Langmuir probe (156). Hess and co-workers (110, 157) found little change in temperatures for varying discharge gases and pressures in a coaxial-type GD. They measured excitation

temperatures between 6500 and 8500 K for a sputtered species (Zn) and between 4500 and 5000 K for discharge gas species (Ar, Ne). Using a Langmuir probe, they determined electron temperatures between 3500-5000 K. Brackett et al. (158), employing a planar glow discharge, measured Ar (I) excitation temperatures between 3000 and 4000 K and found little variation in temperatures with respect to current, pressure, or discharge region. For a Grimm-type glow discharge, Büger (159) reported temperatures between 1560 and 3050 K for Cu lines, 3000 K for Ar lines, and rotational and vibrational temperatures of 2500 K and 3000K for N_2 band emissions. West and Human (160) measured Doppler temperatures ranging from 567 to 2873 K for a Grimm-type GD as a function of operating current and cathode composition. Ferreira et al. (161), using a Grimm GD, found the Doppler temperature of the sputtered atoms reached a maximum within 1mm from the cathode, while the Doppler temperature of the discharge gas decreased with increasing distance from the cathode. Kuraica et al. (162) profiled the temperatures in an argon-hydrogen (97:3) gas mixture for a Grimm GD using Ar(I) and Ar(II) excitation temperatures (4600-5860 K and 28570-29740 K, respectively), Doppler temperatures (950-1110 K), and excited hydrogen temperatures (0.75 - 1.1 x 10^6 K). The Fe(I) and Fe(II) temperatures of a boosted glow discharge lamp were measured by McDonald (163) and were found to be similar (about 4000 K) and independent of operating parameters when sufficient boosting current was applied. Uzelac and Leis (164), using a microwave boosted glow discharge,

reported Doppler gas temperatures ranging between 320-520 K depending on discharge conditions.

Temperature Measurements

The glow discharge presents special considerations for plasma diagnostic measurements because it is not considered to be in local thermodynamic equilibrium (LTE). The collision dynamics of a plasma determine whether it satisfies LTE, which may be defined for a small plasma volume as having a rate of collisional deactivation much greater than radiative deactivation (165, 166). For glow discharges normally operating between 1 and 10 Torr, a major deactivation mechanism is radiative decay, thus giving the characteristic glow of the discharge. As a result, optical temperature measurements based upon an assumption of a Boltzmann distribution will yield different temperatures depending on the species being measured (i.e., neutrals, ions, electrons). As long as their limitations are realized, these "temperatures" determined for low pressure discharges can have a certain diagnostic value as a relative measure of the population of the different excited states for each species. In the case of this study, measurements taken with and without cryogenic cooling of the plasma were of special interest. The temperature measurement theory will be briefly discussed here. For a detailed explanation, there are several excellent reviews on temperature calculations in gas discharges, including references 165, 166, 167 and 168.

Excitation Temperature

The most common method for measuring excitation temperatures is the Boltzmann-plot (slope) technique, which relates the intensity of a spectral line to the excitation energy of that line. The intensity of the line is given by:

$$I_{ki} = VA_{ki}N_k\left(\frac{hc}{\lambda_{ik}}\right) \tag{8}$$

where N_k is the population of the excited atomic state k, A_{ki} is the transition probability from k to i, λ is the spectral line wavelength, V is the probe volume, h is Planck's constant, and c is the velocity of light. For a system in LTE, the population of the excited atomic neutral or ionic species follows a Boltzmann distribution:

$$N_k = N_0\left(\frac{g_k}{Z(T)}\right)\exp\left(\frac{-E_k}{k_BT}\right) \tag{9}$$

where N_o is the total concentration of the neutral atom or ion, g_k is the statistical weight of level k, $Z(T)$ is the partition function, E_k is the excitation energy of level k, and k_B is the Boltzmann constant. Combining equations 1 and 2, and taking the logarithms gives:

$$\log\left(\frac{I_{ki}\lambda_{ik}}{g_kA_{ki}}\right) = \frac{-0.434\,E_k}{k_BT} + \log\left(\frac{Vhc}{Z(T)}\right) \tag{10}$$

Excitation temperatures can be calculated from the Boltzmann plot of $log(I\lambda/Ag)$ versus E_k which gives a slope equal to $-0.434/k_B T_{exc}$, where I is the measured intensity of the line (arbitrary units).

The selection of the elemental species to use as the thermal probe for the temperature determination is one of the most important criteria. Commonly used elements include neutral argon and iron and ionized titanium. The elemental species should have spectral lines that meet the following criteria: (1) wide ranging energies, (2) accurate transition probabilities (within 10%), (3) closely spaced wavelengths, and (4) no spectral overlaps of the lines.

Rotational Temperature

Compared to excited electronic state exchanges, the exchange rate between excited rotational states is very fast. A Boltzmann distribution of the excited rotational states can be assumed (169). In addition, the energy differences between rotational levels is low, and rotational relaxation is very fast, resulting in the excited rotational states being in equilibrium with the kinetic energy of the molecules (169). Consequently, the kinetic gas temperature of the plasma is reasonably approximated by the rotational temperature.

Rotational temperatures can be determined using the band intensities of diatomic molecules. The molecular species that have been used for rotational temperature (T_{rot}) calculations include OH, N_2^+, C_2, and CN. Rotational temperatures determined using the R branch of the N_2^+ emission band are calculated from the following equation (167):

$$\log \frac{\alpha I}{2(K'' + 1)} = \frac{-Bhc}{kT}(K'' + 1)(K'' + 2) \qquad (11)$$

A plot of $\log \alpha I/2(K''+1)$ versus $(K''+1)(K''+2)$ results in the slope being equal to $-Bhc/kT_{rot}$, where K'' is the rotational quantum number, $\alpha = 1$ for even line numbers or $\alpha = 2$ for odd line numbers, I is the line intensity, k is Boltzmann constant, h is Planck's constant, c is the velocity of light, and B is the rotational constant of the vibrational level. Substituting in the values of the constants, the slope is equal to $-1.296/T_{rot}$ (167).

Experimental

The glow discharge source, cryogenic coil and laboratory-built mass spectrometer used in the experiments have been fully described in chapter 3. The glow discharge housing is a six-way cross with 2.75-in. (7.0 cm) flanges that is used primarily as a GD ion source on a mass spectrometer and is fitted with quartz windows that allow optical spectroscopic and mass spectrometric measurements to be performed simultaneously (Figure 45). The cryogenic coil is coaxial with the direct insertion probe and positioned approximately 5 mm behind the edge of the cathode, allowing emission measurements to be made in front of both the cathode and coil. The cathode samples used for the diagnostic measurements were Fe [National Institute of Standards and Technology, Gaithersburg, MD, USA, Standard Reference Material 1265 electrolytic iron

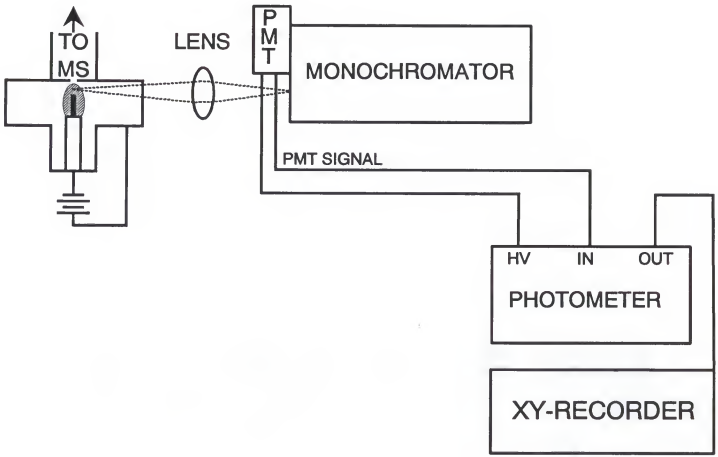

Figure 45. Schematic diagram of the GD optical emission system.

(99.9% Fe)] and tantalum (Johnson Matthey Chemicals, Ward Hill, MA, USA, 99.5% pure). The Fe samples were machined into 2 mm diameter pins from bulk sample disks and the Ta was purchased as a 2 mm diameter wire. Five millimeters of the sample pins were exposed in the discharge. The discharge gases consisted of argon and nitrogen [Liquid Air Corp., Walnut Creek, CA, USA, argon (99.999% pure), nitrogen (99.998% pure)] operating at a nominal pressure of 1 Torr (133.3 Pa). The discharge was run in dc mode with the current ranging between 1-6 mA and the discharge voltage varying from 500-1700 V.

For spectral measurements, the wavelengths of interest were scanned using a 0.5 m Ebert spectrometer (Jarrell Ash, Model 82-516, Waltham, MA, USA) with a grating groove density of 1180 grv/mm and a reciprocal linear dispersion of 1.6 nm/mm. The glow discharge was imaged 1:1 on the entrance slit using a 68 mm diameter quartz biconvex lens with a 160 mm focal length. Spatially resolved measurements of the glow discharge were taken by moving the lens over approximately a 5mm range perpendicular to the optical axis. The entrance and exit slit widths were 25 μm and the entrance slit height was 2 mm. A photomultiplier tube (Hamamatsu Type R1463, Bridgewater, NJ, USA) was used for detection with the high voltage being supplied by a photometer (Pacific Instruments Model 110, Concord, MA, USA). The output current from the PMT was amplified by the photometer and recorded using a strip chart recorder (Houston Instruments, Austin, TX, USA).

Physical temperature measurements were taken with a 1/32 in. (0.079 mm) diameter Type "T" (Copper vs. Copper-Nickel) thermocouple (Omega, Stamford, CT, USA) surrounded by a stainless steel grounded sheath. The temperature readouts in °C were provided by an Omega digital panel meter Model DP460.

Excitation Temperature Measurements

The first diagnostic experiments for determining the effect of cryogenic cooling on the glow discharge processes were the measurement of excitation temperatures (T_{exc}) with and without cooling. An iron cathode sample was used for all excitation temperature measurements. Iron is one of the most commonly used elements for measuring excitation temperatures because its emission lines span a large energy range over narrow wavelength intervals with well-known transition probabilities (167). The seven Fe (I) lines used and their transition probabilities have found previous applications and are listed in Table XI (170). A GD emission spectrum of the Fe sample is shown in Figure 46, and is similar to Fe spectra reported for plasma discharges (171). A typical Boltzmann plot is shown in Figure 47. The stability of the excitation temperature was determined over a 300 min time period (Figure 48). When the discharge is turned on, the T_{exc} decreases for the first 30-60 minutes until reaching a steady-state temperature. This initial drop in temperature roughly corresponds to the time required to clean up the impurities from the plasma without cooling. Therefore, in the absence of cooling, the plasma was allowed to presputter typically 30 min before starting the

Table XI. Assignment of wavelengths, excitation energies, and transition probabilities for the iron spectral lines (170).

λ (nm)	E_k (cm^{-1})	A (10^7 s^{-1})
371.993	26875	1.62
373.486	33695	9.02
373.713	27167	1.42
374.826	27560	0.915
374.949	34040	7.64
375.823	34329	6.34
376.379	34547	5.44

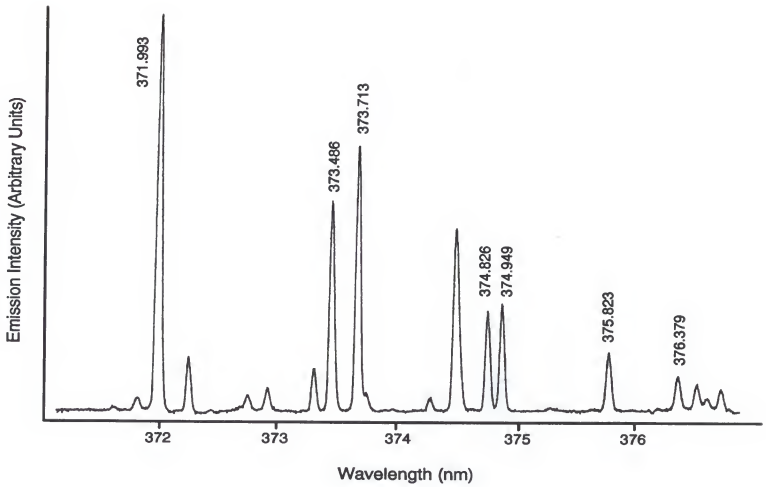

Figure 46. Glow discharge Fe emission spectrum. Iron cathode, 1 Torr argon discharge, 4.0 mA, without cooling.

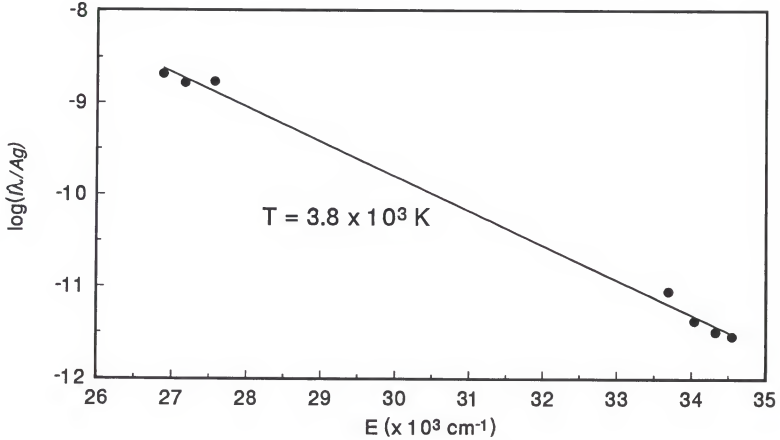

Figure 47. Representative Boltzmann plot for the determination of the Fe(I) excitation temperature. Iron cathode, 1 Torr argon discharge, 4.0 mA, without cryogenic cooling.

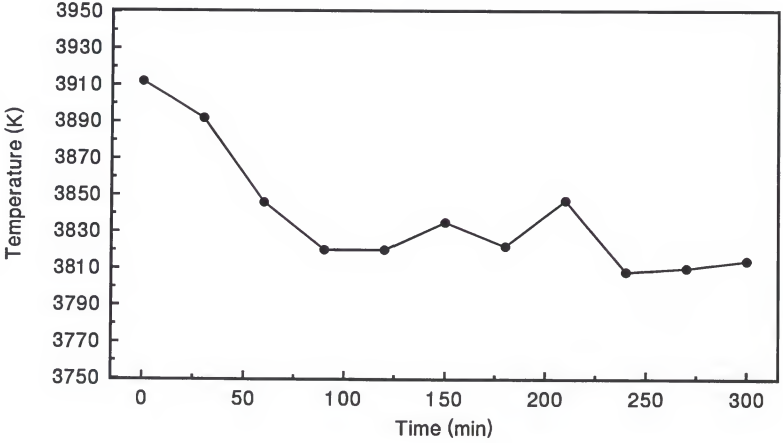

Figure 48. Stability of the Fe(I) excitation temperature measurements. Iron cathode, 1 Torr argon, 4.0 mA.

temperature measurements. Emission spectra and Boltzmann plots were obtained for both the cooled and noncooled discharges. The temperatures calculated throughout this section are an average of three repetitive measurements with error bars of one standard deviation.

Excitation temperature profiles of the GD are shown in Figure 49, with and without cooling. The profiles were obtained using line-of-sight measurements with 1:1 imaging of the GD plasma. For the plasma without cryogenic cooling, there is a noticeable increase in T_{exc} extending from the cathode surface through the cathode dark space to the interface between the cathode dark space and negative glow. The T_{exc} then decreased with increasing penetration into the negative glow. This pattern could correspond to the acceleration of electrons through the electric field of the cathode dark space toward the negative glow, where the electrons now have accumulated enough energy to excite and ionize the atomic species, producing the glow of the plasma. Upon reaching the negative glow, the electrons, atoms and ions randomly diffuse through this relatively field-free region, imparting their energies to cooler gas atoms by inelastic collisions. Temperature measurements were feasible only within the first few millimeters in front of the cathode because of decreasing GD emission intensity with distance. Upon adding liquid nitrogen to the coil, the excitation temperatures were decreased between 50 and 200 K. The overall shape of the profile is similar to the plasma without cooling, except that there is only a slight rise in temperature at the

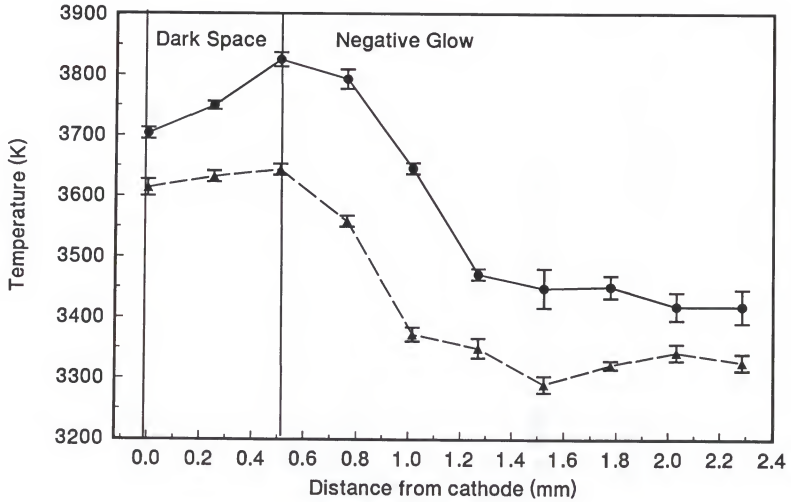

Figure 49. Fe(I) excitation temperature profile of the glow discharge plasma. ● - Without cryogenic cooling, 1 Torr argon, 4.0 mA. ▲ - With cryogenic cooling, 1 Torr argon, 4.0 mA.

cathode dark space and negative glow boundary. The largest temperature difference between the two profiles is at the cathode dark space and negative glow interface, with the difference decreasing with increasing distance from the cathode and coil assembly. It appears that as measurements are taken farther away from the cryogenic coil, a reduced cooling effect is observed for the excited species. The shapes of the excitation temperature profiles agree with the Doppler temperature profiles of Ferreira et al. (161). They found that the sputtered species temperature reached a maximum within 1mm of the cathode surface, depending on the operating parameters. For example, using the Doppler broadening of the Cr 428.9 nm line operating at 800 V and 60 mA, a maximum gas temperature of 1513 K was observed approximately 0.75 mm from the cathode surface.

The stability of the GD is an interdependent function of the operating current, voltage and pressure. When operating in the constant current mode (as in the previous experiments), the resultant discharge voltage will decrease upon cooling. Assuming Ohm's law applies to the GD, cooling (impurity removal) appears to lower the plasma resistance, requiring less voltage to maintain the discharge current. If the GD is operated in the constant voltage mode, the resultant current increases upon cooling because of the decrease in plasma resistance. The effect of cooling was determined for both constant current and constant voltage modes to determine whether the lower excitation temperature was the result of the changing discharge parameters upon cooling. The excitation temperatures were determined at the maximum of the GD temperature profile,

corresponding to the cathode dark space and negative glow interface. The effect of varying the discharge current while holding the pressure constant is shown in Figure 50. The discharge voltage decreased 25-35% while the T_{exc} decreased 100-200 K with cooling. The results of cooling while operating in constant voltage mode are shown in Figure 51 where the discharge current increased 10-40% upon cooling and the T_{exc} still decreased 200-300 K. In addition, the pressure was also varied for both the constant current and constant voltage operating modes, and in both cases, the T_{exc} decreased upon cooling. In summary, plasma temperatures for the noncooled GD are greater than for the cooled GD. It appears cryogenic cooling produces effects in the glow discharge relatively independent of the GD operating parameters.

Excitation temperatures were also determined using titanium ion lines. Titanium is a gettering reagent (an oxygen scavenger) that will eventually "clean up" the plasma. By using a gettering reagent, it should be possible to determine whether the lower excitation temperature is a result of impurity removal or cryogenic cooling. A GD emission spectrum for the titanium ion lines is shown in Figure 52 with the corresponding excitation energies and transition probabilities listed in Table XII. A typical Boltzmann plot is shown in Figure 53. The Ti(II) excitation temperature was determined as a function of sputtering time (Figure 54). When the discharge is first turned on, the T_{exc} is low then begins to increase, reaching a maximum after 20 min of sputtering. During this time, the major ion

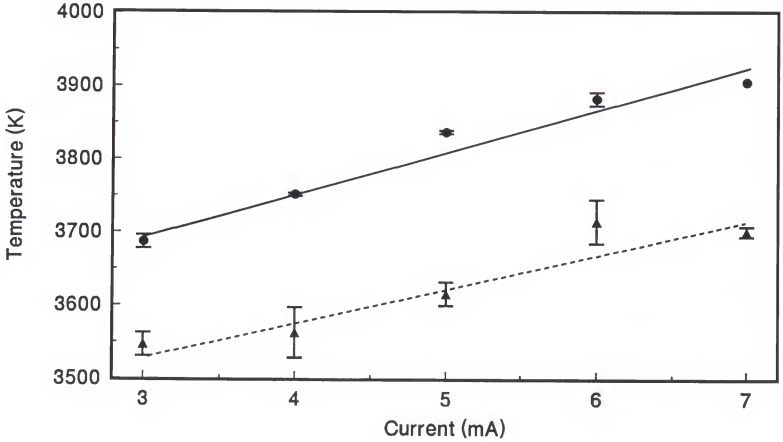

Figure 50. The effect of discharge current of Fe(I) excitation temperatures. ● - Without cryogenic cooling, 1 Torr argon. ▲ - With cryogenic cooling, 1 Torr Argon.

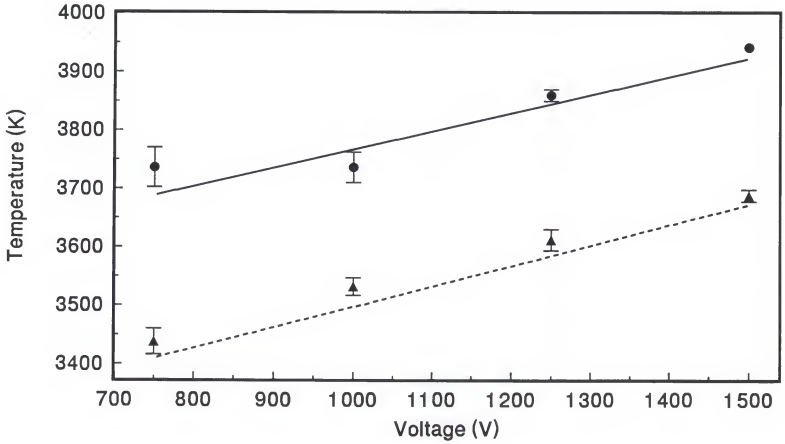

Figure 51. The effect of discharge voltage on Fe(I) excitation temperatures. ● - Without cryogenic cooling, 1 Torr argon. ▲ - With cryogenic cooling, 1 Torr argon.

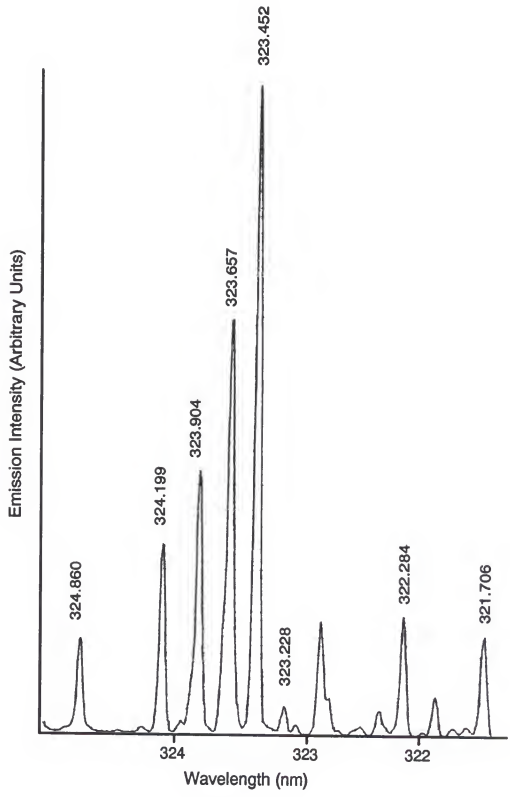

Figure 52. Glow discharge Ti(II) emission spectrum. Titanium cathode, 1 Torr argon, 4.0 mA, without cooling.

Table XII. Assignment of wavelengths, excitation energies, and transition probabilities for the titanium ion spectral lines .

λ (nm)	E_k (cm^{-1})	gA (10^8 s^{-1})
321.706	31301	2.7
322.284	31114	3.1
323.228	39927	6.8
323.452	31301	16.0
323.657	31114	13.0
323.904	30959	9.3
324.199	30837	5.8
324.860	40798	44.0

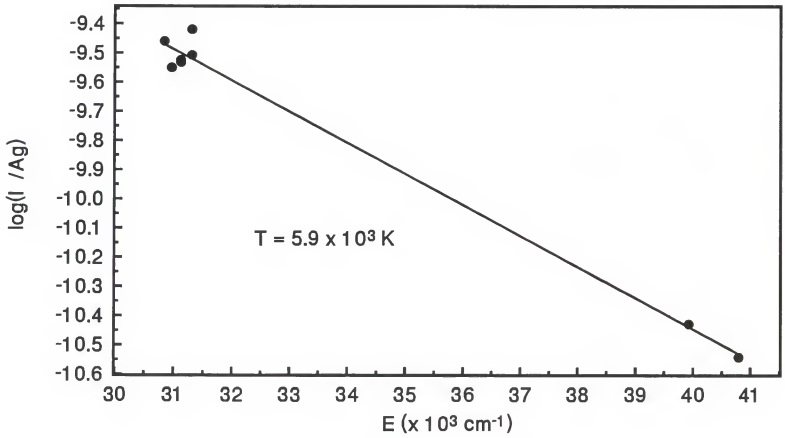

Figure 53. Representative Boltzmann plot for the determination of Ti(II) excitation temperatures. Titanium cathode, 1 Torr argon, 4.0 mA, without cryogenic cooling.

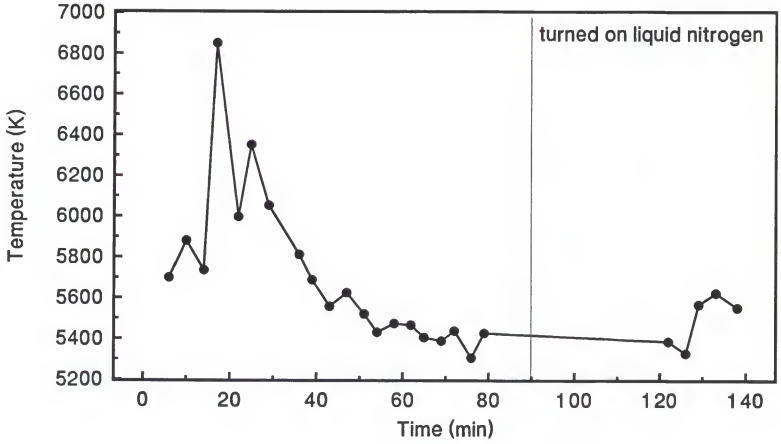

Figure 54. The effect of gettering versus cryogenic cooling on the Ti(II) excitation temperature. Titanium cathode, 1 Torr argon, 4.0 mA.

species observed in the mass spectrum are the impurity species, in particular H_3^+ and H_3O^+. Between 30 - 60 minutes of sputtering, the gaseous impurities start to disappear from the mass spectrum. During the same time period, the T_{exc} drops and reaches a minimum temperature. When the liquid nitrogen flow is turned on, the T_{exc} is still low, and is comparable to the minimum temperature before cooling. These results would suggest that the lower excitation temperatures, as determined by Ti(II), that result from cooling the plasma are due to the removal of the gaseous impurities instead of thermal effects. In equations 8 and 9, it was shown that the line intensity is a function of the total concentration of the neutral atom or ion as well as the temperature (all the other variables are assumed constant). If it is not a temperature effect, then the total neutral atom or ion concentration must be changing. A reduction in discharge voltage is observed when the plasma is cleaned; therefore, the population decrease could be due to less sputtering. This is unlikely because the discharge voltage decreases further when cooling is applied, but a slight temperature rise is observed instead of a greater decrease in temperature. It appears that the impurities are involved in gas-phase reactions that affect the elemental line intensities. The responsible gas-phase reactions have not been identified.

Due to the non-LTE conditions of the GD, excitation temperature measurements are not very useful for comparing the GD to other plasma sources. While the excitation temperatures measured here are similar to the GD excitation temperatures reported by other investigators, they are also comparable to Fe

excitation temperatures for ICPs (3500-9000K) (167). Thus, excitation temperatures measured in the GD are best used for characterizing excitation trends within the plasma. The excitation temperature diagnostics have clearly shown that lower temperatures result from cooling the GD. The lower temperatures reflect the lower excited-state population levels or the redistribution of these levels. Changes in the emission line intensities can result from changes in the free atom population or the electronic temperature in the plasma. It is known that the presence of gaseous impurities can influence the sputtering, excitation, and ionization processes in the glow discharge. Water vapor in the GD plasma has been shown to produce inefficient sample sputtering due to lower molecular weight bombarding species and oxidation of the sample surface, loss of analyte atoms through gas-phase reactions, and quenching of argon metastable atoms that are responsible for excitation and ionization (97, 112). Therefore upon cooling, the free atom population can be altered by the elimination of all or several of these gaseous impurity effects. The mechanism responsible for the lower excitation temperatures has yet to be determined.

Rotational Temperature Measurements

The rotational temperature measurements were performed for the cryogenically cooled glow discharge to investigate the effect of cooling on the plasma gas temperature. The most common molecular species used for rotational temperature (T_{rot}) calculations are OH and N_2^+. Both species are

present in the glow discharge plasma as trace impurities, but their emission bands are not observed or too weak for temperature measurements. Therefore, it is necessary to add water vapor or nitrogen to the argon discharge gas to produce emission signals sufficient for temperature calculations. Nitrogen addition was chosen for rotational temperature determinations since cooling with liquid nitrogen should not "freeze out" nitrogen as it would the water vapor. The 0.5 m monochromator was able to resolve adequately the R branch transitions of the N_2^+ band emission for temperature calculations. A typical N_2^+ emission spectrum is shown in Figure 55. The transition lines that were sufficiently resolved and used for calculating the temperature are listed in Table XIII. A Boltzmann plot for the determination of the N_2^+ rotational temperature is shown in Figure 56. With 10% nitrogen in argon, a rotational temperature of 660 K was calculated at 0.5 mm from the cathode surface. Immediately noticeable is the large difference between the excitation and rotational temperatures. The excitation temperature is on average 5 times larger than the rotational temperature. This temperature discrepancy supports the assumption that the glow discharge is not in local thermodynamic equilibrium. The large differences in the temperature measurements result from the differences in the excitation processes and degree of excitation of the Fe and N_2 species in the glow discharge.

The addition of nitrogen to the discharge can alter somewhat the plasma processes. An initial study was made to determine the effect of N_2 concentration on the T_{rot} without cooling (Figure 57). The GD was operated in constant current

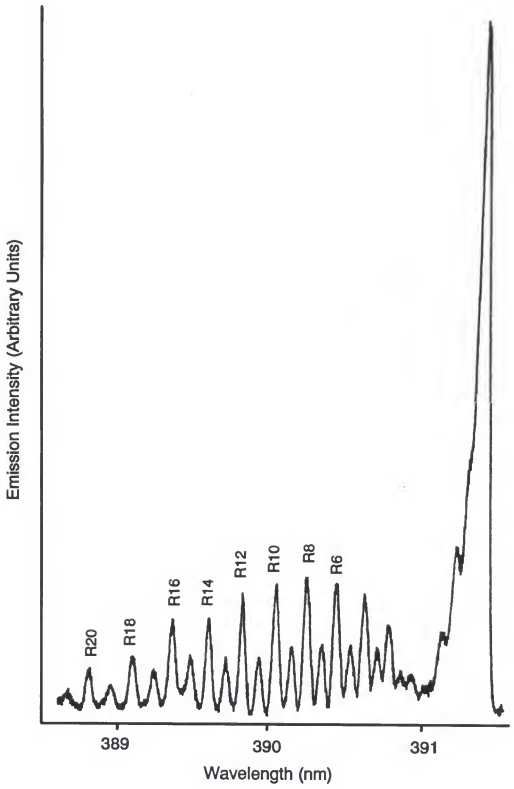

Figure 55. Glow discharge N_2^+ emission spectrum. Iron cathode, 0.9 Torr argon and 0.1 Torr nitrogen, 4.0 mA, without cryogenic cooling.

Table XIII. Assignment of the wavelengths and rotational quantum numbers for the R branch of the N_2^+ emission band (167).

λ (nm)	K"	(K" + 1)(K" + 2)
390.49	6	56
390.29	8	90
390.08	10	132
389.85	12	182
389.60	14	240
389.04	18	380
388.74	20	462

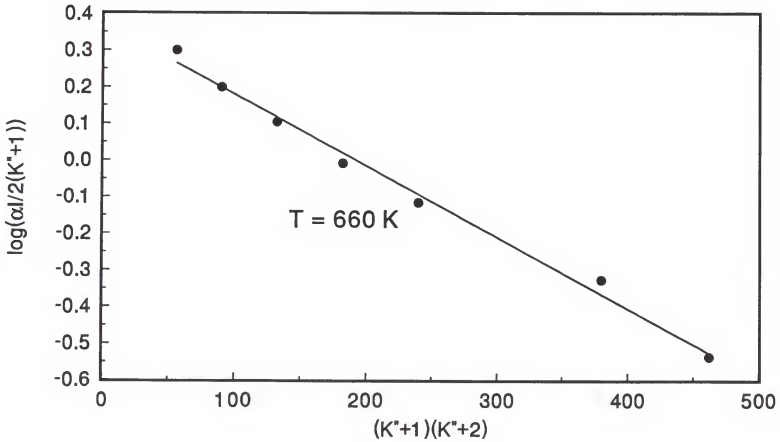

Figure 56. Representative Boltzmann plot for the determination of the N_2^+ rotational temperature. Iron cathode, 0.9 Torr argon and 0.1 nitrogen, 4.0 mA, without cryogenic cooling.

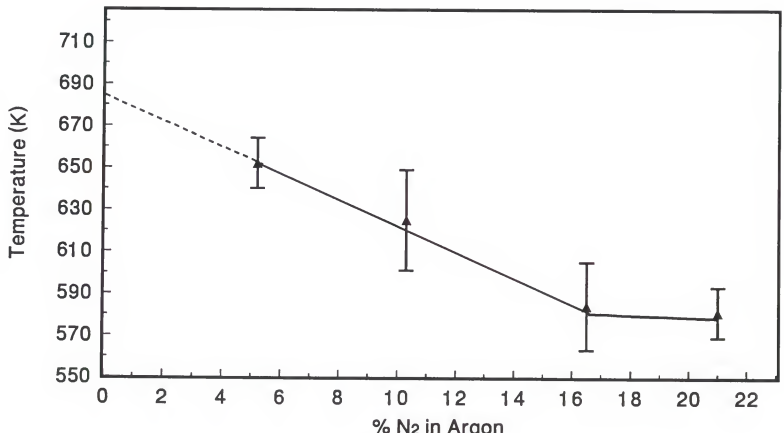

Figure 57. The effect of nitrogen concentration on the glow discharge N_2^+ rotational temperature. Iron cathode, 1 Torr total discharge pressure, 4.0 mA, without cryogenic cooling.

mode with a total discharge pressure of 1 Torr. The pressures were monitored with a capacitance manometer allowing the absolute discharge pressures to be set and maintained without regard to differences in the densities of Ar and N_2. The overall effect of nitrogen introduction was to reduce the gas temperature while increasing the discharge voltage. As the percentage of N_2 was increased from 5 to 15%, the T_{rot} linearly decreased until leveling off at ca. 15% of added N_2. The relative gas temperature at 0% N_2 was determined by extrapolating from the linear portion of the plot to the y-axis, and was estimated to be ca. 685 K at 0.5 mm from the cathode surface. All remaining experiments were performed with 10% N_2 in argon because it provided an adequate N_2^+ emission intensity without completely overwhelming the analyte ion signals that were monitored simultaneously by the mass spectrometer. Additionally, all subsequent rotational temperatures reported are for 10% N_2 addition; the temperatures have not been corrected to 0% N_2.

The stability of the N_2^+ rotational temperature over 200 min is shown in Figure 58. In contrast to the iron excitation temperature, the rotational temperature is relatively stable during this entire time period with a RSD of 2%. Since nitrogen is constantly being added to the discharge, the removal of impurities due to presputtering will not occur. The rotational temperature was also determined for varying discharge voltage and current with and without cooling. The results were similar to the excitation temperature in that the rotational temperatures for the cryocooled case were always lower, typically 25-90 K less.

In an attempt to determine the magnitude of cryogenic cooling induced by the liquid nitrogen coil on the plasma temperature, the distance between the sample cathode and the coil was varied (Figure 59). The coil can be moved over some distance, ranging from a position behind the cathode to an extreme position in contact with the exit orifice plate. For these experiments, the position of the coil was varied but always remained behind the cathode, so that the coil did not interfere with the optical measurements. The closer the coil was to the cathode, the lower the T_{rot} measured. These lower temperatures reflect the reduction of the relative populations of the N_2^+ rotational levels. Note that the coil did not have to be in the maximum cooling position in order to remove gaseous impurities. For example, a compacted sample, with entrapped moisture, may require the coil to be closer to the cathode to remove efficiently the water evolved from the sample, compared to a solid metal sample where adsorbed water vapor is released primarily from the chamber walls. In addition, reproducibility of analyses will depend on the position of the cryogenic coil, given the change in temperature (i.e., plasma processes) with cathode-coil position.

To determine whether the removal of the gaseous impurities contributes to the reduction of the T_{rot}, Ta (a gettering reagent) was used as the sample cathode. A titanium cathode was not used because it had spectral lines that overlapped with the N_2^+ band. It was found that as the reactive Ta cleans the plasma, the T_{rot} increased and the impurity ion signals, as represented by the H_3O^+ ion signal, decreased (Figure 60). After approximately 50 min., the water impurity species

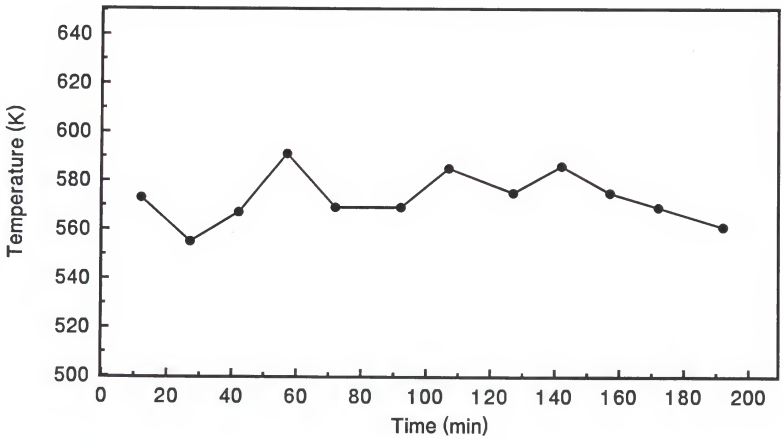

Figure 58. Stability of N_2^+ rotational temperature measurements. Iron cathode, 0.9 Torr argon and 0.1 Torr nitrogen, 4.0 mA, without cooling.

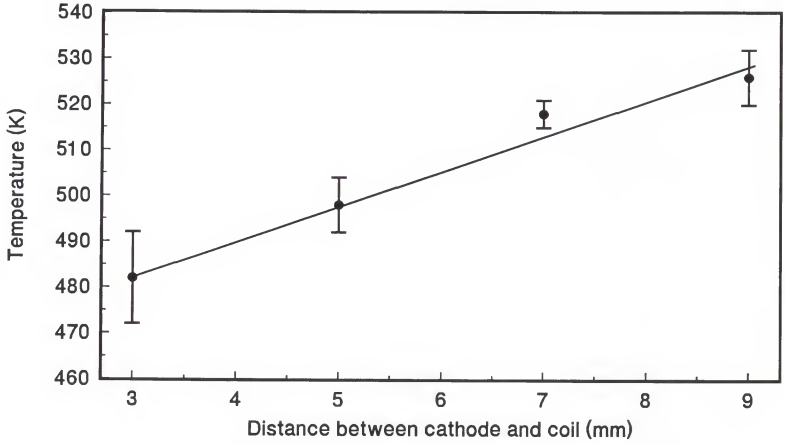

Figure 59. A plot of N_2^+ rotational temperature versus the distance between the sample cathode and the cryogenic cooling coil. Iron cathode, 0.9 Torr argon and 0.1Torr nitrogen, 4.0 mA, with cryogenic cooling.

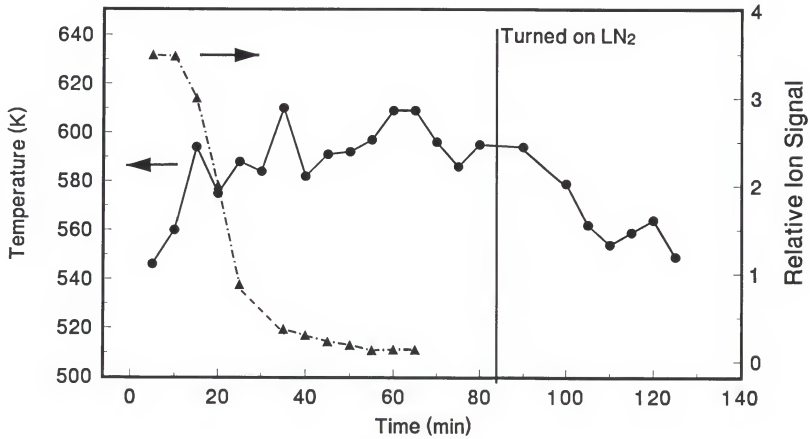

Figure 60. The effect of gettering versus cryogenic cooling on the N_2^+ rotational temperature. Tantalum cathode, 0.9 Torr argon and 0.1 Torr nitrogen, 4.0 mA. ● - rotational temperature, ▲ - H_3O^+ ion signal.

were eliminated and the T_{rot} stabilized near 590±11K. Next, the liquid nitrogen flow through the coil was turned on. After 20 minutes of cooling, the T_{rot} dropped by 50 K. The removal of gaseous impurities increased the T_{rot}, while cryogenic cooling decreased the T_{rot}. The removal of molecular species from the plasma resulted in an increase in the rotational temperature. Therefore, the removal of impurities from the discharge does not, in itself, contribute to the lower gas temperature seen with cryogenic cooling.

The N_2^+ rotational temperature profile of the GD plasma is shown in Figure 61. In contrast to the excitation temperature profile, the T_{rot} appears to decrease slowly with increasing distance from the hot cathode. With the addition of N_2, the regions of the plasma were not easily distinguished and, hence, are not shown on the profile. The T_{rot} with cryogenic cooling is between 50 and 100 K lower than without cooling. As the distance from the cathode is increased, the temperature difference appears to be relatively constant until near the end of the measured distance, where a small decrease in temperature difference is observed, although the weak emission signals at that distance make reliable measurements questionable. The shape of the rotational temperature profile is similar to both the temperature profiles reported by Ferreira et al. (161) for the broadening of a discharge gas line (Ar 415.8 nm) and the profiles reported by Kuraica et al. (162) for the broadening of the Ar 696.54 nm line. It is difficult to compare the magnitude of the gas temperatures measured in these studies, since different GD source configurations as well as operating conditions were used. There is a large

temperature difference when comparing the N_2^+ rotational temperatures (450-700 K) reported here to ICP N_2^+ rotational temperatures (4500-8300 K) (167), as would be expected between the low-powered GD and high-powered ICP.

Thermocouple Temperature Measurements

The rotational temperature is considered a good approximation of the gas temperature; therefore, the gas temperature was measured with a thermocouple for comparison. The smallest practical thermocouple was used to minimize any disturbances to the plasma. By using a physical probe, the temperature of the entire GD source can be profiled. The temperature profile of the GD with and without cooling is shown in Figure 62. In comparing the profile temperatures for the first 3 mm from the cathode, the thermocouple temperatures are similar in profile and approximately 2/3 of the N_2^+ rotational temperatures. In addition, the gas temperature decreased with increasing distance similar to the T_{rot} profiles. The difference between gas temperatures measured optically and physically could be due to the low pressure in the source (fewer collisions) requiring a longer time for the thermocouple probe, which is surrounded by a grounded stainless steel sheath, to reach equilibrium with the surrounding gas. It is also possible that convection processes might partially influence temperature measurements at this pressure. No other reports of thermocouple temperature measurements in the GD have been found for comparison. It is not possible to compare the thermocouple

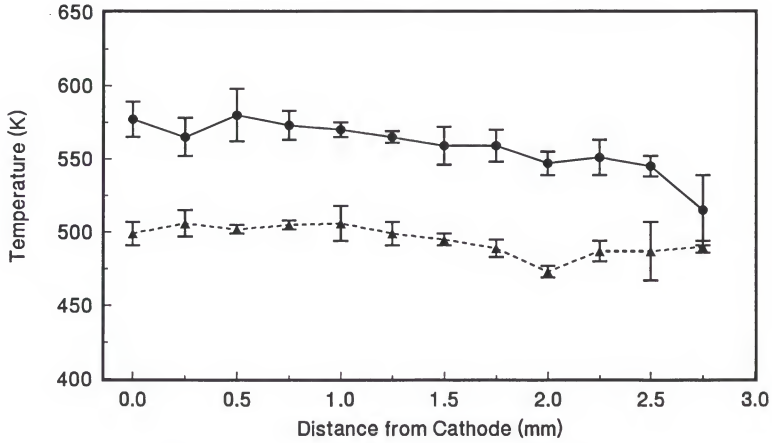

Figure 61. N_2^+ rotational temperature profile of the glow discharge. Iron cathode, 0.9 Torr argon and 0.1 Torr nitrogen, 4.0 mA. ● - Without cryogenic cooling, ▲ - with cryogenic cooling.

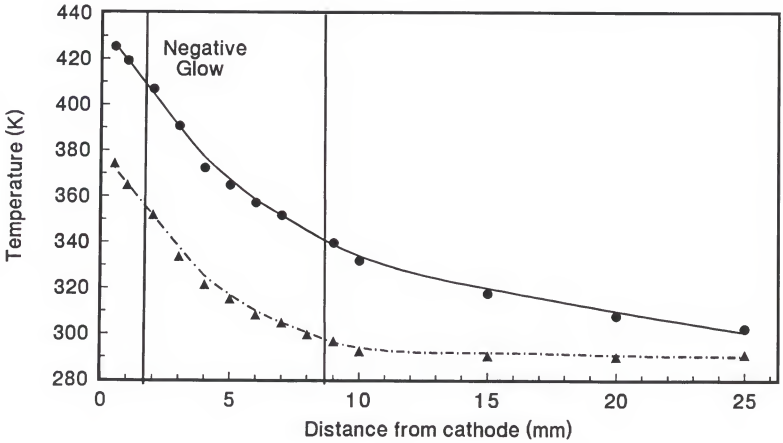

Figure 62. Gas temperature profile of the glow discharge using a thermocouple probe. Iron cathode, 0.9 Torr argon and 0.1 Torr nitrogen, 4.0 mA. ● - without cryogenic cooling, ▲ - with cryogenic cooling.

measurements to ICP or other high power plasmas, because thermocouples are not compatible with the high temperatures found in these plasmas.

Conclusions

The use of liquid nitrogen cooling to remove gaseous impurities from the glow discharge source lowers the temperature of the plasma, as reflected in both optical measurements using the Fe(I) excitation and N_2^+ rotational emission spectra or physical measurements using a thermocouple. With cryogenic cooling, the excitation temperatures decreased 100-300 K, the rotational temperatures decreased 50-100 K, and thermocouple temperatures decreased 25-50 K. The lower rotational and thermocouple temperatures indicate that the thermal temperature (energy) of the plasma decreases with cooling. Why the electronic temperature decreases with cooling has yet to be determined. It is known that trace quantities of impurity species can significantly influence the sputtering, ionization and excitation processes in the glow discharge, which in turn can influence the free atom population and emission intensity. Whether this decrease in temperature with cryogenic cooling will significantly affect quantitative analyses will depend on the magnitude of impurities in the discharge, type of sample to be analyzed, and the analysis method being used.

CHAPTER 7
CONCLUSIONS

Glow discharge mass spectrometry is an elemental analysis technique where atomization, excitation, and ionization of the solid sample occur in the discharge. One disadvantage of the glow discharge is the presence of gaseous impurities, which can reduce the amount of sample sputtering as well as quench excitation and ionization reactions. This dissertation has reported on the effects of cryogenic cooling to remove these gaseous impurities from the glow discharge plasma. By flowing liquid nitrogen through a coil inserted in the GD chamber, impurities were physically removed by their condensation on the coil surface.

The greatest interferences from water vapor and other gaseous impurities occur in the m/z range between 10 - 40. Cryogenic cooling started to reduce the impurities immediately upon turning on the liquid nitrogen flow and within 20 - 30 min removed the impurities, except N^+. Even under the extreme conditions of oil vapor introduction, cryogenic cooling effectively cleaned the plasma of the hydrocarbon impurities. Upon cooling with liquid nitrogen, the water impurities are removed first, followed by the other impurities, with the order of disappearance depending on the condensation point and amount of the impurities. By varying the liquid nitrogen flow rate, it should be possible to eliminate selectively the

impurities from one another. The production of hydride and oxide species in the plasma was also eliminated upon cryogenic cooling.

The operating parameters of the cryogenically cooled glow discharge ion source were found to be similar to the noncooled glow discharge. The optimum sampling distance and discharge pressure were essentially the same with and without cooling. For both constant voltage and current operating modes, lower analyte ion signals were reported for the cooled plasma than the noncooled, but both exhibited increased ion signals with increased voltage and current. The cryogenically cooled glow discharge was found to have less impedance than the noncooled plasma. This decrease in impedance could be due to less energy being consumed by the impurity species for excitation (electronic, vibration, and rotational) and dissociation or by the impurity species forming negative ions by electron attachment. Although the cooled glow discharge has less impedance, the sputter yields and relative ion energies were found not to differ significantly between the cooled and noncooled plasmas. Using metal alloy samples, the relative sensitivity factor values required for quantitative analysis improved in accuracy and precision upon cooling. The limits of detection were also similar for the cooled and noncooled glow discharges.

The greatest achievement of the cryogenic cooling was demonstrated by its ability to remove or reduce the gaseous impurities from a rf glow discharge plasma using a nonconducting sample. The rf-GD mass spectra of ceramic and geological samples without cooling were dominated by the gaseous impurities,

in particular the water or water related ion signals. It was impossible to obtain elemental analyses of these samples. Upon cooling, the impurities were reduced and the analyte ion signals were abundant, making elemental analysis possible.

Plasma diagnostic temperature measurements were performed in the glow discharge to study the effect of cryogenic cooling on the plasma processes. The fundamental plasma processes were investigated by optical temperature measurements from Fe (I) and Ti (II) excitation and N_2^+ rotational emission spectra and physical temperature measurements using a thermocouple probe. Lower temperatures were observed for the cryogenically cooled glow discharge plasma, except for the Ti (II) excitation temperatures. The rotational and thermocouple temperatures are measurements of the thermal temperature of the plasma and, as expected, both temperatures decreased with cooling. For the Fe (I) excitation temperature, the temperature decreased with cooling. The Ti(II) excitation temperature decreased as the Ti cleaned the plasma with and without cooling. The excitation temperature measurements are a reflection of the relative population of the different excited states of the element. From the excitation temperature measurements, it appears that the trace quantities of gaseous impurities influence the free atom population and emission intensities.

Future Studies

These initial experiments provide the impetus for many more exciting investigations into cryogenics and glow discharges. First, there are many

possibilities with regard to the cryogenic cooling system design. While liquid nitrogen has proven to be very effective at removing the gaseous impurities, the effect of other cryogens or refrigerants (Table III) for impurity removal could be investigated. There is also the possibility of developing a cryogenic system without liquid cryogens. The Stirling and Gifford-McMahon coolers are both capable of providing the temperatures required for cooling the glow discharge source and are available in sizes that could be adapted for use in the GD sources. This ability to vary and control the cooling temperature, using either method, would allow the effect of the selective removal of the impurities on plasma chemistry to be investigated.

Other possible areas of investigation include how the glow discharge processes are affected by the cooling system configuration. For example, in order to analyze difficult samples, such as polymers, biological materials, and even frozen aqueous solutions, a cryogenic system that cools the cathode is necessary. Since the cryogenic coil is not in direct contact with the sample cathode, a new design could incorporate the liquid nitrogen flow through tubing in the direct insertion probe. How would such a design affect the glow discharge processes, especially sputtering?

For GDMS to reach its full potential as a solids elemental analysis technique, it needs to prove its capability for compacted powder samples (i.e., rocks, soils, ores). It was shown that cryogenic cooling is essential for the analysis of these nonconducting materials using rf-GDMS. To improve the

cryogenically cooled rf-GDMS analysis method, the technique must be optimized, including sample preparation (i.e., pulverizing, blending, and pressing of the sample) and glow discharge operating parameters (i.e., pressure, power, sampling distance). In addition, the RSF values must be developed and investigated. RSF values have been found to be relatively independent of matrix effect for metal samples, but is this true for complex geological samples? Research in this area has already begun in our laboratory.

It was shown that cooling can remove or reduce carbon, oxygen and possibly nitrogen impurities. It still needs to be determined whether a cryogenically cooled glow discharge source can be used for the quantitative analysis of these elements. Most of the trace elements analyzed by GDMS are metals. Further experiments are needed to determine whether similar improvements are seen for nonmetal trace species. Most nonmetals form negative ions; therefore, how is negative ion formation in the plasma affected by cryogenic cooling?

Finally, while cooling is necessary for mass spectrometric analyses, how about optical emission, absorption, and fluorescence measurements? It is estimated that the GD ionization rate is about 1%, and it is understandable why the presence and removal of gaseous impurities can affect the ion population. But for the more abundant atomic population, the presence of gaseous impurities might not pose as large a problem. In addition, there are many more analyte lines, with varying sensitivities, available in optical measurements than for mass

spectrometry. How these optical techniques will be affected by cryogenic cooling, if at all, needs to be studied.

REFERENCES

(1) Aston, F. W. *Mass Spectra and Isotopes*; Edward Arnold & Co.: London, 1942.

(2) Knewstubb, P. F.; Tickner, A. W. *J. Chem. Phys.* **1962**, *36*, 674.

(3) Knewstubb, P. F.; Tickner, A. W. *J. Chem. Phys.* **1962**, *36*, 684.

(4) Knewstubb, P. F.; Tickner, A. W. *J. Chem. Phys.* **1962**, *37*, 2941.

(5) Knewstubb, P. F.; Dawson, P. H.; Tickner, A. W. *J. Chem. Phys.* **1963**, 38 1031.

(6) Knewstubb, P. F.; Tickner, A. W. *J. Chem. Phys.* **1963**, *38*, 464.

(7) Coburn, J. W. *Rev. Sci. Instr.* **1970**, *41*, 1219.

(8) Coburn, J. W.; Kay, E. *Appl. Phy. Lett.* **1971**, *18*, 435.

(9) Coburn, J. W.; Kay, E. *Appl. Phy. Lett.* **1971**, *19*, 350.

(10) Coburn, J. W.; Taglauer, E.; Kay, E. *J. Appl. Phys.* **1974**, *45*, 1779.

(11) Coburn, J. W.; Eckstein, E. W.; Kay, E. *J. Appl. Phys.* **1975**, *46*, 2828.

(12) Harrison, W. W.; Magee, C. W. *Anal. Chem.* **1974**, *46*, 461.

(13) Colby, B. N.; Evans Jr., C. A. *Anal. Chem.* **1974**, *46*, 1236.

(14) Daughtrey, E. H.; Harrison, W. W. *Anal. Chem.* **1975**, *47*, 1024.

(15) Wallace, J. R.; Natusch, D. F. S.; Colby, B. N.; Evans, C. A. *Anal. Chem.* **1976**, *48*, 118.

(16) Donohue, D. L.; Harrison, W. W. *Anal. Chem.* **1975**, *47*, 1528.

(17) Mattson, W. A.; Bentz, B. L.; Harrison, W. W. *Anal. Chem.* **1976**, *48*, 489.

(18) McCaig, L.; Shi, Z.; Woodrum, T. H.; Brewer, S.; Sacks, R. *Appl. Spectrosc.* **1992**, *46*, 1762.

(19) Bentz, B. L.; Harrison, W. W. *Anal. Chem.* **1982**, *54*, 1644.

(20) Harrison, W. W.; Bentz, B. L. *Anal. Chem.* **1979**, *51*, 1853.

(21) Klingler, J. A.; Savickas, P. J.; Harrison, W. W. *J. Am. Soc. Mass Spectrom.* **1990**, *1*, 138.

(22) King, F. L.; Pan, C. *Anal. Chem.* **1993**, *65*, 735.

(23) Klingler, J. A.; Barshick, C. M.; Harrison, W. W. *Anal. Chem.* **1991**, *63*, 2571.

(24) Klingler, J. A.; Harrison, W. W. *Anal. Chem.* **1991**, *63*, 2982.

(25) Duckworth, D. C.; Marcus, R. K. *J. Anal. Atom. Spectrosc.* **1992**, *7*, 711.

(26) Milton, D. M.; Hutton, R. C. *Spectrochim. Acta* **1993**, *48B*, 39.

(27) Barshick, C. M.; Eyler, J. R. *J. Am. Soc. Mass Spectrom.* **1992**, *3*, 122.

(28) Watson, C. H.; Wronka, J.; Laukien, F. H.; Barshick, C. M.; Eyler, J. R. *Spectrochim. Acta* **1993**, *48B*, 1445.

(29) Watson, C. H.; Wronka, J.; Laukien, F. H.; Barshick, C. M.; Eyler, J. R. *Anal. Chem.* **1993**, *65*, 2801.

(30) Duckworth, D. C.; Barshick, C. M.; Smith, D. H.; McLuckey, S. A. *Anal. Chem.* **1994**, *66*, 92.

(31) McLuckey, S. A.; Glish, G. L.; Duckworth, D. C.; Marcus, R. K. *Anal. Chem.* **1992**, *64*, 1606.

(32) Duckworth, D. C.; Marcus, R. K. *Appl. Spectrosc.* **1990**, *44*, 649.

(33) King, F. L.; McCormack, A. L.; Harrison, W. W. *J. Anal. Atom. Spectrosc.* **1988**, *3*, 883.

(34) McLuckey, S. A.; Glish, G. L.; Asano, K. G.; Grant, B. C. *Anal. Chem.* **1988**, *60*, 2220.

(35) McLuckey, S. A.; Glish, G. L.; Asano, K. G. *Anal. Chim. Acta* **1989**, *225*, 25.

(36) Chambers, D. M.; McLuckey, S. A.; Glish, G. L. *Anal. Chem.* **1993**, *65*, 778.

(37) Zhao, J.; Zhu, J.; Lubman, D. *Anal. Chem.* **1992**, *64*, 1426.

(38) Chien, B. M.; Michael, S. M.; Lubman, D. M. *Anal. Chem.* **1993**, *65*, 1916.

(39) Lauritsen, F. R.; Choudhury, T. K.; Dejarme, L. E.; Cooks, R. G. *Anal. Chim. Acta* **1992**, *266*, 1.

(40) Matsumoto, K.; Kojima, H.; Kazuhiro, Y.; Tsuge, S. *Organic Mass Spectrom.* **1985**, *20*, 243.

(41) Fang, D.; Seegopaul, P. *J. Anal. Atom. Spectrosc.* **1992**, *7*, 1303.

(42) Vieth, W.; Huneke, J. C. *Anal. Chem.* **1992**, *64*, 2958.

(43) Kudermann, K.; Blaufub, K. *Mikrochim. Acta* **1987**, *1*, 269.

(44) Mykytiuk, A. P.; Semeniuk, P.; Berman, S. *Spectrochim. Acta Rev.* **1990**, *13*, 1.

(45) Vassamillet, L. F. *J. Anal. Atom. Spectrosc.* **1989**, *4*, 451.

(46) Kudermann, G.; Blaufuss, K. H.; Luehrs, C.; Vielhaber, W.; Collisi, U. *Fresenius J. Anal. Chem.* **1992**, *343*, 734.

(47) Hutton, R. C.; Raith, A. *J. Anal. Atom. Spectrosc.* **1992**, *7*, 623.

(48) Mizota, T.; Nakamura, T.; Iwasaki, K. *Bunseki Kagaku* **1992**, *41*, 425.

(49) Charalambous, P. M. *Mikrochim. Acta* **1987**, *1*, 295.

(50) Jakubowski, N.; Stuewer, D.; Vieth, W. *Mikrochim. Acta* **1991**, *1*, 302.

(51) Jakubowski, R.; Stuewer, D.; Vieth, W. *Anal. Chem.* **1987**, *59*, 1825.

(52) Itoh, S.; Hirose, F.; Hasegawa, R. *Spectrochim. Acta* **1992**, *47B*, 1241.

(53) Woo, J. C.; Jakubowski, N.; Stuewer, D. *J. Anal. Atom. Spectrosc.* **1993**, *8*, 881.

(54) Duckworth, D. C.; Barshick, C. M.; Smith, D. H. *J. Anal. Atom. Spectrosc.* **1993**, *8*, 875.

(55) Duckworth, D. C.; Barshick, C. M.; Bostick, D. A.; Smith, D. H. *Appl. Spectrosc.* **1993**, *47*, 243.

(56) Tigwell, M.; Clark, J.; Shuttleworth, S.; Bottomely, M. *Mater. Chem. Phys.* **1992**, *31*, 23.

(57) Mei, Y.; Harrison, W. W. *Anal. Chem.* **1993**, *65*, 3337.

(58) Milton, D. M. P.; Hutton, R. C.; Ronan, G. A. *Fresenius J. Anal. Chem.* **1992**, *343*, 773.

(59) Milton, D. M. P.; Clark, J.; Potter, D.; Hutton, R. C. *Anal. Sci.* **1991**, *7*, 1243.

(60) Robinson, K.; Hall, F. H. *J. Metals* **1987**, *39*, 14.

(61) Donohue, D. L.; Petek, M. *Anal. Chem.* **1991**, *63*, 740.

(62) Shimamura, T.; Takahashi, T.; Honda, M.; Nagai, H. *J. Anal. Atom. Spectrosc.* **1993**, *8*, 453.

(63) Luo, F. C. H.; Huneke, J. C. *Proceedings of the 2nd International Conference on Elem. Anal. Coal and Its By-Products*, Singapore, **1991**.

(64) Yang, M. Y.; Lee, S. H.; Wakita, H. *Anal. Sci.* **1991**, *7*, 1269.

(65) Jakubowski, J.; Stuewer, D. *J. Anal. Atom. Spectrosc.* **1992**, *7*, 951.

(66) Hall, D. J.; Sanderson, N. E. *Surf. Interface Anal.* **1988**, *11*, 40.

(67) Van Straaten, M.; Butaye, L.; Gijbels, R. *Second. Ion Mass Spectrom.* **1992**, 629.

(68) Naumidis, A.; Beske, H.; Holzbrecher, H.; Nickel, H.; Schulze, H. A. *Fresenius J. Anal. Chem.* **1987**, *329*, 278.

(69) Raith, A.; Hutton, R. C.; Huneke, J. C. *J. Anal. Atom. Spectrosc.* **1993**, *8*, 867.

(70) Pak, Y. N.; Tanaka, T.; Kawaguchi, H. *Anal. Sci.* **1993**, *9*, 137.

(71) Evetts, I.; Milton, D.; Mason, R. *Biol. Mass Spectrom.* **1991**, *20*, 153.

(72) Mason, R.; Milton, D. *Int. J. Mass Spectrom. Ion Proc.* **1989**, *91*, 209.

(73) Barshick, C. M.; Duckworth, D. C.; Smith, D. H. *J. Am. Soc. Mass Spectrom.* **1993**, *4*, 47.

(74) Barshick, C. M.; Smith, D. H.; Hackney, J. H.; Cole, B. A.; Wade, J. W. *Anal. Chem.* **1994**, *66*, 730.

(75) Jakubowski, N.; Stuewer, D.; Toelg, G. *Spectrochim. Acta* **1991**, *46B*, 155.

(76) Jakubowski, N.; Stuewer, D. *Fresenius J. Anal. Chem.* **1989**, *335*, 680.

(77) Saito, M. *Anal. Sci.* **1991**, *7*, 541.

(78) Mei, Y.; Harrison, W. W. *Spectrochim. Acta* **1991**, *46B*, 175.

(79) Howatson, A. M. *An Introduction to Gas Discharges*; Pergamon Press: New York, 1976.

(80) Llewelyn-Jones, F. *The Glow Discharge*; Methuen: London, 1966.

(81) Cobine, D. C. *Gaseous Conductors*; Dover: New York, 1958.

(82) von Engel, A. *Electric Plasmas: Their Nature and Uses*; International Publications Taylor & Francis Inc.: New York, 1983; ch. 7.

(83) Chapman, B. *Glow Discharge Processes*; Wiley-Interscience: New York, 1980.

(84) Wehner, G. K.; Anderson, G. S. In *Handbook of Thin Flim Technology*; L. I. Maissel and R. Glang, Ed.; McGraw-Hill Co.: New York, 1970; ch. 3.

(85) Herzog, R. F. K.; Poschenrieder, W. P.; Satidiewics, F. K. *Radiat. Eff.* **1973**, *18*, 199.

(86) Boumans, P. W. J. M. *Anal. Chem.* **1972**, *44*, 1219.

(87) Mason, R. S.; Milton, D. M. P.; Pichilingi, M.; Anderson, P. D. J.; Fernandez, M. T. *Rapid Commun. Mass Spectrom.* **1994**, *8*, 187.

(88) von Hippel, A. *Ann. Phys.* **1926**, *81*, 1043.

(89) Carter, G.; Colligan, J. S. *Ion Bombardment of Solids*; American Elesevier: New York, 1968.

(90) Westwood, W. D. *Prog. Surf. Sci.* **1976**, *7*, 71.

(91) Oechsner, H. *Appl. Phys.* **1975**, *8*, 185.

(92) Rosenberg, D.; Wehner, G.K . *J. Appl. Phys.* **1962**, *33*, 1842.

(93) Wehner, G. K.; Laegreid, N. *J. Appl. Phys.* **1961**, *32*, 365.

(94) Wehner, G. K. In *Methods of Surface Analysis*; A. W. Czanderna, Ed.; Elsevier Scientific Publishing Co.: Amsterdam, 1975.

(95) Jones, R. E.; Winters, H. F.; Maissel, L. I. *J. Vac. Sci. Technol.* **1968**, *5*, 84.

(96) Loving, T. J.; Harrison, W. W. *Anal. Chem.* **1983**, *55*, 1526.

(97) Larkins, P. L. *Spectrochim. Acta* **1991**, *46B*, 291.

(98) Bernhard, A. E. *Spectrosc.* **1987**, *2*, 24.

(99) Chakrabarti, C. L.; Headrick, K. L.; Hutton, J. C.; Bicheng, Z.; Bertels, P. C.; Back, M. H. *Anal. Chem.* **1990**, *62*, 574.

(100) Smith, B. W.; Womack, J. B.; Omenetto, N.; Winefordner, J. D. *Appl. Spectrosc.* **1989**, *43*, 873.

(101) Broekaert, J. A. C. In *Glow Discharge Spectroscopies*; R. K. Marcus, Ed.; Plenum Press: New York, 1993; ch. 4.

(102) Harrison, W. W.; Bentz, B. L. *Prog. Anal. Spectrosc.* **1988**, *11*, 53.

(103) King, F. L.; Harrison, W. W. *Mass Spectrom. Rev.* **1990**, *9*, 285.

(104) Penning, F. M. *Electrical Discharges in Gases*; Philips Technical Library: Envdoven, 1957.

(105) Fang, D.; Marcus, R. K. In *Glow Discharge Spectrocopies*; R. K. Marcus, Ed.; Plenum Press: New York, 1993; ch. 2.

(106) Nasser, E. *Fundamentals of Gaseous Ionization and Plasma Electronics*; Wiley: New York, 1971.

(107) Stedman, D. H.; Setser, D. W. *Prog. Reaction Kinetics* **1971**, *6*, 193.

(108) Hecq, M.; Hecq, A.; Fontignies, M. *Thin Solid Films* **1984**, *115*, L45.

(109) Hecq, M.; Hecq, A.; Fontignies, M. *Anal. Chim. Acta* **1983**, *155*, 191.

(110) Smith, R. L.; Serxner, D.; Hess, K. R. *Anal. Chem.* **1989**, *61*, 1103.

(111) Smyth, K. C.; Bentz, B. L.; Bruhn, C. G.; Harrison, W. W. *J. Am. Chem. Soc.* **1979**, *101*, 797.

(112) Ratliff, P. H.; Harrison, W. W. *Spectrochim. Acta Part B* **1994**, Accepted.

(113) Velazco, J. E.; Kolts, J. H.; Setser, D. W. *J. Chem. Phys.* **1978**, *69*, 4357.

(114) *CRC Handbook of Chemistry and Physics*; CRC Press, Inc.: Boca Raton, 1990; Vol. 70 th.

(115) Scurlock, R. G. *Cryogenics* **1990**, *30*, 483.

(116) Sittig, M. *Cryogenics: Research and Applications*; D. Van Nostrand Company, Inc.: Princeton, NJ, 1963.

(117) Meyer, B. *Low Temperature Spectroscopy*; Elsevier Publishing Company, Inc.: New York, 1971.

(118) *Cryogenics Safety Manual*; Butterworth-Heinemann Ltd.: Oxford, 1991.

(119) Ozin, G. A.; Moskovits, M. *Cryochemistry*; John Wiley & Sons: New York, 1976.

(120) Little, W. A. In *Advances in Cryogenic Engineering*; R. W. Fast, Ed.; Plenum Press: New York, 1990; Vol. 35; 1305.

(121) Kohler, F. W. L. In *Progress in Cryogenics*; K. Mendelssohn, Ed.; Academic Press Inc.: New York, 1960; Vol. 2; 41.

(122) Nambudripad, N. In *Cryogenic Engineering*; B. A. Hands, Ed.; Academic Press: London, 1986; pp 431.

(123) Gifford, W. E. In *Progress in Cryogenics*; K. Mendelssohn, Ed.; Academic Press Inc.: New York, 1961; Vol. 3; pp 49.

(124) Lyon, D. N. In *Cryogenic Technology*; R. W. Vance, Ed.; John Wiley & Sons: New York, 1963; Ch. 2.

(125) *Melcor Frigichip Technical Catalog*; Materials Electronic Products Corp.: Trenton, NJ, .

(126) Lott, D. E.; Jenkins, W. J. *Rev. Sci. Instr.* **1984**, *55*, 1982.

(127) Krock, K. A.; Ragunathan, N.; Wilkins, C. L. *J. Chromatogr.* **1993**, *645*, 153.

(128) Alves, L. C.; Wiederin, D. R.; Houk, R. S. *Anal. Chem.* **1992**, *64*, 1164.

(129) Koppenall, D. W.; Barinaga, C. J.; Smith, M. R. In *1994 Winter Conference on Plasma Spectrochemistry*; San Diego, CA, 1994; pp 292.

(130) Lancaster, G. M.; Honda, F.; Fukuda, Y.; Rabalais, J. W. *J. Am. Chem. Soc.* **1979**, *101*, 1951.

(131) Jonkman, H. T.; Michl, J. *J. Am. Chem. Soc.* **1981**, *103*, 733.

(132) Orth, R. G.; Jonkman, H. T.; Powell, D. H.; Michl, J. *J. Am. Chem. Soc.* **1981**, *103*, 6026.

(133) Orth, R. G.; Jonkman, H. T.; Michl, J. *Int. J. Mass Spectrom. Ion Proc.* **1982**, *43*, 41.

(134) Ervin, M. H.; Wood, M. C.; Winogard, N. *Anal. Chem.* **1993**, *65*, 417.

(135) Holzhauer, J. K.; McGee, J., H. A. *Anal. Chem.* **1969**, *41*, 24.

(136) Blanchard, L. P.; Le Goff, P. *Can. J. Chem.* **1959**, *37*, 515.

(137) Daughtrey, E. H.; Harrison, W. W. *Anal. Chem.* **1975**, *47*, 1024.

(138) Foss, G. O.; Svec, H. J.; Conzemius, R. J. *Anal. Chim. Acta* **1983**, *147*, 151.

(139) U.S. Patent No. 4, 8., 539, **1989**,

(140) King, F. L. Ph.D. Dissertation, University of Virginia, Charlottesville, VA, 1989.

(141) Bentz, B. Ph.D. Dissertation, University of Virginia, Charlottesville, VA, 1979.

(142) Savickas, P. J. Ph.D. Dissertation, University of Virginia, Charlottesville, VA, 1984.

(143) Miller, P. E.; Benton, M. B. *J. Chem. Ed.* **1986**, *63*, 617.

(144) *Quadrupole Mass Spectrometry and its Applications*; Dawson, P. H., Ed.; Elsevier Scientific Publishing Co.: Amsterdam, 1976.

(145) Winchester, M. R.; Duckworth, D. C.; Marcus, R. K. In *Glow Discharge Spectroscopies*; R. K. Marcus, Ed.; Plenum Press: New York, 1993; pp Ch. 7.

(146) Stern, E.; Caswell, H. L. *J. Vac. Sci. Technol.* **1966**, *4*, 128.

(147) Rakshit, A. B.; Warneck, P. *J. Chem. Phys.* **1981**, *74*,

(148) Ohorodnik, S. K.; DeGendt, S.; Tong, S. L.; Harrison, W. W. *J. Anal. Atom. Spectrosc.* **1993**, *8*, 859.

(149) Konig, H.; Helwig, G. *Z. Phys.* **1951**, *129*, 491.

(150) Laegreid, N.; Wehner, G. K. *J. Appl. Phys.* **1961**, *32*, 365.

(151) Fischer, W.; Naoumidis, A.; Nickel, H. *J. Anal. Atom. Spectrosc.* **1994**, *9*, 375.

(152) Vieth, W.; Huneke, J. C. *Spectrochim. Acta* **1991**, *46B*, 137.

(153) Smithwick III, R. W.; Lynch, D. W.; Franklin, J. C. *J. Am. Soc. Mass Spectrom.* **1993**, *4*, 278.

(154) Shick, C. R.; Raith, A.; Marcus, R. K. *J. Anal. Atom. Spectrosc.* **1993**, *8*, 1043.

(155) Fang, D.; Marcus, R. K. *J. Anal. Atom. Spectrosc.* **1988**, *3*, 873.

(156) Fang, D.; Marcus, R. K. *Spectrochim. Acta* **1990**, *45B*, 1053.

(157) Angstadt, A. D.; Whelan, J.; Hess, K. R. *Microchem. J.* **1993**, *47*, 206.

(158) Brackett, J. M.; Mitchell, J. C.; Vickers, T. J. *Appl. Spectrosc.* **1984**, *38*, 136.

(159) Buger, P. A. *Z. f. Naturforsch.* **1975**, *30A*, 216.

(160) West, C. D.; Human, H. G. C. *Spectrochim. Acta* **1976**, *31B*, 81.

(161) Ferreira, N. P.; Human, H. G. C.; Butler, L. R. P. *Spectrochim. Acta* **1980**, *35B*, 287.

(162) Kuraica, M.; Knojevic, N.; Platisa, M.; Pantelic, D. *Spectrochim. Acta* **1992**, *47B*, 1173.

(163) McDonald, D. C. *Spectrochim. Acta* **1982**, *37B*, 747.

(164) Uzelac, N. I.; Leis, F. *Spectrochim. Acta* **1992**, *47B*, 877.

(165) Cabannes, F.; Chapelle, J. In *Reactions Under Plasma Conditions*; M. Venugopalan, Ed.; Wiley-Interscience: New York, 1971; Vol. 1.

(166) Thorne, A. P. *Spectrosphysics*; Chapman and Hall: London, 1988.

(167) Mermet, J. M. In *Inductively Coupled Plasma Emission Spectroscopy Part 2 Applications and Fundamentals*; P. W. J. M. Boumans, Ed.; John Wiley & Sons: New York, 1987; ch. 10.

(168) Hasegawa, T.; Umemoto, M.; Haraguchi, H.; Hsiech, C.; Montaser, A. In *Inductively Coupled Plasmas in Analytical Atomic Spectrometry*; A. Montaser and D. W. Golightly, Ed.; VCH Publishers, Inc.: New York, 1992.

(169) Bastien, F. In *Electrical Breakdown and Discharges in Gases Part B: Macroscopic Processes and Discharges*; E. E. Kunhardt and L. H. Luessen, Ed.; Plenum Press: New York, 1981; ch. 7.

(170) Wiese, W. L. *Spectrochim. Acta* **1991**, *46B*, 831.

(171) Abdallah, M. H.; Mermet, J. M. *Spectrochim. Acta* **1982**, *37B*, 391.

BIOGRAPHICAL SKETCH

Susan Ohorodnik was born on February 7, 1963 in Detroit, Michigan. She began her undergraduate career at Wayne State University in 1983. Due to family obligations, she transferred to the University of California, San Diego in 1985 and then to Old Dominion University in 1987 where she received her Bachelor of Science degree in chemistry in May 1988. In May 1990, she obtained her Master of Science degree in analytical chemistry under the direction of Dr. Kenneth G. Brown at Old Dominion University. For her master's thesis, she developed a pulsed gas chromatographic method to measure the chemisorption properties of carbon monoxide oxidation catalysts. In the fall of 1990, she began her Ph.D. studies at the University of Florida where she joined Dr. Willard W. Harrison's research group. She completed her graduate career with a Doctor of Philosophy degree in August 1994.

I certify that I have read this study and that in my opinion it conforms to acceptable standard of scholarly presentation and is fully adequate, in scope and quality, as a dissertation for the degree of Doctor of Philosophy.

Willard W. Harrison, Chairman
Professor of Chemistry

I certify that I have read this study and that in my opinion it conforms to acceptable standard of scholarly presentation and is fully adequate, in scope and quality, as a dissertation for the degree of Doctor of Philosophy.

James D. Winefordner
Graduate Research Professor of Chemistry

I certify that I have read this study and that in my opinion it conforms to acceptable standard of scholarly presentation and is fully adequate, in scope and quality, as a dissertation for the degree of Doctor of Philosophy.

Richard A. Yost
Professor of Chemistry

I certify that I have read this study and that in my opinion it conforms to acceptable standard of scholarly presentation and is fully adequate, in scope and quality, as a dissertation for the degree of Doctor of Philosophy.

John R. Eyler
Professor of Chemistry

I certify that I have read this study and that in my opinion it conforms to acceptable standard of scholarly presentation and is fully adequate, in scope and quality, as a dissertation for the degree of Doctor of Philosophy.

Reza Abbaschian
Professor of Materials Science and Engineering

This dissertation was presented to the Graduate Faculty of the Department of Chemistry in the College of Liberal Arts and Sciences and to the Graduate School and was accepted as partial fulfillment of the requirements for the degree of Doctor of Philosophy.

August 1994

Dean, Graduate School